Article:
Basilici, G., Lorenzoni, P., Mesquita, Á. F. et al. (2024) Can palaeosols reveal palaeoenvironmental variability of fluvial systems? An example from the upper portion of the Bauru Group (Upper Cretaceous, SE Brazil). Sedimentary Geology, 464. 106604. ISSN: 0037-0738

https://doi.org/10.1016/j.sedgeo.2024.106604

Can palaeosols reveal palaeoenvironmental variability of fluvial systems? An example from the upper portion of the Bauru Group (Upper Cretaceous, SE Brazil)

Giorgio Basilici[a,b,*], Paolo Lorenzoni[c], Áquila Ferreira Mesquita[a], Juraj Janocko[d], Luca Colombera[e], Grace I.E. Cosgrove[f], Nigel Philip Mountney[f], Carlos Roberto Souza Filho[a], Alexandre Ribeiro Cardoso[a], Agustín Guillermo Martinelli[g], Lucas Ernesto Fiorelli[b], Richard Guillermo Vasconez Garcia[a], Thiago da Silva Marinho[h,i], André Marconato[l]

[a]Departamento de Geologia e Recursos Naturais, Instituto de Geociências, Universidade Estadual de Campinas, 13083-870, Campinas, SP, Brazil.

[b]Centro Regional de Investigaciones Científicas y Transferencia Tecnologica de La Rioja (Prov. de La Rioja-UNLaR-SEGEMAR-UNCa-CONICET), Anillaco, Entre Ríos y Mendoza sn, CP 5301, La Rioja, Argentina

[c]Professional consultant, Largo Trasimeno 1, 02100, Rieti, Italy.

[d]Institute of Geosciences, Faculty BERG, Technical University of Kosice, Letna 9, 040 11 Košice, Slovakia

[e]Dipartimento di Scienze della Terra e dell'Ambiente, Università di Pavia, Via Ferrata 1, 27100, Pavia, Italy

[f]School of Earth and Environment, Institute of Applied Geoscience, University of Leeds, Woodhouse, Leeds, LS2 9JT

[g]CONICET - Sección Palaeontología de Vertebrados, Museo Argentino de Ciencias Naturales "Bernardino Rivadavia", Av. Ángel Gallardo 470, CP1405, Buenos Aires, Argentina.

[h]Instituto de Ciências Exatas, Naturais e Educação (ICENE), UFTM, Av. Randolfo Borges Jr. 1700, Univerde cidade, 38064-200, Uberaba, MG, Brazil.

[i]Centro de Pesquisas Paleontológicas L. I. Price, Complexo Cultural e Científico Peirópolis, Pró-Reitoria de Extensão Universitária, Universidade Federal do Triangulo Mineiro, Uberaba, Minas Gerais, Brazil.

[l]Institute of Geosciences, University of São Paulo, Rua do Lago, 562, Cidade Universitária, São Paulo - SP, 05580-080.

Correspondent author: *e-mail: giorgio@unicamp.br

ABSTRACT

Palaeosols are common in sedimentary successions of continental origin, notably they comprise the majority of the thickness of some accumulated successions of fluvial origin. Yet, detailed investigation of palaeosols and evaluation of their palaeoenvironmental significance is not routinely undertaken in detail in many sedimentological studies. A careful analysis of palaeosols may, however, reveal that sedimentary units, which appear similar if based solely on the facies analysis, indeed show strongly distinct palaeoenvironmental and depositional characteristics.

This is the case of the upper portion of the Bauru Group, a 100-190 m-thick Maastrichtian red sandstone unit of fluvial origin, present over an area of c. 180,000 km^2 in south-eastern Brazil. In this study, the palaeosols of this unit, which constitute 25-92% of the succession by thickness, are used to decipher palaeoenvironmental climate conditions, sediment source areas, and relationships between pedogenic and depositional processes. Through the combined study of macroscopic, micromorphological, and geochemical aspects of the palaeosols and of facies analysis of the deposits, the upper portion of the Bauru Group succession is separated into three sectors: north-western, north-eastern, and south-eastern. Although these three areas are all characterised by similar lithology types and lithofacies, indicative of deposition in alluvial systems, the palaeosol analysis highlights that they were each characterised by different climate, different clastic source areas and different dynamics and

interaction of the pedogenic and sedimentary processes. This research reveals the critical significance of the palaeosols for discriminating otherwise apparently similar depositional units.

Keywords: palaeoclimatology; cycles of palaeosols and deposits; distributive fluvial systems; palaeosols geochemistry

1. INTRODUCTION

Although palaeosols are widely recognised as a valuable element in the palaeoenvironmental reconstruction of ancient continental sedimentary successions (Driese and Nordt, 2013; Basilici et al., 2022), few prior studies have demonstrated how the systematic analysis of palaeosols can be applied to (i) better inform and characterise the sedimentary architecture of depositional systems, and (ii) support studies of the sequence stratigraphic evolution of continental sedimentary basin fills (Bown and Kraus, 1981, 1987; Kraus and Aslan, 1993; Wright and Marriott, 1993; McCarthy and Plint, 1998; Kraus, 1999). From an applied standpoint, palaeosols are not routinely used to predict the geometry and distribution of subsurface sedimentary bodies in the exploration for natural resources. Yet, palaeosols are extremely common in continental sedimentary successions and act as proxies that are especially sensitive to palaeoenvironmental conditions and variations thereof; in many cases more so than primary sedimentary facies (Retallack, 2001; Tabor et al., 2017; Beverly et al., 2018; Basilici et al., 2022). Due to the specialised methodological field- and laboratory-based approaches required to study palaeosols in detail, their potential value as indicators of palaeoenvironmental conditions are overlooked by many sedimentologists and stratigraphers.

Since the publication of pioneering articles in the 1980s and 1990s (e.g., Bown and Kraus, 1981, 1987, 1993; Marriott and Wright, 1993; Wright and Marriot, 1993), only a modest number of more recent published studies have focussed on the stratigraphic aspects of palaeosols. Some of these cases are briefly commented on hereafter. In their analysis of the Cenomanian Dunvegan Formation McCarthy and Plint (2013) documented how palaeosols vary in type along a sequence boundary as a function of

changes in depositional landscape. Benvenuti et al. (2021) demonstrated that the classical model of well-developed and well-drained palaeosols at the transition from lowstand to transgressive systems tracts (*sensu* Wright and Marriot, 1993) is not necessarily applicable when sea-level variations are characterised by rapid fall and rise. Dzombak et al. (2021) drew attention to small-scale lateral variations in palaeosols; this aspect, which in pedology is known as a toposequence or catena, demonstrates that a palaeosol cannot be considered a unique geological body within a sedimentary basin.

Ancient continental sedimentary successions of great lateral extent, and characterised by apparently relatively homogeneous lithology and similar facies units, can result in routine sedimentological and palaeoenvironmental interpretations that propose largely unchanging palaeoenvironmental systems. However, when these continental sedimentary successions are typified by alternations of deposits and palaeosols (a very common circumstance; Basilici et al., 2022), the combined study of palaeosols and their host deposits can reveal marked differences within the same sedimentary succession in different portions of the basin. This is the case of the upper portion of the Bauru Group, an Upper Cretaceous sandstone unit of the Bauru Basin, located in SE Brazil. Although early studies of this sedimentary succession - which is exposed over an area of ca. 70,000 km^2 - convincingly argued that it may be classed as a single depositional system, more recent studies have highlighted several differences in the succession between distinct geographic areas (Basilici et al., 2009; Basilici and Dal Bó, 2010; Batezelli and Ladeira, 2016; Batezelli et al., 2019; Soares et al., 2020a), thereby suggesting a more complex depositional and palaeoenvironmental context than has previously been recognised. Given this, new data have been acquired to integrate our own dataset with existing literature-derived data, the purpose being to identify and describe putative palaeoenvironmental and depositional differences in this sedimentary succession (cf. Soares *et al.*, 1980). Our analysis is based on the macroscopic, microscopic, and geochemical characterisation of the palaeosols and their hosting deposits, and their mutual vertical and horizontal relationships.

The aim of this paper is to show how the integrated study of related palaeosols and deposits constitutes a powerful method to reveal stratigraphic and palaeoenvironmental aspects of continental sedimentary successions. Specific research objectives are to demonstrate the following: (i) that in the same sedimentary basin, the controlling factors that induce alternation of palaeosols and deposits can vary spatially; and (ii) that palaeosols are an effective tool for detecting subtle spatial depositional variations in the same sedimentary basin.

2. STUDY AREA AND STRATIGRAPHIC CONTEXT OF THE BAURU GROUP

The Bauru Group is an Upper Cretaceous lithostratigraphic unit, c. 300 m thick, in SE Brazil (Goias, Mato Grosso do Sul, São Paulo, and Paraná states) (Fig. 1). This unit overlies the Serra Geral Formation, which is a thick and extensive basaltic effusive unit generated during the rifting of southern Gondwana (cf. Cañón-Tapia, 2018). The lower portion of the Bauru Group consists of the Araçatuba, Adamantina, and Uberaba formations, and the upper portion of the Marília Formation (Serviço Geológico do Brasil - CPRM, 2004a; 2004b; 2004c; Batezelli et al., 2019; Soares et al., 2018) (Fig. 1D). This last unit was previously subdivided into three members: Echaporã, Serra da Galga, and Ponte Alta. However, based on a new approach to the organisation of sedimentary architecture, Soares et al. (2020b) proposed a new formation for the NE area of the Marília Formation, called Serra da Galga Formation. Yet, since the depositional architectural lateral relationships and limits of these various units are still unclear, in this paper the term "upper portion of the Bauru Group" is simply used to indicate the study succession. The upper portion of the Bauru Group is 100-190 m thick, and is constituted of red (10R 5/8), moderately to well-sorted sandstone, occasionally interlayered with sandy orthoconglomerate and rarer thin beds of mudstone. Most of the deposits are generated by fluvial activity and only a small part is deposited by wind (Basilici et al. 2009; 2016). The palaeosols constitute 25 to 92% of the thickness of the measured succession (Basilici et al., 2009; Basilici et al., 2016; Batezelli et al., 2019). This paper reports on the study of three exposed areas of the upper portion of the Bauru Group: north-

western, north-eastern and south-eastern sectors (Fig. 1). The north-western sector is located to the west of the Paraiba River in Goias and Mato Grosso do Sul states. The studied area is delimited by the cities of Cassilândia, Itajá, Itarumã, and Quirinópolis (Fig. 1A), and is present over an area of c. 20,000 km^2. The north-eastern sector extends between the localities of Peirópolis, Uberaba, Prata, Campina verde, Gurinhatã, and Uberlândia for an area of c. 9,000 km^2 (Fig. 1B). The south-eastern sector includes the municipalities of Echaporã, Marília, Garça and Lins over an area of c. 3,000 km^2 (Fig. 1C). Palaeontological studies of vertebrate remains of Sauropoda (Santucci and Bertini, 2001; Martinelli et al. 2011; Martinelli and Teixeira, 2015; Martinelli et al., 2018), fishes (Candeiro et al., 2024), ostracods and charophytes (Gobbo-Rodrigues et al., 1999a, 1999b; Dias-Brito et al., 2001) and palynological remains (Arai and Diaz-Brito, 2023) demonstrate that all three mentioned sectors of the upper portion of the Bauru Group are Maastrichtian age. Batezelli and Ladeira (2016) and Batezelli et al. (2019) consider the deposits in all three sectors to represent by the same lithostratigraphic unit attributing them to a single depositional system. Biostratigraphic and lithostratigraphic data are considered to be sufficiently reliable to ascribe the upper portion of the Bauru Group as coeval in the three sectors.

3. METHODS

Different methods of data collation were employed in the study of sediments and palaeosols of the studied succession. Six sections were measured and described at centimetre-scale resolution in the north-western sector, 11 in the north-eastern sector and 18 in south-eastern sector. The thickness of each of the measured sections varies from 1.8 to 24 m (overall c. 200 m of measured sections). In the field, the sediments were described in terms of lithology, grain size (sedimentary textures), types and distribution of sedimentary structures, and bounding surfaces. The sedimentary units were organised into architectural elements. In the laboratory, 24 sediment hand-specimen samples were prepared as polished slabs to highlight sedimentary structures. Analyses of the clast composition of the conglomerates were realised by classifying all the clasts with an axis length greater than 20 mm over a

defined area of 1 m^2. Two sets of counting were performed for each conglomerate bed. In total nine beds were analysed. Detailed petrographic analyses were performed. Counting was done on 49 thin sections of palaeosols and deposits; at least 300 points were counted in each thin section. The grain surface textures of 25 medium- and coarse-grained sand clasts were described using scanning electron microscope (SEM—mod. LEO 430) in secondary electron imaging mode. In the field, palaeosols have been distinguished into horizons by recording colours (Munsel Color, 2013), structures, boundaries (distinctness and topography), grain size, biological remains, redoximorphic features, slickensides. The macroscopic descriptions and applied nomenclatures were made following Schoeneberger et al. (2012) and Vepraskas (2015). One or more palaeosol samples were collected for each horizon. They have been used for micromorphological and geochemical characterisation, and scanning electron microscope imaging. Seventy-five thin sections were made for micromorphological analyses from samples impregnated with epoxy resin and methylene blue stain. Description and interpretation of the thin sections followed the methods detailed in the manuals of Bullock et al. (1985), Stoops (2003), and Stoops et al. (2010). Geochemical analyses of c. 90 samples consisted of the determination of major and minor oxides and trace elements by an X-ray fluorescence spectrometer (Philips PW2404). Thirty-five samples were examined using a scanning electron microscope via secondary electron imaging to describe micromorphological features. Weathering molar ratios of major, minor and trace elements were used to obtain information of provenance of the parent material and apply palaeoclimate empirical equations, based on CIA-K (Chemical Index of Alteration less K) (Maynard, 1992; Fedo et al., 1995), ΣBases/Al (Sheldon et al., 2002) and CALMAG (Nordt and Driese, 2010). Principal Component Analysis and box-and-whisker plots were employed to discriminate the distribution of the major and minor geochemical elements in the three study sectors and to define palaeoenvironmental and palaeodepositional aspects of the parent material of the palaeosols (cf., Retallack, 1994a; Sheldon et al., 2002; Kraus and Riggins, 2007; Sheldon and Tabor, 2009; Nordt and Driese, 2010). Palaeosols are

described as pedotypes (cf., Retallack, 1994b). The designations of the horizons and the classification of the palaeosols into orders or suborders were based on the criteria by Soil Survey Staff (1999, 2014).

4. SEDIMENTOLOGICAL AND PALAEOPEDOLOGICAL CHARACTERISTICS OF UPPER PORTION OF THE BAURU BASIN

The sedimentological and palaeopedological characteristics of the three sectors of the upper portion of the Bauru Group are described and interpreted next.

4.1. North-western sector

In north-western sector, the upper part of the Bauru Group consists of sandstone and less commonly of sandy orthoconglomerate; its overall thickness is c.190 m (Serviço Geológico do Brasil - CPRM, 2004a).

4.1.1 Deposits

The deposits are organised in two architectural elements: (i) planar-parallel, horizontal or low-angle, laminated sandstone beds and (ii) sandstone and conglomerate sheet bodies.

4.1.1.1 Planar-parallel, horizontal or low-angle, laminated sandstone beds

Description. This architectural element consists of sets of well-sorted laminated sandstone, 0.2-0.6 m thick, 2.5 to 40 m in lateral extent, organised in stratal packages up to 6 m thick and separated by planar erosional surfaces. The laminations are planar, horizontal or low-angle (up to 10 degrees), 1.5 to 18 mm thick, and constituted of very fine- and fine-grained sandstone, grading upwards to medium-coarse-grained sand clasts (Fig. 2A, B). Alignment of very fine-grained black heavy-mineral sand clasts at the bottom of the laminations is very common (Fig. 2B). Sand clasts are mainly of quartz and volcanic lithic fragments (Fig. S1A), typically rounded or subrounded; distinctive microtextures occur as low relief, bulbous edges, elongated depressions and upturned plates; these are common on the surface of the medium- or coarse grained quartz clasts (Fig. 2C).

197 *Interpretation*. The shape and planar erosional surfaces of the sets, the geometry and inverse
198 gradation of the laminations, and the textural and microtextural characteristics of the sand grains allow
199 the deposits of this architectural element to be interpreted as climbing wind-ripple strata (Hunter, 1977;
200 Kocurek and Dott, 1981; Mountney, 2006). Upturned plates, elongated depressions and bulbous edges
201 are microtextures typical of wind transported clasts (Vos et al., 2014). Migrating and climbing wind
202 ripples commonly deposit inversely graded laminae often with a thin lamination of very fine-grained
203 sand, named pin stripe lamination (Freyberg and Schenk, 1988). Various depositional aeolian events
204 generate sets of horizontal or low-angle laminations with planar erosional bases (Mountney, 2006).
205 Basilici et al. (2009) and Basilici and Dal Bó (2010) interpreted this architectural element to have been
206 formed by the deposition of nabkha dunes, 0.3 to 2 m high (cf. Basilici and Dal Bó, 2014), and deposited
207 in a sand sheet across a dry flood plain area.
208 4.1.1.2 Sandstone and conglomerate sheet bodies
209 "Sandstone and conglomerate sheet bodies" (*sensu* Friend et al., 1979) are typically 3.5 m thick,
210 more than 3 km long, in direction parallel to reconstructed palaeocurrents, and up to 500 m wide,
211 perpendicular to the palaeocurrents. Basal bounding surfaces are concave up, with scour up to 0.9 m;
212 uppermost bounding surfaces are planar and horizontal.
213 "Sandstone sheet bodies" consist of vertically alternating unorganised bed of structureless poorly
214 sorted medium-grained litharenites (Fig. S1B), that are 0.15 to 1 m thick and up to 200 m in lateral
215 extent, and sandy conglomerates that are 0.1 to 0.2 m thick and up to 30 m in lateral extent (Figs. 3A,
216 B; S2A, B). Additionally, lenses of intraformational matrix-supported sandy conglomerates are present in
217 some instances. The intraclasts present in these lenses comprise palaeopedogenised and cemented
218 sandstone or muddy sandstone (Fig. S2C). These lenses have concave and erosional basal surfaces,
219 flat top surfaces, a thickness up to 0.7 m and a lateral extent of c. 4 m (Fig. 3A, B).
220 "Conglomerate sheet bodies" consist of three of four beds, each 0.6 to 0.95 m thick, 50 to 100 m in
221 lateral extent, showing an erosive basal bounding surface, and composed internally of clast-supported

conglomerate that is weakly normally graded from cobbles to small pebbles. In places, conglomerate beds are overlain fine to medium-grained sandstone beds, up to 0.15 m thick and of variable lateral extent (Fig. 3C-E). The conglomerate beds have a poorly sorted medium- to coarse-grained sandstone matrix; few imbricate clasts are present and no open-work structures are visible. Ventifact pebbles and cobbles are common (Fig. S2D). The sandstone beds at the top of the conglomerate show thin planar parallel laminations, characterised by weak, ungraded grain-size variations with local thin alignments of granules or small pebbles (Fig. 3E).

Clast composition of the pebble and cobble clasts of two channelised sheet bodies (excluding the intraformational clasts) is displayed in figure S1B. The sandstones consist of volcanic lithic fragments and quartz clasts (Fig. S1C). Reconstructed palaeocurrent directions of the depositional flows measured from imbricated clasts in the "Sandstone and conglomerate sheet bodies" indicate flows towards S and SSW (Figs. S3A, B).

Interpretation. The erosive concave bases and the flat tops of "sandstone and conglomerate sheet bodies", and the architectural association with aeolian deposits and palaeosols (see below) allow these deposits to be interpreted as the product of subaqueous flows in confined river channels (Miall, 1988; Holbrook, 2001; Miall, 2006).

In the "sandstone sheet bodies" the absence of well-define sedimentary structures (such as cross stratification) shows that the depositional flows were characterised by high sediment concentration, inhibited turbulence and reduced settling velocity (Middleton and Southard, 1984); deposition was dominantly from hyperconcentrated flows (Martin and Turner, 1998). More concentrated flow, attributable to hyperconcentrated density flows (cf. Mulder and Alexander, 2001) or non-cohesive debris flows, may have been the origin of the lenses of intraformational matrix-supported sandy conglomerates.

The erosive bottom, rough normal grading, absence of internal erosional surfaces and sand cover shows that the single beds of the "conglomerate sheet bodies" constitute individual and distinct

depositional units. Additionally, the absence of open-work structures, high amount of sandy matrix and rare occurrence of imbricated flattened clasts demonstrates hydraulic flows that possessed a high concentration of transported sediment and that underwent rapid waning (Basilici et al., 2009; Hassan, 2005). The characteristics of these conglomerate beds matches with the description of sheets of massive conglomerate of Ramos and Sopeña (1983) and unit-bar of Hassan (2005), associated by these authors to longitudinal bars. Furthermore, Hassan (2005) highlighted that rare imbrications, a high amount of sandy matrix and an absence of armoured surfaces are aspects typical of ephemeral rivers in arid environment.

4.1.2. Palaeosols

Aridisols, Entisols, Vertisols and Alfisols are the palaeosols recognised in this sector (Basilici and Dal Bó, 2010). The most common pedotypes are described below: Itajá pedotype (Aridisol) and Avá pedotype (Entisol). Their parent material is fine to medium-grained, moderately to poorly-sorted sandstones, defined as sublitharenite (Fig. S1D).

4.1.2.1 Itajá pedotype (Aridisol)

Description. The Itajá pedotype (Dal Bó et al., 2010) is, on average, 1.5 m thick and consists of the following horizons: A-Bt (Btk) - Bk (Bkm) - C (Fig. 4A). The top and bottom distinctness are very abrupt and the topography smooth. The distinctness between the horizons is gradual or diffuse and the topography is smooth. Where present, the A horizon is light red (10R 6/8), massive, <0.1 m thick. However, it is commonly is absent. Sand-filled, vertical cylindrical structures, tapering downwards and laterally branching, up to 0.4 m long, and 30-50 mm wide, are common. The B horizon is red (10R 4/8), 0.9 m thick on average, and consists of Bt or Btk and Bk or Bkm subdivisions. The Bt and Btk horizons have strongly developed medium to fine angular blocky or very coarse prismatic peds, which can be subdivided into smaller angular blocky peds (Fig. 4B). In thin section, the c/f (coarse-fine) related distribution pattern is chitonic, the b-fabric is granostriated and the main pedofeature is a clay-oxide coating on sandy grains (Fig. 4C). The clay content consists of palygorskite, smectite, and sepiolite

(Basilici et al., 2009; Dal Bó et al., 2010). The Bk horizon shows typic micritic calcite nodules, with distinct outer boundaries, and a diameter between 5-50 mm; they are isolated or coalescent, and have an areal distribution between 20-40% (Fig. 4D). In thin section, c/f related distribution pattern is chitonic or closed porphyric; there are crystalline pedofeatures, and calcite coatings of sandy grains (Fig. 4E). The Bkm horizon consists of brecciated calcium carbonate concentration (Fig. 4F); it is up to 0.6 m thick and discontinuously extended up to 30 m (Fig. 4G). The C horizon is red (10R 5/8), has an average thickness of 0.3 m, is massive, and shows residual planar parallel laminations.

Interpretation. The weak colour of the A horizon and the lack of any other pedogenic characteristic allow it to be attributed to ochric epipedon (Soil Survey Staff, 1999). Sand-filled, vertical cylindrical structures are attributable to root casts (Klappa, 1980). Illuviated clay coating in the Bt horizon and concentration of calcium carbonate in Bk and Bkm horizons, define argillic and calcic subhorizons, respectively (Soil Survey Staff, 1999). These aspects, in addition to well-developed pedogenic structure, are characteristics that enable the Itajá pedotype to be interpreted as Aridisol (Nettleton and Peterson, 1983; Soil Survey Staff, 1999; 2014). The concentration of calcium carbonate in the B horizon is indicative of soil with hydric deficit, typical of arid or semiarid climate. However, clay coatings of sand-sized grains – which typify the Bt and Btk horizons, and are due to the clay illuviation – testify to the existence of temporary (seasonal) or longer wetter periods (Watson, 1992). Well-developed pedogenic structures (prismatic and angular blocky peds) are related to soils with a long formation time, which is also indicated by the morphology of the calcium carbonate concentration in the Bk horizon. This relates to stages II and III, and in Bkm horizon relates to the stage IV of Gile et al. (1966), Machette (1985) and Monger et al. (1991). The stages III and IV indicate development times longer than 10^4-10^5 yr (Machette, 1985; Zamanian et al., 2016). Palygorskite and sepiolite are common in arid environments and in Aridisols (Yaalon and Wieder, 1976; Watts, 1980; Singer, 1984).

4.1.2.2 Avá pedotype (Entisol)

296 *Description.* This pedotype is red (10R 5/8 or 2.5YR 5/8), 0.4 m thick and consists of A and C
297 horizons (Fig. 5A, B). Sand-filled, vertical tubular forms, 3-10 mm wide and 0.3 m long, and small
298 calcareous nodules are relatively common. The top and the bottom surfaces of this pedotype show very
299 abrupt distinctness and smooth topography; the A and C horizon transition has clear or gradual
300 distinctness and smooth topography. The A horizon is massive and 0.1 m thick; the C horizon, 0.3 m
301 thick, shows residual planar laminations (Fig. 5A, B).
302 *Interpretation.* The absence of the B horizon and peds, and the presence of relics of sedimentary
303 features define the Avá pedotype as an Entisol (Soil Survey Staff, 1999; Grossman, 1983; Soil Survey
304 Staff, 2014). Entisols form under poor development conditions, mostly in relation to short development
305 time (a few 10^2 yr), although particular climate conditions (e.g., hydric deficit) or particular types of
306 parent material can be also important. The concentration of calcite nodules indicates that this palaeosol
307 developed in semiarid or arid climate environments (Buol et al., 2011).
308 4.1.3 Distribution and relationships between palaeosols and deposits
309 "Planar-parallel, horizontal or low-angle, laminated sandstone beds", "sandstone sheet bodies" and
310 "conglomerate sheet bodies" constitutes 28%, 4% and 3% of the thickness of the succession,
311 respectively. Itajá (Aridisol) and Avá pedotype (Entisol) form 38 and 16% in thickness of the entire
312 succession, respectively. Vertisols and Alfisols constitute 6 and 5 % of the succession (Table S1).
313 The Itajá (Aridisol) and Avá pedotypes (Entisol) commonly alternate with "planar-parallel, horizontal
314 or low-angle, laminated sandstone beds" (Fig. 6A). The upper transition of the palaeosol profile to the
315 deposits is always erosional, commonly planar and horizontal, but in places it is characterised by an
316 undulose surface (Fig. S4A-C); the lower transition to the deposits is always gradual. The macro- and
317 microtextural characteristics of the parent material of the palaeosols reveal that they formed on deposits
318 of "planar-parallel, horizontal or low-angle, laminated sandstone beds".
319
320 ***4.2. North-eastern sector***

The north-eastern sector of the upper portion of the Bauru Group (Fig. 1B) is 70 m thick and consists of dominant sandstones, with few conglomerate beds and rare sandy mudstones. Batezelli et al. (2019) and Soares at al. (2020a) interpreted it as a sedimentary succession representing a distributive fluvial system, which from east to west and/or northwest transitioned from proximal to distal areas. The proximal area is located to east of Uberaba; the medial area is approximately between Uberaba and Prata; and the distal area corresponds to the portion comprises between the towns of Gurinhatã and Uberlândia (Fig. 1B) (Batezelli et al., 2019, their Fig, 18C; Soares et al., 2022a, their Fig. 1). Herein, the architectural elements (deposits and palaeosols) of these three areas are described, highlighting their differences and relative distribution.

4.2.1 Deposits

4.2.1.1 Sheet sandstone bodies

Description. "Sheet sandstone bodies" are constituted of medium- to coarse-grained sandstones, which consist of litharenites: dominantly quartz clasts with subordinate fragments of metamorphic rocks (Fig. S1E). Aligned small pebbles (mainly of metamorphic rocks) occur at the bottom of the sandstones sets of the bodies (Fig. S1F). The bodies are up to 2.5 m thick and more than 100 m in lateral extent in orientations perpendicular to reconstructed palaeocurrent. The bottom is erosive and slightly concave up, the top is flat. In places, muddy sandstone beds or palaeopedogenised muddy sandstone separate these sandstone bodies (Figs. 7A-D and 8A, C). Two alternating types of "sheet sandstone bodies" have been distinguished: (i) "sheet sandstone bodies" with sets of tabular or trough cross-stratification and (ii) "sheet sandstone bodies" with large lenticular sets of trough cross-stratification (Fig. 7A-D). The first type (Fig. 7A-D, cf. "sheet sandstone bodies" n. 1 and 2) presents a sequence of tabular or trough cross-stratification with angular foreset terminations at the set bases, and an upwards decrease in set thickness (from 0.1 to 0.5 m thick) and grain size (from medium-coarse- to fine-medium-grained sandstone). The second type of "sheet sandstone bodies" (Fig. 7A-D, cf. "sheet sandstone body" n. 3) is made of coarse- and medium-grained sandstone organised in large lenticular sets (0.8-1.4 m thick

346 and 10-15 m wide) of trough cross-stratification with low-angle foresets with tangential toes. This second
347 type does not exhibit upward vertical variation in the size of the sets or in grain size. "Sheet sandstone
348 bodies" exposed in medial areas are similar to those described above, but exhibit fine- to medium-
349 grained sandstone and have greater width/thickness ratio (Soares et al., 2020a; their Fig. 4) (Fig. S4D,
350 E).

351 Indicators of palaeocurrent (mainly foreset azimuths of cross strata), reveal palaeoflows towards NW
352 (Fig. S3 C, D). Batezelli et al. (2019; their Fig. 18D) report a large number of palaeocurrent data for this
353 area generally showing westward-directed flows.

354 *Interpretation.* The lower bounding surfaces of the sheet sandstone bodies and the nature of their
355 internal deposits demonstrate the presence of channelised fluvial deposits (Miall, 1988; Holbrook, 2001;
356 Miall, 2006). The tabular and trough cross-stratified sets of the first type of channel deposits represent
357 the product of migration of small transverse bars with sinuous crests in a small braided river,
358 characterised by permanent and relatively steady stream flow (cf. Bridge, 2003; Miall, 2006). The
359 upward decrease in size and grain size of the sets of cross-strata could be linked to the upward growth
360 of the bar and the associated decrease of current velocity in shallower waters (Haszeldine, 1983; Miall,
361 2006; Scherer et al., 2015; Soares et al., 2018; Martinelli et al., 2019). The second type of channel
362 deposit shows characteristics suggestive of different formative hydrodynamic conditions. Analogous
363 lenticular sets of through cross-stratifications were described by Røe (1987) and interpreted as dunes
364 formed below high-velocity currents at the transition from lower-stage dune to upper-stage plane-bed
365 fields. These structures and the absence of grading and of sedimentary structures more typical of lower
366 flow regime indicate the highly energetic and variable character of the river currents, typical of rivers
367 with high discharge fluctuations, as is common in dryland environments characterised by strong
368 seasonal rainfalls (Fielding et al., 1999; Fielding, 2006). In both types of channel deposits, there is no
369 evidence of interruption of the water flows, such as mud drapes, oscillatory ripples, mud cracks, or
370 incipient palaeopedogenesis; therefore, they can both be interpreted as the products of perennial rivers.

371 Yet, the different style of filling allows recognition of paroxysmal water discharge characteristics in the
372 second type of channel (Soares et al., 2018; Martinelli et al., 2019). Sheet sandstone bodies exposed in
373 medial area of the distributive fluvial systems suggest relatively wider and shallow braided channels
374 (Nichols and Fisher, 2007; Soares et al., 2020a).

375 4.2.1.2 Muddy sandstone beds

376 *Description*. "Muddy sandstone beds" are interlayered with "sheet sandstone bodies" in proximal and
377 medial areas (Fig. 7A) and consist of fining-upward sequences of climbing-ripple cross-laminated, very
378 fine-grained sandstone and laminated mudstone beds with thickness 0.2-0.8 m and lateral continuity up
379 to 6 m (Soares et al., 2018; their Fig. 8).

380 *Interpretation*. Sandy mudstone thin beds represent floodplain deposits formed by episodic and low
381 energetic flows (Soares et al., 2020a).

382 4.2.1.3 Tabular bed of sandstone grading to mudstone

383 *Description*. This architectural element is constituted of 0.2-2 m beds that are $\geq$ 100 m wide; they
384 consist of fine-grained sandstone, characterised of mud clast alignments, planar laminations, current
385 ripples, and upward grading to mudstone. This element is typical of the distal area (Fig. 8E).

386 *Interpretation*. "Tabular bed of sandstone grading to mudstone" constitute low-energy water flood
387 deposits of terminal splay (Nichols and Fisher, 2007; Coronel et al., 2020) and/or of interchannel areas
388 (Batezelli et al., 2019).

389 4.2.1.4 Ribbon sandstone bodies

390 *Description*. "Ribbon sandstone bodies" find in distal area; they are 0.7-1.5 m thick, 6-10 m wide and
391 slightly asymmetric in palaeocurrent direction. The bottom is concave-up and erosional, the top flat or
392 slightly convex-up. These bodies have single-storey, medium- to fine-grained sandstone filling, showing
393 trough cross stratification or more commonly they are structureless (Fig. 7E).

394 *Interpretation*. Ribbon sandstone bodies are attributed to stable river channel (Friend et al., 1979;
395 Gibling, 2006) and their limited asymmetry indicated a low sinuosity of the river course (Jobe et al.,

2010). The common absence of sedimentary structures and the low sediment sorting can be linked to high flow concentration and rapid deposition (Cain and Mountney, 2009).

4.2.2 Palaeosols

The north-eastern sector of the upper portion of the Bauru Group contains Entisols, Inceptisols, Vertisols and Aridisols.

4.2.2.1 Krenak pedotype (Entisol)

Description. Krenak pedotype is constituted of light red (2.5YR 6/8), fine-grained sandstone in proximal and medial area and sandy mudstone in distal area of the fluvial system. In the distal area close to Uberlândia, some profiles are light olive (10Y 5/4) or greyish green (5GY 5/2) (cf. Soares et al., 2020a; their Fig. 9). The palaeosol profile is 0.2-0.5 n thick and consists of A-C horizons (Fig. 7A and 8A, C, E, H); top distinctness and topography, transitioning to deposits, are abrupt and smooth, respectively (cf. Martinelli et al., 2019); the bottom distinctness and topography are diffuse and smooth, respectively. The A horizon is massive and shows common tubules, filled of sandstone, or mudstone, 0.15 m long and 10-20 mm wide, tapering downward. The C horizon may be characterised by relics of cross- or planar laminations. Calcareous nodules are common in both the horizons, though less than in NE distal area (Fig. 8H).

Interpretation. As discussed previously, the absence of the B horizon and defined pedogenic features in palaeosol profiles is typical of Entisols, i.e., soils with a low degree of development. The light red colour and calcareous nodules testify drained and oxidising conditions for most of these palaeosol, but in the NW distal area, near Uberlândia (Fig. 1B), the pedotype shows greyish colour, accordingly evidence of poorly drained environmental conditions.

4.2.2.2 Pataxó pedotype (Inceptisol)

Soares et al. (2020a) distinguished two types of pedotypes. The first is red (10R 5/8) and characterised by the followings horizons (A)-Bw-(Bwk)-Bk-C-(Ck) (Fig. 8A, C, E). The profile thickness is 0.4-1 m and consists of fine-grained sandstone, mainly constituted of quartz clasts and fragments of

metamorphic rocks (Fig. S1G). The A horizon shows sand cemented by calcite, downward branching tubes, attributable to rhizotubules (Kraus and Hasiotis, 2006) or sand-filled cylindrical tubes with greenish-grey halos, attributable to rhizohaloes (Kraus and Hasiotis, 2006) (Fig. 7F). In thin section, c/f related distribution is monic and the microstructure is simple packing voids. Bw horizon does not show clear pedogenic structures; locally only clay coatings are present (Fig. 7G); c/f related distribution is monic-chitonic. Bk or Bwk are characterised by isolated calcareous nodules, 5 mm in diameter. In thin section, b-fabric is crystallitic and c/f related distribution is porphyric (Fig. 7H) (Soares et al., 2020a; their Fig. 8J, K and L). The C horizon is massive.

The second type is constituted of greyish green (5GY 5/2) muddy sandstone and shows Ag-Bwg-Cg horizons. The profile is 0.6 m thick and it is distributed prevalently in the NW distal area near Uberlândia (Fig. 8H). The Ag horizon is characterised of abundant rhizohaloes (Kraus and Hasiotis, 2006). In thin section, c/f related distribution is single-porphyric. The Bwg horizon does not show macroscopic structures. In thin section, this consists of subangular blocky microstructure, single-porphyric c/f related distribution and impregnative redox pedofeatures of Fe-Mn oxides (Soares et al., 2020a; their Fig. 9G and H).

Interpretation. The presence of a Bw horizon without evident macroscopic pedogenic features identifies this as a cambic horizon, which characterises the Inceptisols. The differences between the first and second type of the Pataxó pedotype are due to different drainage conditions of the soil. The first type developed in drained and dry conditions; the second type developed in temporarily water-logged conditions, where Fe and Mn were depleted and concentrated in redoximorphic impregnative concentration (Lindbo et al., 2010).

4.2.2.3 Aranã pedotype (Vertisol)

Description. This pedotype is present only in the medial area (Fig. 8C). It is light red (7.5R 6/8) or red (7.5R 5/8) and is constituted of a sandy mudstone parent material. The profile has a thickness up to 1 m and consists of Ass-Bssk-(Bssg). The top distinctness of the Ass horizon is abrupt and the topography

446 is wavy. The Bssk horizon is characterised by slickensides surfaces, which separate wedge-shape
447 structures, and accumulation of isolated calcareous nodules. Locally, the Bssg horizon is present; it
448 displays redoximorphic impregnative features (Soares et al., 2020a; their Fig. 12I and J). In thin section,
449 c/f related distribution is typically porphyric and b-fabric is cross-striated (Soares et al., 2020a; their Fig.
450 12F).

451 *Interpretation*. The muddy parent material, abundant slickensides, wedge-shape structures, wavy top
452 of the profile (which can be identified as gilgai micromorphology), and, in this section, porphyric c/f
453 related distribution allow this pedotype to be interpreted as Vertisol, i.e. a soil subjected to frequent
454 swelling and shrinking as consequence of the clay parent material and the periodic variations in
455 humidity (Soil Survey Staff, 1999, 2014; Ahmad, 1983; van Breemen and Buurman, 2002). Calcareous
456 nodules indicate a usually drained condition, whereas the presence of redoximorphic features indicates
457 temporarily water-logged conditions.

458 4.2.2.4 Mukuriñ pedotype (Aridisol)

459 *Description*. Batezelli et al. (2019) described Aridisols in medial area of the fluvial system (Fig. 8C).
460 This pedotype is red (10R 4/8), consists of fine-grained sandstone and it is constituted of Bk-Ck
461 horizons. The Bk horizon shows well-developed blocky or prismatic structures and high concentration of
462 isolated calcareous nodules. In thin section, b-fabric is crystallitic.

463 *Interpretation*. As already discussed, according to the described macroscopic and
464 micromorphological characteristics this pedotype is interpreted as Aridisol; a well-developed soil formed
465 in hydric deficit environment (Batezelli et al., 2019).

466 4.2.3 Distribution and relationships of deposits and palaeosols

467 “Sheet sandstone bodies” are typical of the proximal and medial area of the fluvial system. “Sheet
468 sandstone bodies” constitute 57% of the thickness of the in proximal area, whereas in the medial area
469 they are 22% of the thickness. “Ribbon sandstone bodies” occur only in the distal area, where they
470 constitute 8% of the thickness. “Muddy sandstone beds” are interlayered with sheet sandstone bodies

and constitute 6% of the thickness of the sedimentary succession in proximal area and 13% in medial area. “Tabular beds of sandstone grading to mudstone” are typical of the distal portion of the fluvial system and here constitute 62% of the thickness of the sedimentary succession. The Krenak pedotype (Entisol) has a thickness distribution of 10%, 34% and 17% in the proximal, medial and distal area, respectively. Pataxó pedotype (Inceptisol) decreases in thickness from 27% to 14%, to 8% from proximal, to medial, to distal area, respectively. The Aranã pedotype (Vertisol) and Mukuriñ pedotype (Aridisol) occur only in the medial area, where they constitute 10 and 7% of the thickness of the measured successions, respectively. A summary of the distribution of the architectural elements is in Table S1.

In the proximal area, Krenak pedotype (Entisol) constitutes thin profiles that separate partially amalgamated channels represented by “Sheet sandstone bodies”. In the same area, Pataxó pedotype (Inceptisol) covers and underlies sequences of amalgamated channels (“Sheet sandstone bodies”) (Fig. 8A). In medial area, a vertical and horizontal organisation of palaeosols and deposits was observed (Soares et al., 2020a; their Fig. 14). Pataxó pedotype (Inceptisol) covers isolated and abandoned channels (“Sheet sandstone bodies”). Close to the channel belts, Krenak pedotype (Entisol) alternates to floodplain deposits (“Muddy sandstone beds”). Even further from the channel belt, Aranã pedotype (Vertisol) alternates to muddier floodplain deposits (“Muddy sandstone beds”). Mucuriñ pedotype (Aridisol) occasionally occur above channel deposits (“Sheet sandstone bodies”) (Fig. 8C). In distal area, Krenak pedotype (Entisol) is the most common palaeosols and it is typically alternated to unchannelised deposits (“Tabular beds of sandstone grading to mudstone”); by contrast, Pataxó pedotype (Inceptisol) cover the channel deposits of “ribbon sandstone bodies” (Fig. 8E). In NW distal area, Krenak pedotype (Entisol) and Pataxó pedotype (Inceptisol) show horizons with greenish-grey colour (Ag and/or Bwg) indicating poor-drained conditions associated to shallow groundwater.

4.3. South-eastern sector

In this sector, the upper portion of the Bauru Group is c. 150 m thick (cf. Basilici et al., 2016; their Fig. 14). The deposits constitute 8% of the entire thickness of the succession and the palaeosols 92%.

4.3.1. Deposits

The deposits show a single architectural element: tabular sandstone beds.

4.3.1.1 Tabular sandstone beds

Description. "Tabular sandstone beds" have a thickness of 0.9-3 m (Figs. 9A) and lateral extent is over 160 m without significant variations in thickness (Fig. 9A). The lower and upper boundaries are abrupt and flat; rarely small scours (0.1 m deep and 1 m wide) are observed at the bottom. Their lower portion (0.1-0.6 m) consists of thin tabular layers (40-90 mm thick) of alternating light red (2.5YR 7/6) coarse-grained sandstone and yellowish red (5YR 5/8) pebble- or cobble mud clasts (Fig. 9B); pebbles show *a*-axes aligned parallel to the bedding plane and sometimes *a*(p) *a*(i) clast imbrications. These alternating sandstone/pebble layers are overlain by medium and coarse-grained sandstones, up to 0.1 m thick, with apparent planar laminations (Fig. 10A). The remaining part of the bed (up to 90% of the thickness) consists of moderately sorted fine - and medium -grained sandstone, characterised by pedogenic features. Sometimes the tabular sandstone beds are overlain by thin (0.05-0.2 m thick) bright reddish brown (2.5YR5/6) clay mudstone, which are completely palaeopedogenised (Fig. 10A).

Interpretation. Due to palaeopedogenesis, most of the deposits have lost the original sedimentary structures. However, the shape and thickness of the beds, their lower and upper bounding surfaces, the general vertical grain-size distribution, and the sedimentary structures preserved at the base of the beds enable inferences to be made regarding the processes responsible for sediment transport and deposition. The significant lateral extent of these beds, the lack of relevant thickness variations and their flat bottom suggest that the sandstone beds were deposited from widespread unconfined alluvial flows (North and Davidson, 2012). Four depositional steps can be recognised in each sandstone bed (Fig. 10). (i) At the base of the bed, thin layers of coarse-grained sandstone with flat mudstone pebbles, aligned parallel to the stratification at the top, represent deposition by high-concentration laminar flows,

probably driven by overlying turbulent flows, in a bipartite flow configuration (Enos, 1977). The mechanisms of sediment transport and deposition of this portion can be compared with those of a diffusely stratified traction-carpet (cf. Todd, 1989 and Sohn, 1997). (ii) Waning turbulent flow deposited medium-grained sandstone with planar laminations generated in the upper flow regime. (iii) Although entirely palaeopedogenised, most of the sandstone bed (homogenous moderately sorted medium- and fine-grained sandstone) demonstrates that sedimentation occurred in steady and depletive, probably turbulent, conditions (cf. Kneller, 1995). (iv) A thin bed of clayey mudstone represents the last episode of sedimentation, which was deposited from standing water in the aftermath of an unconfined alluvial flood.

4.3.2. Palaeosols

Two pedotypes were recognised: Echaporã (Inceptisol) (Fig. 10A) and Kaingang pedotypes (Vertisol) (Fig. 10B, C).

4.3.2.1 Echaporã pedotype (Inceptisol)

Description. The parent material of the Echaporã pedotype (Basilici et al., 2016) consists of fine-to medium- grained sandstone, constituted mainly of quartz and secondarily of feldspars (Fig. S1H). The thickness varies from 0.9 to 2.4 m and the typical profile is constituted of A-Bw-(Bwk)-C horizons (Fig. 10A). The A horizon is reddish yellow (5YR 6/8), massive and is not always preserved; its maximum thickness is 0.2 m (Fig. 9C). The top distinctness with the overlying beds (bottom part of "tabular sandstone beds") is very abrupt and the top topography smooth. The distinctness with the lower Bw horizon is gradual, the topography smooth or wavy. Sand-filled cylindrical tubes, tapering downward and branching laterally, and showing redoximorphic depletion features around the margins cover c. 15% of the exposure area; they correspond to root cast of Klappa (1980) (Fig. 9C). The Bw horizon is reddish yellow (5YR 6/6), and 0.3-2 m thick. The lower distinctness to the Bwk horizon is gradual, the topography smooth. The c/f related distribution pattern is chitonic or coarse monic. Sand-sized grains

546 are partially coated with clay or clay-oxide (Fig. 9D). Incipient pedogenic structures generate a grade of
547 pedality between weakly and moderately developed: they consist of prismatic peds (150 mm high and
548 80 mm wide) and angular blocky peds (50-80 mm wide), separated by discontinuous calcium carbonate
549 coatings (Fig. 9E). There are very small calcium carbonate rhizocretions (Klappa, 1980) and
550 rhizotubules (Kraus and Hasiotis, 2006). The Bwk horizon is reddish yellow (7.5YR6/8), 0.1-0.25 m
551 thick. The distinctness of the bottom of the C horizons is gradual and the topography smooth. This
552 horizon shows subspherical calcareous nodules, 1-50 mm in diameter, whose distribution is 10-20% of
553 the exposed area. The c/f related distribution pattern is coarse monic or locally chitonic. A small number
554 of Bw horizons show more developed prismatic peds and a little higher quantity of clay, which is
555 stressed by a slight increase of the Al/Si weathering molar ratio (Fig. 11A) and by the greater
556 occurrence of grain clay coatings (Fig. 9D). These horizons appear to be incipient Bt horizons. The C
557 horizon is 0.2-1.2 m thick and it is constituted of reddish yellow (7.5YR 7/6). Macroscopically, relics of
558 planar laminations are visible.

559 Weathering molar ratios of Ba/Sr, Rb/Sr, hydrolysis (ΣBases/Al), and the CIA (Chemical Index of
560 Alteration) were calculated for all the horizons of seven profiles of this pedotype (Fig. 11B, C, D, and E;
561 Tables S2 and S3). Ba/Sr ratio varies from 2.50 to 5.11, the coefficient of variation is 9.4%; Rb/Sr ratio
562 varies from 0.34 to 0.91, the coefficient of variation is 15.05%; the hydrolysis values are from 1.01 to
563 1.67, their coefficient of variation is 14.44%; the CIA values vary from 54.23 to 67.83, their coefficient of
564 variation is 6.77%. Note that in all these ratios we excluded the values corresponding to horizons (Bk,
565 Bwk, Ck) with calcium carbonate concentration because (i) the Sr is incorporated in calcite crystalline
566 lattice (Buggle et al., 2011) and the ratio of Ba/Sr and Rb/Sr result to be extremely low and (ii) the high
567 CaO concentration in Bwk horizons generates anomalous peak of hydrolysis and CIA.

568 *Interpretation.* The A horizon (epipedon) was identified through the high root trace concentration (Fig.
569 9C and 10A). The light colour is ascribable to scarce or absent organic matter, and the absence of
570 pedogenic structures identify this horizon as ochric (Soil Survey Staff, 1999). The following peculiar

571 characteristics of the Bw and Bwk horizons indicate limited development of the macro- and
572 micromorphologic pedogenic features: (i) incipient prismatic structures (Fig. 9E and 10A); (ii) few thin
573 clay coatings around sand grains (Fig. 9D and 10A), which do not permit definition of an argillic horizon
574 (Soil Survey Staff, 1999); (iii) some weatherable minerals (Fig. 9D); (iv) an absence of redoximorphic
575 features; (v) isolated and small calcareous nodules in Bwk horizons, which indicate first stages of
576 development of a calcic horizon (Gile et al., 1966). Even the geochemical aspects of this palaeosol
577 indicate weak pedogenic development. The weathering molar ratios of Ba/Sr and Rb/Sr are used as
578 proxies of leaching because the Sr is more soluble than Ba and Rb and these three elements have
579 similar atomic radii and chemical behaviour (Sheldon, 2006; Sheldon and Tabor, 2009; Liu *et al*., 2014).
580 The values of Ba/Sr (excluding the peaks in Bwk horizons, which are anomalous for the reasons
581 explained above) are constant and very similar to the value of the original parent material (C horizons).
582 This means that the Ba/Sr and Rb/Sr ratio present the same values inherited from the sedimentary
583 material and therefore cannot be traced back to pedogenic processes. Likewise, the weathering molar
584 ratios associated with hydrolysis and the CIA do not show remarkable vertical variations. Notably, the
585 values of CIA (from 54.23 to 67.83) are close to the value of the pure K-feldspar or granite and
586 granodiorite (Nesbitt and Young, 1982). Furthermore, the Bw and Bwk horizons do not present peculiar
587 macroscopic, micromorphological and geochemical characteristics that allow attributing it to specific
588 subsurface horizons (such as argillic, oxic, spodic, or other), but it can be defined as a cambic horizon
589 (Soil Survey Staff, 1999). Ochric epipedon and the cambic subsurface horizons constitute the intrinsic
590 characteristics that allow defining Inceptisol, a type of soil more developed than Entisol, but whose B
591 horizon does not show specific characteristics that allow attributing to a more developed soil (Foss *et*
592 *al*., 1983; Soil Survey Staff, 1999; Buol et al., 2011).

593 4.3.2.2 Kaingang pedotype (Vertisol)

594 *Description*. The Kaingang pedotype has red (2.5YR 5/8) sandy mudstone parent material (Fig.
595 10B). This pedotype is uncommon in the south-eastern sector. The typical profile can be subdivided into

596 Bss-Bssk-C horizons, it is 0.7-1.3 m thick, and shows macroscopic yellow (2.5Y 8/6) redox depletion
597 features, whose distribution varies from 20-75% of the exposed surface (Fig. 10C). The Bss horizon is
598 0.15-0.3 m thick; the transition to overlying deposits is very abrupt. Its top surface is characterised by
599 weak undulations that continue within the horizon as smooth low-angle surfaces with striations and
600 grooves (slickensides) (Fig. 10B and C). Few medium- and fine-grained sand clasts are scattered in a
601 muddy micromass. The c/f related distribution pattern is single or double-spaced porphyric. The b-fabric
602 is stipple speckled and greyish-green redox depletions are common in thin sections. The Bssk horizon is
603 0.7-0.9 m thick and shows a net of low-angle smooth striated surfaces (slickensides), which intersect at
604 angles of 30º and 150º to the horizontal, thus separating wedge-shaped structural aggregates (cf.
605 mukkara structure) (Fig. 10C). Calcite cement, 2-10 mm thick, fills the planar voids among the
606 slickensides. The c/f related distribution pattern and b-fabric are similar to those of the Bss horizon. The
607 C horizon is a reddish yellow (7.5YR 7/6), medium-grained sandstone, 0.1-0.3 m thick, and shows relics
608 of planar laminations.
609 *Interpretation.* This pedotype is attributed to Vertisol based on the following: (i) high content of
610 micromass, probably constituted of expandable smectite clays, (ii) high bulk density of the micromass,
611 (iii) presence of slickensides, (iv) wedge-shaped aggregates, (v) mukkara structure, (vi) weak undulation
612 at the top, attributable to gilgai surface structure (Soil Survey Staff, 1999, 2014; Ahmad, 1983; van
613 Breemen and Buurman, 2002). Vertisol are soils formed in expandable clay parent material in various
614 climate regimes, but which always show marked alternations of wet and dry periods (Ahmad, 1983). The
615 presence of the Bssk horizon is expected to be caused by the negative hydric balance.
616 4.3.3 Distribution and relationships of deposits and palaeosols
617 In south-eastern sector, palaeosols are dominant: 92% of the thickness of the measured sections.
618 Echaporã pedotype (Inceptisol) is 90% of the thickness of the succession, while Kaingang pedotype
619 (Vertisol) is 2%. The deposits ("Tabular sandstone beds") constitute 8% of the succession (Table S1).

The upper portion of the Bauru Basin is formed almost exclusively of alternating beds of “Tabular sandstone beds” and Echaporã pedotype (Inceptisol), 0.9-3 m thick (Fig. 12A). The bottom of each cycle “Tabular sandstone beds”/ Echaporã pedotype (Inceptisol) is abrupt, flat and locally characterised by small erosional scours. The upward transition from deposit to palaeosol is gradual or diffuse and the top of the palaeosol is abrupt.

5. PALAEOSOLS AS PROXIES OF CLIMATE, PROVENANCE AND RECURRENCE TIME OF DEPOSITIONAL PROCESSES TO DISCERN ANCIENT FLUVIAL SYSTEMS

The upper portion of the Bauru Basin, based exclusively on sedimentological and stratigraphic data, has been attributed to a unique fluvial system, probably distributive, trending from east to west (Soares et al., 1980; Fernandes and Coimbra, 2000; Fernandes and Ribeiro, 2015; Basilici et al., 2016; Batezelli et al. 2019; Soares et al. 2020a). In this study, via analysis of palaeosols and by considering interactions between palaeosols and deposits as palaeoenvironmental and architectural proxies, the upper portion of the Bauru Basin is shown to consist in three differentiated fluvial systems constrained by different (i) climate, (ii) provenance of detrital material, and (iii) cyclical alternations of palaeosols/deposits, including differences in the timespan of accumulation.

5.1. Climate

Climate is one of the main factors controlling the pedogenesis (Buol et al., 2011), consequently the palaeosols are an excellent palaeoclimatic proxy (Retallack, 2001). In upper portion of the Bauru Basin, the palaeosols with strong climatic control are Aridisols (Itajá and Mukuriñ pedotypes) and Vertisols (Aranã and Kaingang pedotypes). Aridisols are characterised by accumulation of calcium carbonate (Bk or Bkm horizons), which indicate hydric deficit; furthermore their general reddish colour and the absence of redoximorphic features reveal deep groundwater and drained soil conditions. Aridisols are soils typical of arid or semiarid areas, i.e. environments characterised by scattered vegetation, negative water

balance and in general with annual precipitation around or less than 500 mm (Nettleton and Peterson, 1983; Watson, 1992; Mack and James, 1994; Schaetzl and Anderson, 2005; Buol et al., 2011). Aridisols are common in north-western sector of the study succession, they are very rare in north-eastern sector and absent in south-eastern sector. Vertisols are soils with parent material made of expandable clays, developed in climatic conditions characterised by marked differentiation between dry and humid season (Ahmad, 1983; Mermut et al., 1996). Vertisols were identified in all three sectors; their diffusion is rather limited due to the infrequent clay deposits in upper portion of the Bauru Group.

Empirical formulae (climofunctions), based on physical and geochemical characteristics of the palaeosols, can be applied to obtain quantitative values of mean annual precipitations (MAP) (Sheldon and Tabor, 2009). The depth of carbonate accumulation (Bk or Bkm horizon) in the soil profile is a direct function of the annual precipitation amount. Retallack (2005) created a formula that directly related the mean annual precipitation with the depth of the carbonate accumulation. Quantitative estimations of the mean annual precipitation may also be obtained from formulae that consider the degree of chemical alteration of a palaeosol horizon: (i) CIA-K (Maynard, 1992; Fedo et al., 1995) for Bt horizons; (ii) ΣBases/Al for Bk horizons (Sheldon et al., 2002; their formulae [1] and [3]); and (iii) CALMAG weathering index [Al2O3 /(Al2O3 + CaO + MgO) × 100] for Vertisols (Nordt and Driese, 2010).

In the north-western sector, from the depth of the Bk horizon of five Aridisol profiles, MAP displays values between of 322-679 mm/y. Applying the CIA-K and ΣBases/Al formulae to Bt or Bk horizons of Aridisols, the MAP mean values obtained are between 518-775 and 502-541 mm/y, respectively (Tab. S4). The difference of these values with those obtained from the depth of the Bk horizon may be due to possible erosion of the top of the palaeosol profile, resulting in a depth of the Bk horizon smaller than the original value. Mean of MAP of this sector is 535 mm/y (Tab. S4). In the proximal area of the north-eastern sector, climofunctions based on the degree of chemical alteration of Bk horizons of Inceptisols indicate MAP of 737 and 752 mm/y. Mean of MAP of this area is 744 mm/y (Tab. S4). In the medial area of the same sector, climofunctions based on Bk depth show mean value of MAP of 406 and 532 mm/y;

whereas climofunctions based on the degree of chemical alteration of Bk and Bt horizons of Inceptisols indicate 431 and 460 mm/y, respectively (Tab. S4). Mean of MAP of this area is 457 mm/y (Tab. S4). In the south-eastern sector, climofunctions based on Bk depth show value of 814 and 899 mm/y; whereas climofunctions based on the degree of chemical alteration of Bt horizons of Inceptisols indicate MAP values between 633-1229 mm/y (Tab. S4). Mean of MAP of this sector is 977 mm/y (Tab. S4).

Climate proxies can be compared in the three sectors with the types of the deposits. The north-western sector (Fig. 6) is typified of aeolian deposits, which correspond to the accumulation of small nabkha dunes in an aeolian sand sheet (Basilici et al., 2009), and sandstone and conglomerate sheet bodies, which reveal the existence of rivers characterised by rapid and highly concentrated flows, typical of rivers in drylands (Tooth, 2000). In the north-eastern sector (Fig. 8), sedimentary structures and architectural organisation of the sheet sandstone bodies demonstrate that the deposits were formed in channels with perennial water flow, although with variable morphological and hydraulic conditions (Soares et al., 2018; Martinelli et al., 2019). In the south-eastern sector (Fig. 12), the "tabular sandstone beds" likely formed by paroxysmal unchannelised subaqueous flows at the mouths of fluvial channels (Basilici et al., 2016).

To conclude, using an integrated dataset of palaeosols types, climofunctions and deposits, as climate proxies, it has been possible to reconstruct geographic variations in climate from north-western (mean of MAP 535 mm/y) to south-eastern (mean of MAP 977 mm/y) sectors, indicating a transition gradient from semiarid/arid to subhumid climatic conditions (Fig. 13). In the north-eastern sector, the differences between MAP in proximal area (mean 744 mm/y) and medial area (mean 457 mm/y) (Fig. 13) are probably linked to palaeomorphological factors, since the eastern and proximal portion was originally located close to a coeval topographic high (the Alto Paranaíba uplift; Batezelli et al., 2019).

5.2. Provenance of the detrital material

Geochemical data of the parent material of the palaeosols can help to define the source of the clastic material. The Principal Component Analysis of the major and minor chemical elements shows a clear differentiation of the geochemical composition of the palaeosols of the three sectors (Fig. 14A). The first component (P1) explains the 35% of the total variance of the distribution of the chemical variables. The loading plot (Fig. S5) displays a positive correlation for MnO, MgO, CaO, P_2O_5, and LOI (loss on ignition) and a negative one for SiO_2, TiO_2, Al_2O_3, Fe_2O_3, Na_2O, and K_2O. This allows separation of the palaeosol horizons with larger content in calcium carbonate from those that are relatively richer in silica and other oxides. The second component (P2) explains the 33% of the total variance. In this case, the loading plot (Fig. S5) displays SiO_2 as having negative correlation and the other oxides positive ones, with the highest values of Fe_2O_3 and TiO_2. Thus, the analysis allows discerning palaeosols with relatively higher components of TiO_2 and Fe_2O_3 from those with relatively higher component of SiO_2. Analysing the distribution of the samples on the biplot, it is possible to observe that the south-eastern sector (blue circles in Fig. 14A) is characterised by a relatively greater occurrence of SiO_2 in most horizons, which decreases where CaO and LOI increase. TiO_2 and Fe_2O_3 values appear here to be smaller than in the other sectors. The geochemical distribution of the north-western sector samples (orange squares in Fig. 14A) shows a greater content of Fe_2O_3 and TiO_2 and a lower quantity of SiO_2 compared to the south-eastern sector. The north-eastern sector partially overlaps the other two areas (green "X" in Fig.14A). Samples from this sector have similar SiO_2 content to those from the south-eastern sector, but a higher and variable amount of Fe_2O_3 and TiO_2. The inverse relationship of SiO_2 with CaO and LOI is typical of all the sectors and can be explained by the presence of Bk or Bkm horizons where the pedogenic content of $CaCO_3$ increases, thereby decreasing the relative content of SiO_2.

The distribution of TiO_2 and Fe_2O_3 is significant for discerning the origin of the sediments. Small concentrations of these two oxides are observed in the palaeosols of the south-eastern sector while higher values are found in the north-eastern sector and in particular in the north-western sector (Fig. 14B, C). The different concentrations of Fe_2O_3 and TiO_2 can be linked to the original characteristics of

719 the parent material; these two oxides being more common in mafic rocks: for example, basaltic rocks
720 have 0.5-2% of TiO_2 and 5-14% of Fe_2O_3, while granitic rocks have 0.3% TiO_2 and 2.9% Fe_2O_3 (Wilson,
721 1989).

722 The TiO_2/Al_2O_3 weathering molar ratio can indicate the provenance of the palaeosol parent material.
723 De facto, these elements are few mobile and the original ratio remains unchanged during the
724 pedogenesis and diagenesis (Sheldon and Tabor, 2009). However, under particular conditions, related
725 to a long time of pedogenesis and/or acidic pH soils, this ratio may vary with respect to the original
726 parent material. Thus, to guarantee that the TiO_2/Al_2O_3 ratio from the palaeosol horizons corresponds to
727 the original TiO_2/Al_2O_3 ratio of the parent material, this ratio was determined along the profile of poorly
728 developed palaeosols (Entisol and Inceptisols) and in palaeosols formed under basic conditions
729 (Aridisols) (Fig. 14D). The mean and whisker plot (Fig. 14E) shows that the TiO_2/Al_2O_3 ratio is extremely
730 low (<0.15) in the south-eastern sector, whereas it is higher in the north-western and north-eastern
731 sectors (>0.3), although with larger variance in the latter. The relatively modest variability of these ratios
732 across the palaeosol profiles of the same sector indicates the reduced mobility of these elements in
733 palaeosol profile and a common provenance of the parent material (Fig. 14D). High values of TiO_2/Al_2O_3
734 ratio (>0.2) are believed to indicate a mafic volcanic origin of the parent material, while low values of
735 TiO_2/Al_2O_3 ratio (<0.15) are associated with a sedimentary and/or felsic origin (Sheldon and Tabor,
736 2009; Myers et al., 2014).

737 The pebble and cobble composition of the conglomerates and the petrography of the sandstones
738 integrate with and corroborate geochemical data (Fig. S1B, F). In the north-western sector clast
739 composition of conglomerates and petrographic assemblage of the fluvial sandstone reveal source
740 areas from the northern portion of this sector. In fact, this portion is constituted of mafic rocks (basalts of
741 Serra Geral Formation – Lower Cretaceous) and sandstone with chert (quartzarenites of Botucatu
742 Formation – Upper Jurassic) (cf. 1:1,000,000 geological map of Goiânia; Serviço Geológico do Brasil -
743 CPRM, 2004a). In the north-eastern sector, pebble clasts in sheet sandstone beds of the proximal part

744 of the fluvial system and petrography of fluvial sandstone and palaeosols suggest a source areas
745 constituted of metamorphic rocks, currently widely exposed to the east of this sector (cf. 1:1,000,000
746 geological map of Belo Horizonte, Serviço Geológico do Brasil - CPRM, 2004b). In the south-eastern
747 sector, the petrography of the parent material of the palaeosols indicates that the source of sediments
748 lies in felsic intrusive and/or sedimentary rocks.
749 Palaeoflow directions of the north-western sector are toward S-SSW; in the north-eastern the
750 palaeoflows are toward W or NW; no data are available for the south-eastern sector (Fig. S3).
751 In synthesis geochemical data, clast composition, sand petrography and palaeocurrent directions of
752 the river flows demonstrate that the three sectors display distinct catchment areas.
753
754 5.3. Cyclical alternation palaeosols/deposits, and time and span of accumulation
755 The palaeosol profiles described in all the three sectors were identified as compound. Compound
756 palaeosol profiles are separated at the bottom and top by deposits, i.e. beds with preserved
757 sedimentary structures (Duchaufour, 1982; Marriott and Wright, 1993; Kraus, 1999). In this type of
758 palaeosols, the C horizon has a gradual transition to the deposits below, whereas the A horizon (or B
759 when A is missing due to erosion) has an abrupt contact with the deposits above. This type of palaeosol
760 profile is developed in relation to sudden and rapid depositional events, which caused rapid deposition
761 of a package of sediment thick enough to bury and interrupt the pedogenesis on the topographic
762 surface (Kraus, 1999). The presence of compound palaeosol profiles in a sedimentary succession
763 means that the depositional and palaeopedogenic events were clearly separated in time. Therefore, by
764 examining the development time of the palaeosols, it is possible to define the recurrence time of the
765 depositional events which buried the soils and from this discover the factors which controlled the
766 processes of the accumulation of the continental sedimentary succession (Basilici et al., 2022).
767 In the north-western sector, compound profiles of palaeosols alternate with aeolian sandstone
768 deposited in an aeolian sand sheet (Fig. 6A) (Basilici and Dal Bó, 2010). Sixty-seven percent of the

alternations is constituted of the Itajá pedotype (Aridisol) and 30% of the Avá pedotype (Entisol). The formation time of the Itajá pedotype (Aridisol) was long, as suggested by strongly developed pedogenic structures (prismatic and angular blocky peds), thick accumulation of clay for illuviation, and coalescent calcareous nodules and brecciated petrocalcic horizons, which take several 10^4 yr and some 10^5 yr to form (Gile *et al.*, 1966; Machette, 1985; Marriott and Wright, 1993). Sheldon (2003) produced a chronofunction, based on data of Markevitch et al. (1990), which relates the thickness of Bt horizons with the time of palaeosol formation. Applying this chronofunction (cf. Sheldon, 2003; Sheldon and Tabor, 2009) to 12 Bt profiles of the Itajá pedotype, the reconstructed formation time of this pedotype varies from $46.4x10^3$ and $367.5x10^3$ yr (mean: $144x10^3$ yr) (Table S5). Although the accumulation of the clay over time may not be constant, depending on source input and climatic variations (Watson, 1992), and the reconstructed formation time values obtained are variable, these are of the same order of magnitude in time as expected from the other macroscopic palaeopedogenic features (see above) (Basilici et al., 2009; Basilici and Dal Bó, 2010). The Avá pedotype (Entisol) indicates a very short time of development of less than 10^3 yr (Grossman, 1983; Buol et al., 2011). The transition from Itajá or Avá pedotypes to aeolian deposits represents a sharp change from a stable topographic surface, where the sparse vegetation cover hindered erosion and transport of sand by the wind (Fig. 6B, D), to a barren more arid topographic surface, where the wind becomes the main morphodynamic agent (Fig. 6C). Basilici et al. (2009) and Basilici and Dal Bó (2010) interpreted these cyclical alternations of high frequency (of the order of 10^4 to 10^5 yr for the Itajá pedotype and less than 10^3 yr for the Avá pedotype) controlled by climate variations from semiarid to arid conditions (Fig. 6).

In north-eastern sector, “sheet sandstone bodies“, “muddy sandstone beds” and “tabular bed of sandstone grading to mudstone”, generated by river channel, floodplain flows and floods of terminal splay, respectively, alternate with compound palaeosols profiles (Fig. 8A, C, E, H). Consequently, in this sector, river flow processes are at the origin of the interruption of the pedogenic processes and constitute the parent material of the palaeosols. The Pataxó pedotype (Inceptisol) developed above

amalgamated channel sequences or isolated channel deposits ("sheet sandstone bodies") (Fig. 8B, D, G, F). Inceptisol require some thousands of years to form (Buol et al., 2011). Isolated carbonate nodules contained in the Bk horizon of this pedotype correspond to the stage II and III of carbonate concentration (Gile et al., 1966; Machette, 1985; Zamanian et al., 2016) and are regarded as features formed in the order of 10^4 years. The Pataxó pedotype (Inceptisol) developed on abandoned fluvial ridge in drained conditions; it was sheltered by the sedimentary processes induced by flooding because located in raised position, thus it had sufficient time to develop. The Krenak pedotype (Entisol) generated above floodplain deposits close to the river channel or above the deposits of terminal splay ("tabular bed of sandstone grading to mudstone") in distal area of the fluvial system (Fig. 8B, D, G, F). Aranã pedotype (Vertisol) developed above muddier deposits of flood plain. Entisol and Vertisol are soils developed in a very short time of the order of a few hundred years (Grossman, 1983; Ahmad, 1983). Both these pedotypes developed in lowland area of the flood plain where sedimentary processes frequently interrupted the pedogenic processes (Fig. 8B, D, G, F). The rare Mukuriñ pedotype (Aridisol), which records development time in the order of 10^4 yr, could evidence raised areas on the flood plain (terraces) away from deposition for several tens of thousands of years (Fig. 8C). In north-eastern sector, the presence of the palaeosols increases from proximal to medial area and drastically decrease in distal area, testifying the progressive increase of the depositional processes in distal area (Table S1). Moreover, the pedotypes show a distinctive distribution from proximal to distal areas of the distributive fluvial system. The Pataxó pedotype (Inceptisol) decreases gradually from proximal to distal area in parallel with a decrease of the channelised bodies. The Krenak pedotype (Entisol) increases in medial area, in parallel with the presence of the Aranã pedotype (Vertisol) and decreases in distal area, highlighting the greater frequency of overbank deposits in medial area. Overall, in the north-eastern sector the pedogenesis was strictly controlled by morpho-depositional processes of the distributive fluvial system.

In the south-eastern sector, the compound profiles of palaeosols are characterised by cycles of "tabular sandstone beds" and Echaporã pedotype (Inceptisols), which represent the alternation of high-concentrated paroxysmal unchannelised depositional flows with relatively long periods of pedogenesis (Fig. 12A). Several macroscopic features allow deducing the development time of the Echaporã pedotype. Isolated carbonate nodules, present in Bwk horizons, are regarded by Gile et al. (1966) and Machette (1985) as features formed in the order of 10^4 years. Prismatic and angular blocky peds, although moderately developed in Bw horizons, need a few tens of thousands of years to form (Birkeland, 1999). Using the empirical relationship of Retallack (2005), who linked the time of nodule formation with its size, the age of the larger nodules (0.5 mm) of $6.7x10^3$ yr was obtained (Table S5). By applying the empirical chronofunction proposed by Sheldon (2003) to three incipient Bt horizons (see above), times of development between 8.9 $x10^3$ and $38.5x10^3$ yr (mean: 20,790 yr) were obtained (Table S5). This prediction matches the moderately developed pedogenic features and the other quantitative values obtained. Since no evidence of cumulative or composite profiles was observed, it may be inferred that the recurrence time of the proximal unchannelised depositional flows was roughly from several thousands to few tens of thousands of years. The rare Kaingang pedotype (Vertisol) formed on clayey parent material, which was deposited at the more distal portions of the unchannelised deposits. Vertisols form in few hundreds of years and remain constant for a long time, thus they do not provide effective development time insights (Ahmad, 1983; Mermut et al., 1996; Buol et al., 2011).

The palaeosol/deposit ciclicity reveals that the upper portion of the Bauru Group can be divided into distinct regions (sectors) with distinct controlling factors and rhythms of sedimentation, and consequent generation of accommodation. In north-western sector, the palaeosol/deposit alternations are linked to climate variations, whereas variability in river flow factors controlled deposition and palaeosol development in the other two sectors. In the north-western sector, the abundance of Aridisols with development time of 10^4-10^5 yr demonstrates a low accommodation generation. In north-eastern sectors, the common presence of Entisols and Inceptisols with development time around 10^2-10^3 yr

843 reveals a high rate of accommodation generation. The south-eastern sector, which is characterised by
844 Inceptisol with development time around in the order of 10^4 yr, indicates an intermediate rate of
845 accommodation space generation.
846
847 **6. CONCLUSIONS**
848 In continental sedimentary successions, lithological homogeneity and similarity in sedimentological
849 characteristics can be mistakenly considered as indicative of depositional and palaeoenvironmental
850 uniformity. Yet, the palaeosols, which are commonly present in continental sedimentary successions
851 and are effective tools for palaeoenvironmental reconstructions and for revealing the dynamic of the
852 depositional processes and the architecture of continental sedimentary successions, allow to unravel
853 the composite nature of apparently homogeneous sedimentary succession. Applying an integrated
854 study of palaeosols and sediments to the upper portion of the Bauru Basin, for long considered a
855 homogenous depositional system, it is unveiled that it is constituted of three distinct fluvial systems
856 (Table S6). The main findings of this paper are listed below.
857 1. Macroscopic, micromorphological and geochemical features of palaeosols allowed to define
858 qualitative and quantitative estimations of the palaeoprecipitations. In upper portion of the Bauru Group,
859 this paper showed a palaeoprecipitation gradient increasing from north-western sector to south eastern
860 sector, identifying a climate variation from semi-arid to sub-humid palaeoenvironment. Deposits of
861 ephemeral rivers and aeolian dunes (nabkhas) in north-western sector and deposits of unchannelised
862 paroxysmal flows in south-eastern sector combine with this interpretation. The north-eastern sector
863 shows a palaeoprecipitation gradient controlled by the palaeomorphology: from more humid conditions
864 in proximal areas, close to palaeohighs (Alto Paranaíba uplift), to semi-arid conditions in distal area.
865 2. Geochemical data of the parent material of the palaeosols defined the source of the clastic
866 material. The statistical distribution of Fe_2O_3 and TiO_2 and the Ti/Al molar weathering ratio defined
867 different source and river catchment areas for the three sectors. Combining these data with

conglomerate clast composition, sandstone petrography and palaeocurrent directions arrayed that the basaltic and sedimentary clastic rocks were the source of the north-western sector, while the north-eastern sector received clastic material from eastern metamorphic rocks and the south-eastern sector from eastern felsic magmatic and/or sedimentary rocks.

3. The relationships between the characteristics of deposits and palaeosols in continental sedimentary successions constituted of compound palaeosol profiles allowed to define (i) the factor that controlled the phases of palaeopedogenesis and sedimentations, and (ii) the recurrence time of the depositional processes and wherefore the generation of the accumulation space. In the north-western sector the climate was the controlling factor, which caused pedogenesis during the more humid periods and aeolian deposits in more arid conditions. In this sector, the more developed palaeosols (Aridisols) demonstrate long recurrence time of the depositional processes and consequently low generation of accommodation space. In the north- and south-eastern sectors, the alternation between palaeosols and channelised or unchannelised river deposits demonstrates that the fluvial processes controlled the palaeopedogenesis. The north-eastern sector is dominated by Entisols and Inceptisols, revealing short time of recurrence of the depositional processes and high creation of accommodation space. The south-eastern sector, which is characterised by more developed Inceptisols, shows intermediate conditions of accommodation space creation.

The application of palaeopedogenic analyses to the study of continental sedimentary succession is needed to refine sedimentological, architectural, palaeoenviromental or basin analysis studies. In this case, the palaeosols help to define three fluvial systems in upper portion of the Bauru Basin with distinct types and rhythms of sedimentation. Academic research and exploration of natural resources in continental sedimentary succession can have noteworthy benefits practicing this methodological study.

ACKNOWLEDGEMENTS

The authors would like to thank FAPESP (project 2012/23209-0 of G.B.), CNPq (Universal 4742272013-8 of G.B.; Research Grant 309767/2022-9 of C.R.S.F and PRH/ANP 19.1 (Exploração Petrolífera e Geologia de Reservatórios) for the financial support. Two anonymous reviewers and the Editor-in-Chief, Catherine Chagué, are thanked for giving excellent advice for the revision of this paper.

REFERENCES

Ahmad, N., 1983. Vertisols. In: Wilding, N.L.P., Smeck, E., Hall, G.F. (Eds.), Pedogenesis and Soil Taxonomy II. The Soil Orders. Developments in Soil Science, 11B. Elsevier, Amsterdam, pp. 91–123.

Arai, M., Dias-Brito, 2023. Supersequência Bauru (Cretáceo da Bacia do Paraná). Revisão estratigráfica com base em dados paleontológicos recentes. Derbyana 44, 1-31 (In Portuguese with English abstract)

Basilici, G., Dal Bó, P.F.F., Ladeira, F.S.B., 2009. Climate-induced sediment-palaeosol cycles in a Late Cretaceous dry aeolian sand sheet: Marília Formation (North-West Bauru Basin, Brazil). Sedimentology 56, 1876–1904.

Basilici, G., Dal Bó P.F.F., 2010. Anatomy and Controlling Factors of a Late Cretaceous Aeolian Sand Sheet Depositional System: the Marília and the Adamantina formations, NW of the Bauru Basin, Brazil. Sedimentary Geology 226, 71-93.

Basilici, G., Dal' Bó, P.F.F., 2014. Influence of subaqueous processes on the construction and accumulation of an aeolian sand sheet. Earth Surface Processes and Landforms 39, 1014-1029.

Basilici, G., Dal' Bó, P.F.F., Oliveira, E.F., 2016. Distribution of palaeosols and deposits in the temporal evolution of a semiarid fluvial distributary system (Bauru Group, Upper Cretaceous, SE Brazil). Sedimentary Geology 341, 245–264.

Basilici, G., Benvenuti, M., Cojane, I., Varela, A. 2022. Editorial preface to special issue: Palaeosols in the sedimentary record: Implications for understanding the depositional processes, sedimentary architecture and the palaeoenvironment. In: Basilici, G., Benvenuti, M., Cojan, I., Varela, A. (Eds.)

Palaeosols in the sedimentary record: implications for assessing the depositional processes, architecture and the palaeoenvironment. Palaeogeography, Palaeoclimatology, Palaeoecology 602, 111153. https://doi.org/10.1016/j.palaeo.2022.111153.

Batezelli, A., Ladeira, F.S.B., 2016. Stratigraphic framework and evolution of the Cretaceous continental sequences of the Bauru, Sanfranciscana, and Parecis basins, Brazil. Journal of South American Earth Sciences 65, 1-24.

Batezelli, A., Ladeira, F.S.B., Nascimento do, D.L., Silva, M.L., 2019. Facies and palaeosol analysis in a progradational distributive fluvial system from the Campanian–Maastrichtian Bauru Group, Brazil. Sedimentology, 66, 699-735.

Benvenuti, M., Andreetta, A., Huertas, A.D., Canicelli, S., 2021. Palaeosols in an Upper Pliocene fluvial to shallow marine succession (Valdelsa Basin, central Italy): a sequence-stratigraphic perspective. In: Basilici, G., Benvenuti, M., Cojan, I., Varela, A. (Eds.) Palaeosols in the sedimentary record: implications for assessing the depositional processes, architecture and the palaeoenvironment. Palaeogeography, Palaeoclimatology, Palaeoecology 584, 110684. https://doi.org/10.1016/j.palaeo.2021.110684.

Beverly, E.J., Lukens W.E., Stinchcomb, G.E., 2018. Paleopedology as a Tool for Reconstructing Paleoenvironments and Paleoecology. In: Croft, D. A., Su, D.f., Simpson, S.W. (Eds.), Methods in Paleoecology. Reconstructing Cenozoic Terrestrial Environments and Ecological Communities, Springer, Switzerland, 151-183.

Birkeland, P.W., 1999. Soils and Geomorphology. Oxford University Press, New York, 448 pp.

Bluck, B., J., 1979. Structure of coarse grained braided stream alluvium. Transactions of the Royal Society of Edinburgh, 70, 181-221.

Bown, T.M., Kraus, M.J., 1981. Lower Eocene alluvial paleosols (Willwood Formation, Northwest Wyoming, U.S.A.) and their significance for paleoecology, paleoclimatology, and basin analysis. Palaeogeography, Palaeoclirnatology, Palaeoecology 34, 1-30.

942 Bown, T.M., Kraus, M.J., 1987. Integration of channel and floodplain suites in aggrading fluvial
943 systems. I. Developmental sequence and lateral relations of lower Eocene alluvial paleosols, Willwood
944 Formation, Bighorn Basin, Wyoming, Journal of Sedimentary Petrology 57, 587-601.
945 Bown, T.M., Kraus, M.J., 1993. Time-stratigraphic reconstruction and integration of paleopedologic,
946 sedimentologic, and biotic events, Willwood Formation, Lower Eocene, northwest Wyoming, USA.
947 Palaios 8, 68–80.
948 Bridge, J. S., 2003. Rivers and Floodplains. Blackwell, Oxford, 491 pp.
949 Bronger, A. and Catt, J.A. (1989). Paleosols: problems of definition, recognition and interpretation.
950 Catena Supplement, 16, 1-7.
951 Buggle, B., Glaser, B., Hambach, U., Gerasimenko, N., Marković, S., 2011. An evaluation of
952 geochemical weathering indices in loess-palaeosol studies. Quaternary International 240, 12–21.
953 Bullock, P., Fedoroff, N., Jongerius, A., Stoops, G., Tursina, T., 1985. Handbook for Soil Thin
954 Section Description. Waine Research Publications, Wolverhampton, 152 pp.
955 Buol, S.W., Southard, R.J., Graham, R.C., McDaniel, O.A., 2011. Soil Genesis and Classification,
956 Sixth edition. Wiley-Blackwell, Oxford, 543 pp.
957 Cain, S.A., Mountney, N.P., 2009. Spatial and temporal evolution of a terminal fluvial fan system: the
958 Permian Organ Rock Formation, South-east Utah, USA. Sedimentology 56, 1774–1800.
959 Candeiro, C.R.A., Marques Brito, P., Cavin, L., Alves, Y.M., Canile, F., Muniz, F., Queiroz, G.K.,
960 Santos, D., Toriño, P., 2024. First record of Siluriformes from the northernmost portion of the Bauru
961 Group (Upper Cretaceous) in the Center-West region of Brazil. Journal of South American Earth
962 Sciences 133, 104690. https://doi.org/10.1016/j.jsames.2023.104690.
963 Cañón-Tapia, E., 2018. The Paraná-Etendeka Continental Flood Basalt Province: A historical
964 perspective of current knowledge and future research trends. Journal of Volcanology and Geothermal
965 Research, 355, 287–303.

966 Church, M., Jones, D., 1982, Channel bars in gravel bed rivers. In Hey R.D., Bathurst, J.C., and
967 Thorne, C.R., eds., Gravel Bed Rivers: Chichester, U.K., Wiley, pp. 291–338.
968 Coronel, M.D., Isla, M.F., Veiga, G.D., Mountney, N.P., Colombera, L., 2020. Anatomy and facies
969 distribution of terminal lobes in ephemeral fluvial successions: Jurassic Tordillo Formation, Neuquén
970 Basin, Argentina. Sedimentology, 2020, 67(5), pp. 2596–2624. https://doi.org/10.1111/sed.12712
971 Dal Bó, P. F. F., Basilici, G., Angélica, R. S., 2010. Factors of paleosol formation in a late cretaceous
972 eolian sand sheet paleoenvironment, Marília Formation, South-eastern Brazil. Palaeogeography,
973 Palaeoclimatology, Palaeoecology, 1-15.
974 Dal' Bó, P.F.F., Basilici, G., 2015. Intermontane eolian sand sheet development, Upper Tulum
975 Valley, central-western Argentina. Brazilian Journal of Geology, 45 (Suppl 1), 97-115.
976 Dias-Brito, D., Musacchio, E.A., Castro, J.C., Maranhão, M.S.A.S., Suarez, J.M., Rodrigues, R.,
977 2001. Grupo Bauru: uma unidade continental do Cretáceo no Brasil - concepções baseadas em dados
978 micropaleontológicos, isotópicos e estratigráficos. Revista de Paleobiologia 20, 245-304. (In Portuguese
979 withEnglish abstract)
980 Duchaufour, P., 1982. Pedology. Allen & Unwin, 448 pp.
981 Dzombak, R.M., Midttun, N.C., Stein, R.A., Sheldon, N.D., 2021. Incorporating lateral variability and
982 extent of paleosols into proxy uncertainty. In: Basilici, G., Benvenuti, M., Cojan, I., Varela, A. (Eds.),
983 Palaeosols in the Sedimentary Record: Implications for Assessing the Depositional Processes,
984 Architecture and the Palaeoenvironment, Palaeogeography, Palaeoclimatology, Palaeoecology, 582.
985 110641. https://doi.org/10.1016/j.palaeo.2021.110641.
986 Driese, S.G., Nordt, L.C., 2013 New Frontiers in Paleopedology and Terrestrial Paleoclimatology. In:
987 Driese,S.G., Nordt, L.C. (Eds.). New Frontiers in Paleopedology and Terrestrial Paleoclimatology,
988 SEPM Special Publication, 104, pp. 1-3.
989 Enos, P., 1977. Flow regimes in debris flow. Sedimentology, 24, 133-142.

990 Fedo, C.M., Nesbitt, H.W., Young, G.M., 1995. Unraveling the effects of potassium metasomatism in
991 sedimentary rocks and paleosols, with implications for paleoweathering conditions and provenance.
992 Geology 23, 921–924.
993 Fernandes, L.A., Coimbra, A.M., 2000. Revisão estratigáfica da parte orietnal da Bacia Bauru
994 (Neocretaceo). Revista Brasileira de Geociências 30, 717-728.
995 Fernandes, L. A., Ribeiro, C.M.M., 2015. Evolution and palaeoenvironment of the Bauru Basin
996 (Upper Cretaceous, Brazil). Journal of South American Earth Sciences 61, 71-90.
997 Fielding, C.R., Alexander, J., McDonald, R., 1999. Sedimentary facies from GPR surveys of the
998 modern, upper Burdekin River of north Queensland, Australia: consequences of extreme discharge
999 fluctuations. In: Smith, N.D., Rogers, J. (Eds.), Fluvial Sedimentology VI. International Association of
1000 Sedimentologists Special Publication 28, Oxford, UK, pp. 347–362.
1001 Fielding, C.R., 2006. Upper flow regime sheets, lenses and scour fills: extending the range of
1002 architectural elements for fluvial sediment bodies. Sedimentary Geology 190, 227–240.
1003 Foss, J.E., Moormann, F.R., Rieger, S., 1983. Inceptisols. In: Wilding, N.L.P., Smeck, E., Hall, G.F.
1004 (Eds.), Pedogenesis and Soil Taxonomy II. The Soil Orders. Developments in Soil Science, 11B.
1005 Elsevier, Amsterdam, Netherlands, pp. 355-381.
1006 Friend, P.F., Slater, M.J., Williams, R.C., 1979. Vertical and lateral building of river sandstone
1007 bodies, Ebro Basin, Spain. Journal Geological Society of London 136, 39-46
1008 Frostick, L.E. and Reid, I. (1977) The origin of horizontal laminae in ephemeral stream channel-fill.
1009 Sedimentology 24, 1–9.
1010 Fryberger, S.G., Schenk, C.J., 1988. Pin stripe lamination: a distinctive feature of modern and
1011 ancient eolian sediments. Sedimentary Geology. 55, 1–15.
1012 Gibling, M.R., 2006. Width and thickness of fluvial channel Bodies and valley fills in the geological
1013 record: a literature compilation and classification. Journal of Sedimentary Research 76, 731–770.

1014 Gile, L.H., Peterson, F.F., Grossman, R.B., 1966. Morphological and genetic sequences of
1015 carbonate accumulation in desert soils. Soil Science 101, 347–360.
1016 Gobbo-Rodrigues, S.R., Petri, S., Bertini, R.J., 1999a. Ocorrências de ostrácodes na Formação
1017 Adamantina do Grupo Bauru, Cretáceo Superior da Bacia do Paraná e possibilidades de correlação
1018 com depósitos isócronos argentinos. Parte I - Família Ilyocyprididae. Acta Geol. Leopoldensia 23 (49),
1019 3e13. (In Portuguese with English abstract)
1020 Gobbo-Rodrigues, S.R., Petri, S., Bertini, R.J., 1999b. Ocorrências de ostrácodes na Formaçáo
1021 Adamantina do Grupo Bauru, Cretáceo Superior da Bacia do Paraná e possibilidades de correlaçáo
1022 com depósitos isócronos argentinos. Parte II - Família Limnocytheridae. Revista Universidade
1023 Guarulhos -Geociências 6, 5e11. (In Portuguese with English abstract)
1024 Grossman, R.B. (1983) Entisols. In: Wilding, L.P., Smeck, N.E., Hall, G.F. (Eds.) Pedogenesis and
1025 Soil Taxonomy II - The Soil Orders -Development in Soil Science. Elsevier, Amsterdam, Netherland, pp.
1026 55–90.
1027 Hassan, M.A., 2005. Characteristics of gravel bars in ephemeral streams. Journal of Sedimentary
1028 Research, 75, 29-42.
1029 Haszeldine, R.S., 1983. Fluvial bars reconstructed from a deep, straight channel, Upper
1030 Carboniferous coalfield of northeast England. Journal of Sedimentary Petrology 53, 1233-1248.
1031 Holbrook, J., 2001. Origin, genetic, interrelationships, and stratigraphy over the continuum of fluvial
1032 channel-form bounding surfaces: and an illustration from middle Cretaceous strata, southeastern
1033 Colorado. Sedimentary Geology 144, 179-222.
1034 Hunter, R.E., 1977. Basic types of stratification in small eolian dunes. Sedimentology 24, 361–387.
1035 Jobe, Z.R., Bernhardt, A., Lowe, D.R., 2010. Facies and architectural asymmetry in a conglomerate-
1036 rich submarine channel fill, Cerro Toro Formation, Sierra del Toro, Magallanes Basin, Chile. Journal of
1037 Sedimentary Research 80, 1085–1108

1038 Klappa, C.F., 1980. Rhizoliths in terrestrial carbonates: classification, recognition, genesis and
1039 significance. Sedimentology 27, 613–629.
1040 Kneller, B.C., 1995. Beyond the turbidite paradigm: physical models for deposition of turbidites and
1041 their implications for reservoir prediction. In: Hartley, A.J., Prosser, D.J. (Eds.), Characterization of Deep
1042 Marine Clastic Systems. Geological Society Special Publication94, London, UK, pp. 31–49.
1043 Kocurek, G., Dott, R., H., Jr. 1981. Distinctions and uses of stratification types in the interpretation of
1044 eolian sand. Journal of Sedimentary Petrology 51, 579-595
1045 Kraus, M.J., Aslan, A., 1993. Eocene hydromorphic paleosols: significance for interpreting ancient
1046 floodplain processes. J. Sediment. Petrol. 63, 453–463.
1047 Kraus, M.J., 1999. Paleosols in clastic sedimentary rocks: their geologic applications Earth-Science
1048 Reviews 47, 41–70.
1049 Kraus, M.J., Hasiotis, S.T., 2006. Significance of different modes of rhizolith preservation to
1050 interpreting. Palaeoenvironmental and palaeohydrologic settings: examples from Palaeogene
1051 palaeosols, Bighorn Basin, Wyoming, USA. Journal of SedimentaryResearch 76, 633–646.
1052 Kraus, M.J, Riggins, S., 2007. Transient drying during the Paleocene–Eocene Thermal Maximum
1053 (PETM): Analysis of paleosols in the bighorn basin, Wyoming. Palaeogeography, Palaeoclimatology,
1054 Palaeoecology 245, 444–461.
1055 Lindbo, D.L., Stolt, M.H., Vepraskas, M.J., 2010. Redoximorphic Features. In: Stoops, G., Marcelino,
1056 V., Mees, F. (Eds.), Interpretation of Micromorphological Features of Soils and Regoliths. Elsevier,
1057 Amsterdam, pp. 129–147.
1058 Liu, B., Jin, H., Sun, L., Sun, Z., Niu, Q., Xie, S., Li, G., 2014, Holocene moisture change revealed by
1059 the Rb/Sr ratio of aeolian deposits in the south-eastern Mu Us Desert, China. Aeolian Research 13,
1060 109–119.

1061 Machette, N.M., 1985. Calcic soils of the southwestern United States. In: Weide, D.L. (Ed.), Soils
1062 and Quaternary Geology of the Southwestern United States. The Geological Society of America -
1063 Special Paper 203, Boulder, Colorado, pp. 10–21.
1064 Mack, G.H., James, W.C., 1994. Paleoclimate and the Global Distribution of Paleosols. The Journal
1065 of Geology, 102, 360-366.
1066 Markewich, H.W., Pavich, M.J., Buell, G.R., 1990. Contrasting soils and landscapes of the Piedmont
1067 and Coastal Plain, eastern United States. Geomorphology 3, 417–447.
1068 Marriott, S.B., Wright, V.P., 1993. Palaeosols as indicators of geomorphic stability in two Old Red
1069 Sandstone alluvial suites, South Wales. Journal of The Geological Society of London 150, 1109–1120.
1070 Martin, C.A.L., Turner, B.R., 1998. Origins of massive-type sandstones in braided river systems.
1071 Earth-Science Reviews, 44, 15–38
1072 Martinelli, A.G., Teixeira, V.P.A., 2015. The Late Cretaceous vertebrate record from the Bauru Group
1073 at the Triângulo Mineiro, southeastern Brazil. Boletín Geologico y Minero de España, 126, 129-158.
1074 Martinelli, A.G., Marinho, T., Iori, F., Ribeiro, L.C.B., 2018. The first Caipirasuchus
1075 (Mesoeucrocodylia, Notosuchia) from the Late Cretaceous of Minas Gerais, Brazil: new insights on
1076 sphagesaurid anatomy and taxonomy. PeerJ 6, e5594. https://doi.org/10.7717/peerj.5594 .
1077 Martinelli, A.G., Riff, D., Lope, R.P., 2011. Discussion about the occurrence of the genus
1078 Aeolosaurus Powell 1987 (Dinosauria, Titanosauria) in the Upper Cretaceous of Brazil. Gaea - Journal
1079 of Geoscience 7, 34-40.
1080 Martinelli, A.G., Basilici, G., Fiorelli, L.E., Klock, C., Karfunkele, J., Diniz, A.C., Soares, M.V.T.,
1081 Marconato, A., Silva, J.I., Ribeiro, L.C.B., Marinho, T.S., 2019. Palaeoecological implications of an
1082 Upper Cretaceous tetrapod burrow (Bauru Basin; Peirópolis,Minas Gerais, Brazil). Palaeogeography,
1083 Palaeoclimatology, Palaeoecology 528, 147–159.
1084 Maynard, J.B., 1992. Chemistry of modern soils as a guide to interpreting Precambrian paleosols.
1085 Journal of Geology 100, 279–289.

McCarthy PJ, Plint, A.G. 1998. Recognition of interfluve sequence boundaries: Integrating paleopedology and sequence stratigraphy. Geology 26, 387–390.

McCarthy, P.J., Plint, A.G., 2013. A pedostratigraphic approach to nonmarine sequence stratigraphy: a three-dimensional paleosol-landscape model from the Cretaceous (Cenomanian) Dunvegan Formation, Alberta and British Columbia, Canada. In: Driese,S.G., Nordt, L.C. (Eds.). New Frontiers in Paleopedology and Terrestrial Paleoclimatology, SEPM Special Publication 104, Tulsa, Oklahoma,pp. 159–177.

Mermut, A.R., Padmanabham, E., Eswaran, H., Dasog, G.S., 1996. Pedogenesis. In: Ahmad, N., Mermut, A. (Eds.), Vertisols and Technologies for their Management. Developments in Soil Science, vol. 24. Elsevier, Amsterdam, pp. 43–61.

Miall, A.D., 1988. Reservoir heterogeneity in fluvial sandstone: lessons from outcrop studies. American Association Petroleum Geology Bulletin 72, 682-687.

Miall, A.D., 2006. The Geology of Fluvial Deposits. Springer-Verlag Berlin Heidelberg, Ney York, NY, 582 pp.

Middleton, G.V. and Southard, J.B. (1984) Mechanics of Sediment Transport, 2nd edn. SEPM, Eastern Section Short Course 3 Providence, 401 pp.

Myers, T.S., Tabor, N.J., Rosenau, N.A., 2014. Multiproxy approach reveals evidence of highly variable paleoprecipitation in the Upper Jurassic Morrison Formation (western United States). Geological Society Bulletin 126, 1105–1116.

Monger, H.C., Daughert, A., Gile, L.H., 1991. A microscopic examination of pedogenic calcite in an Aridisol of Southern New Mexico. In: Nettleton, W.D. (Ed.), Occurrence, Characteristics, and Genesis of Carbonate, Gypsum, and Silica Accumulations in Soils. SSSA Special Publication 26, Madison, Wisconsin, pp. 37–60.

1109 Mountney, N.P., 2006. Eolian facies models. In: Posamentier, H.W., Walker, R.G. (Eds.), Facies
1110 models revisited. Society for Sedimentary Geology - Special Publication 84, Tulsa, Oklahoma, pp. 19–
1111 83.
1112 Mulder, T., Alexander, J., 2001. The physical character of subaqueous sedimentary density flows
1113 and their deposits. Sedimentology, 48, 269-299.
1114 Munsell Color, 2013. Munsell Soil-Color Charts. Munsell Color, Grand Rapids, MI.
1115 Nesbitt, H.W., Young, G.M., 1982. Early Proterozoic climates and plate motions inferred from major
1116 element chemistry of lutites. Nature 299, 715–717.
1117 Nettleton, W.D. and Peterson, P.F. (1983) Aridisols. In: Pedogenesis and Soil Taxonomy: II. The Soil
1118 Orders (Eds L.P. Wilding, N.E. Smeck and G.F. Hall), Dev. Soil Sci., Elsevier, 11B, 165–215.
1119 Nichols, G.J., Fisher, J.A., 2007. Processes, facies and architecture of fluvial distributary system
1120 deposits. Sedimentary Geology 195, 75-90.
1121 Nordt, L.C. and Driese, S.G., 2010. New weathering index improves paleorainfall estimates from
1122 Vertisols Geology, 38, 407–410.
1123 North, P.C., Davidson, S.K., 2012. Unconfined alluvial flow processes: Recognition and
1124 interpretation of their deposits, and the significance for palaeogeographic reconstruction. Earth-Science
1125 Reviews 111, 199–223.
1126 PiPujol, M.D., Buurman, P., 1998. Analyzing ground-water gley and surface-water (pseudogley)
1127 effects in paleosols. Quat. Int. 51-52, 77–79.
1128 Ramos, A., Sopeña, A., 1983. Gravel bars in low-sinuosity streams (Permian and Triassic, central
1129 Spain). In: Collinson, D., Lewin, J. (Eds.), Modern and Ancient Fluvial Systems. Blackwell Scientific
1130 Publications, Oxford, UK, pp. 301-312.
1131 Reid, I., Frostick, L.E., 2011. Channel form flows and sediments of endogenous ephemeral rivers in
1132 deserts. In: Thomas, D.S.G. (Ed.), Arid Zone Geomorphology. Process, Form and Change in Drylands.
1133 Wiley-Blackwell, Chichester, UK, pp. 301-332.

1134 Retallack, G.J., 1994a. The environmental factor approach to the interpretation of paleosols. In:
1135 Amundson, R., Harden, J., Singer, M. (Eds.), Factors in Soils Formation: A Fiftieth Anniversary
1136 Retrospective. Soil Science Society of America, Madison, Wisconsin,pp. 31–64.
1137 Retallack, G.J., 1994b. A pedotype approach to latest Cretaceous and earliest Tertiary paleosols in
1138 eastern Montana. Geologica! Society of America Bulletin 106, 1377-1397.
1139 Retallack, G.J., 1997. A Colour Guide to Paleosols. John Wiley and Sons, Chichester, UK. 175 pp.
1140 Retallack, G.J., 2001. Soil of the past: An Introduction to Paleopedology. Allen and Unwin, London,
1141 UK, 520 pp. Retallack, G.J., 2005. Pedogenic carbonate proxies for amount and seasonality of
1142 precipitation in paleosols. Geology 33, 333–336.
1143 Røe, S.L., 1987. Cross-strata bedforms of probable transitional dune to upper-stage plane-bed origin
1144 from a Late Precambrian fluvial sandstone, northern Norway. Sedimentology 34, 89–101.
1145 Santucci, R.M., Bertini, R.J., 2001. Distribuição Paleogeográfica e Biocronológica dos Titanossauros
1146 (Saurishia, Sauropoda) do Grupo Bauru, Cretáceo Superior do Sudeste Brasileiro. Brazilian Journal of
1147 Geology 31, 307–315 (In Portuguese with English abstract).
1148 Schaetzl, R., Anderson, S., 2005. Soil-Genesis and Geomorphology. Cambridge University Press,
1149 Cambridge, UK, 817 pp.
1150 Schenk, C.J., 1983. Textural and structural characteristics of some experimentally formed eolian
1151 strata. In: M.E. Brookfield and T.S. Ahlbrandt (Editors), Eolian Sediments and Processes.
1152 (Developments in Sedimentology, 38) Elsevier, Amsterdam, pp. 41-49.
1153 Scherer, C.M.S., Goldberg, K., Bardola, T., 2105. Facies architecture and sequence stratigraphy of
1154 an early post-rift fluvial succession, Aptian Barbalha Formation, Araripe Basin, northeastern Brazil,
1155 Sedimentary Geology 322, 43–62.
1156 Schoeneberger, P.J., Wysocki, D.A., Benham, E.C.,Soil Survey Staff, 2012. Field Book for
1157 Describing and Sampling Soils 3.0. Natural Resources Conservation Service - National Soil Survey
1158 Center, Lincoln, NE, 312 pp.

1159 Serviço Geológico do Brasil - CPRM, 2004a. Carta Geológica do Brasil ao Milionésimo, Folha SE22,
1160 Goiânia, Secretaria de Minas e Metalurgia e Ministério de Minas e Energia, Brasília.
1161 https://geosgb.sgb.gov.br/geosgb/downloads.html
1162 Serviço Geológico do Brasil - CPRM, 2004b. Carta Geológica do Brasil ao Milionésimo, Folha SE23,
1163 Belo Horizonte, Secretaria de Minas e Metalurgia e Ministério de Minas e Energia, Brasília.
1164 https://geosgb.sgb.gov.br/geosgb/downloads.html
1165 Serviço Geológico do Brasil - CPRM, 2004c. Carta Geológica do Brasil ao Milionésimo, Folha SF22,
1166 Paranapanema, Secretaria de Minas e Metalurgia e Ministério de Minas e Energia, Brasília.
1167 https://geosgb.sgb.gov.br/geosgb/downloads.html
1168 Sheldon, N.D., 2003. Pedogenesis and geochemical alteration of the picture gorge subgroup,
1169 Columbia River Basalt, Oregon. Geological Society of America Bulletin 115, 1377–1387.
1170 Sheldon, N.D., 2006. Abrupt chemical weathering increase across the Permian–Triassic boundary.
1171 Palaeogeography, Palaeoclimatology, Palaeoecology 231, 315– 321
1172 Sheldon, N.D., Retallack, G., Tanaka, S., 2002. Geochemical climofunctions from North American
1173 soils and application to palaeosols across the Eocene Oligocene boundary in Oregon. Journal of
1174 Geology 110, 687–696.
1175 Sheldon, N.D., Tabor, N.J., 2009. Quantitative paleoenvironmental and paleoclimatic reconstruction
1176 using paleosols. Earth-Science Reviews, 95, 1–52
1177 Singer, A., 1984. Pedogenicpalygorskite in the arid environment. In: Singer, A., Galan, E. (Eds.),
1178 Palygorskite– Sepiolite: Occurrences, Genesis, and Uses - Development in Sedimentology 37. Elsevier,
1179 Amsterdam, Netherlands, pp. 169-176.
1180 Soares, P. C., Landim, P. M. B., Fúlfaro, V. J., Sobreiro Neto, A. F., 1980. Ensaio de caracterização
1181 do Cretáceo no Estado de São Paulo: Grupo Bauru. Revista Brasileira de Geociencias 10, 177–185 (In
1182 PortuguesewithEnglish abstract).

1183 Soares, M.V.T., Basilici, G.,Dal' Bó, P.F.,Marinho, T.S., Mountney,N.P., Colombera, De Oliveira,
1184 E.F., Silva, K.E.B., 2018. Climatic and geomorphologic cycles in a semiarid distributive fluvial system,
1185 Upper Cretaceous, Bauru Group, SE Brazil. Sedimentary Geology 372, 75–95.
1186 Soares, M.V.T., Basilici, G., Lorenzoni, P., Colombera, L., Mountney, N.P., Martinelli, A. G.,
1187 Mesquita, A.F., Marinho, T.S., Vasconez, R.G.G., Marconato, A., 2020a. Landscape and depositional
1188 controls on palaeosols of a distributive fluvial system (Upper Cretaceous, Brazil). Sedimentary Geology
1189 409, 105774. https://doi.org/10.1016/j.sedgeo.2020.105774.
1190 Soares, M.V.T., Basilici, G., Lorenzoni, P., A.F., Marinho, Martinelli, A. G., Marconato, A., Mountney,
1191 N.P., Colombera, L., Mesquita, T.S., Julia Tucker Vasques, J.T., Abrantes Junior, F. R., Ribeiro, L.C.B.,
1192 2020b. Sedimentology of a distributive fluvial system: The Serra da Galga Formation, a new
1193 lithostratigraphic unit (Upper Cretaceous, Bauru Basin, Brazil). Geological Journal 56, 951–975.
1194 Sohn, Y.K., 1997. On traction-carpet sedimentation. Journal of Sedimentary Research 67, 502-509.
1195 Soil Survey Staff, 1999. Soil taxonomy. In: Soil Survey Staff (Ed.), A Basic System of Soil
1196 Classification for Making and Interpreting Soil Surveys. US Department of Agriculture - Natural
1197 Resource Conservation Service, Washington, D.C, 871 pp.
1198 Soil Survey Staff, 2014. Keys to Soil Taxonomy. USDA-Natural Resources Conservation Service,
1199 Washington, DC, 360 pp.
1200 Stoops, G., 2003. Guidelines for Analysis and Description of Soil and Regolith Thin Sections. Soil
1201 Science Society of America, Madison, Wisconsin, 181 pp.
1202 Stoops, G., Marcelino, V., Mees, F., 2010. Interpretation of Micromorphological Features of Soils and
1203 Regoliths. Elsevier, Amsterdam, Netherlands, 720 pp.
1204 Tabor, N.J., Myers, T.S., Michel, L.A., 2017. Sedimentologist's Guide for Recognition, Description,
1205 and Classification of Paleosols. In: Zeigler, K.E., Parker, W.G. (Eds.), Terrestrial depositional systems:
1206 Deciphering Complexities through Multiple Stratigraphic Methods. Elsevier,Amsterdam, Netherlands,
1207 pp. 65-208.

1208 Todd, S.P., 1989. Stream-driven, high-density gravelly traction carpets: possible deposits in the
1209 Trabeg Conglomerate Formation, SW Ireland and some theoretical considerations of their origin.
1210 Sedimentology 36, 513-530.
1211 Tooth, S., 2000. Process, form and change in dryland rivers: a review of recent research. Earth-
1212 Science Reviews 51, 67–107.
1213 van Breemen, N., Buurman, P., 2002. Soil Formation. Kluwer academic publishers, Dordrecht,
1214 Netherlands, 404 pp.
1215 Vepraskas, M.J., 2015. Redoximorphic Features for Identifying Aquic Conditions: North Carolina
1216 State University. College of Agriculture and Life Sciences, 30 pp.
1217 Vinogradov, A.P., 1959. Geochemistry of Core and Dispersed Chemical Elements in Soils.
1218 Translated by Consultants Bureau, New York. 209 pp.
1219 Vos, K., Vandenberghe, N., Elsen, J., 2014. Surface textural analysis of quartz grains by scanning
1220 electron microscopy (SEM): from sample preparation to environmental interpretation. Earth-Science
1221 Reviews. 128, 93–104.
1222 Watson, A., 1992. Desert soils. In: Martini, IP, Chesworth, W. (Eds.), Weathering, Soils &Paleosols.
1223 Elsevier, Amsterdam, Netherlands, pp. 225–260.
1224 Watts, N.L. (1980) Quaternary pedogenetic calcretes from Kalahari (southern Africa): mineralogy,
1225 genesis and diagenesis. Sedimentology, 27, 661–686.
1226 Wilson, M., 1989. Igneous petrogenesis. Springer, Dordrecht, Netherlands, 466 pp.Wright, V.P.,
1227 Marriott, S.B., 1993. The sequence stratigraphy of fluvial depositional systems: the role of floodplain
1228 sediment storage Sedimentary Geology, 86, 203-210.
1229 Yaalon, D.H., Wieder, M., 1976. Pedogenic palygorskite in some arid brown (calciorthid) soils in
1230 Israel. Clay Mineralogy 11, 73-80.
1231 Zamanian, K., Pustovoytov, K., Kuzyakov, Y., 2016. Pedogenic carbonates: Forms and formation
1232 processes. Earth-Science Reviews, 157, 1–17.

CAPTIONS

Figure 1. Location and geological maps of the study areas. (A) North-western sector. (B) North-eastern sector. (C) South-eastern sector. The geological map and the stratigraphy are modified from Serviço Geológico do Brasil - CPRM (2004a,b,c). In these geological maps, we renamed the original Marília Formation as the upper portion of the Bauru Group (UpB) and the Vale do Rio do Peixe Formation as the Adamantina Formation (Ad). (D) Schematic lithostratigraphy of the Bauru Group. The Serra da Galga Formation was previously part of Marília Formation and subdivided in two members, Serra da Galga and Ponte Alta Member. Lithostratigraphic data modified from Batezelli et al. (2019) and Soares et al. (2020b).

Figure 2. (A) Planar-parallel, horizontal or low-angle, laminated sandstone beds. Horizontal, or low-angle planar laminations, are formed by climbing wind ripples. Thin lighter and in-relief laminae correspond to very fine-grained sand and coarse silt deposits named pin stripe lamination by Fryberger and Schenk (1988) (see arrows). Coin: 20 mm in diameter. (B) Planar-parallel, horizontal or low-angle, laminated sandstone beds. Microphotograph of subcritical climbing translatent strata (Hunter, 1977). Note the very fine-grained and coarse silt accumulation at the bottom of each lamina (white arrows). The inverse grading, resulting from the accumulation of coarse-grained clasts at the top of the wind ripple, is barely evident. White patches are calcium carbonate palaeopedogenic precipitation. (C) Photomicrography of medium-grained quartz grain. Rounded, low-relief clast showing microtextures and characterised by bulbous edges (a), elongated depressions (b) and upturned plates (c) highlights aeolian transport (Vos et al., 2014).

Figure 3. (A and B) Sandstone sheet bodies. Figure B emphasises the features of the picture (Figure A). This tabular body is exposed along the road GO178, close to Itajá. The fill consists of poorly sorted and structureless sandstones (a) interlayered with lenticular beds of sandy conglomerate (b). Sometimes the sandstones show planar parallel laminations (c). The upper part of the "sandstone sheet

bodies" displays crudely cross-stratifications (d) and an erosional trough filled with sandy intraformational conglomerates (e). (C) Conglomerate sheet bodies. "Conglomerate sheet bodies" exposed along the road GO164 c. 35 km north to Quirinópolis. Three episodes of conglomerates, structureless and crudely graded to sandstone constitute this channelised bed. (D) Conglomerate tabular bodies. Photo of the second episode of sedimentation (highlighted by dotted lines) of the succession portrayed in figure 3A. Note the upward transition from cobble-sized to pebble-sized clasts. Hammer: 0.3 m high. (E) Conglomerate tabular bodies. The sandstone bed at the top of each conglomerate episode is characterised by planar lamination formed in the upper flow regime (arrowed). This sandstone bed testifies to the abandonment of the bar. Pencil: 145 mm.

Figure 4. (A) Sketch of Itajá pedotype. See text for detailed descriptions. (B) Itajá pedotype. Prismatic structures of Bt horizon on a horizontal bed surface view. Note the clay coatings delimiting the margins of the peds (arrows). Pencil: 145 mm. (C) Itajá pedotype. Photomicrograph of Bt horizon. A mixing of clay and oxides coats the sandy grain constituting a chitonic c/f related distribution pattern. cl-ox = clay-oxide coating; Qz = quartz grain; Lv = basalt fragment. XPL. (D) Itajá pedotype. Coalescent calcareous micritic nodules constitute the Bk horizon. Coin (arrowed): 20 mm. (E) Itajá pedotype. Photomicrograph of Bk horizon. This horizon is characterised by crystallitic b-fabric and calcite coatings around the grains. c = calcite coating; Qz = quartz grain; Ls = chert fragment. XPL. (F) Itajá pedotype. Bkm horizon shows breccias of micritic laminated calcite. (G) Itajá pedotype. Bkm horizon (arrowed) is constituted of micritic calcite and it is typically laterally discontinuous; its lateral extent is up to 30 m and the thickness is up to 0.6 m. The cliff is c. 15 m high.

Figure 5. (A) Sketch of Avá pedotype. See text for detailed descriptions. (B) Avá pedotype. This palaeosol has no more than 0.4 m of thickness and is constituted of A and C horizons. A is massive and C shows relics of planar laminations deposited by climbing wind ripples. Both horizons contain pedogenic calcareous nodules.

Figure 6. Sketch showing the cyclical alternation between depositional processes and pedogenesis in north-western area of the upper portion of the Bauru Group. In this area the cyclicity palaeosols/deposits is controlled by climate. A more humid climate favoured the growth of the vegetation, which promoted the pedogenesis sheltering the topographic surface; a more arid climate caused the rarefication of the vegetation, the death of the soil and the erosion, transport and deposition by wind action. (A) Typical section in the north-western area. (B) Ephemeral rivers which are active in more humid climatic phase. (C) Desert sand sheet areas with nabkha dunes during the more arid climatic phase. (D) Pedogenesis and generation of Aridisols or Entisols during the more humid climatic phase.

Figure 7. North-eastern sector of the upper portion of the Bauru Group. (A-D) Proximal area of the distributive fluvial system. (A) Stratigraphic section showing a sequence of four "sheet sandstone bodies", interpreted as river channels, separated at the extremity by two Pataxó pedotype (Inceptisol) and interlayered to Krenak pedotype (Entisol) or “muddy sandstone beds” (floodplain deposits). The "sheet sandstone bodies" n. 1, 2 and 4 correspond to the first type described, whereas the "sheet sandstone bodies" n. 3 coincides with the second type. See text for more details. (B-D) These images represent (B) the original picture, (C) the identifications of sedimentary structures and bounding surfaces by field drawings and (D) the architectural interpretative sketch. (E) Distal area of the fluvial distributary system. Ribbon-shaped channel deposits are interlayered with palaeopedogenised floodplain deposits. (F) Proximal area of the fluvial distributary system. Greenish-grey rhizohaloes (arrowed) in Bw horizon of Pataxó pedotype (Inceptisol) are indicative of temporary conditions of stagnant waters within the roots channels. Lafarge Quarry, Ponte Alta (MG). Coin: 25 mm. (G) Proximal area of the fluvial distributary system. Clay coating pedofeature can be sometimes found in Bw horizons of Pataxó pedotype (Inceptisol). (H) Medial area of the fluvial distributary system. Photomicrograph of Bwk horizon of Pataxó pedotype (Inceptisol) in the medial portion of the fluvial system. cl = thin clay coating; cr = crystallitic b-fabric. XPL.

Figure 8. Sketch showing the cyclical alternation between depositional processes and pedogenesis in the north-eastern sector of the upper portion of the Bauru Group. The cyclicity of palaeosols/deposits is controlled by alluvial depositional processes. (A) Typical section in the proximal area of the fluvial system in the north-eastern sector. (B) Perennial river deposits dominate the proximal part; palaeosols are Inceptisols and Entisols. (C) Typical section in the medial area of the fluvial system in the north-eastern sector. (D) In the medial area, channel rivers decrease in size and the palaeosol abundance increases. Inceptisols and Entisols are dominant. (E) Typical section in NW distal area of the fluvial system in north-eastern sector. (F) The NW distal area was probably dominated by high ground water. The palaeosols, commonly Inceptisols, show ground water gley. (G) Typical section in the W distal part of the fluvial system in the north-eastern sector. (H) In the W distal area depositional processes by unconfined subaqueous flow dominated and palaeosol (Entisols) are less abundant.

Figure 9. South-eastern sector of the upper portion of the Bauru Group. (A) Tabular sandstone beds are the typical architecture of this area. Most of the thickness of these beds shows pedogenic features; sometimes only 0.1-0.6 m at the base still displays sedimentary structures. (B) Base of the tabular beds with alternated alignments of mud clasts which are interpreted as traction carpet sedimentary structure. Coin: 22 mm. (C) Upper distinctness of this Echaporã pedotype (Inceptisol) is abrupt upper with unconfined deposits. Note in A horizon root casts (yellow arrow) and rhizohaloes (light blue arrows) distinctness Pencil: 145 mm. (D) Photomicrograph of Bw horizon of Echaporã pedotype (Inceptisol). Quartz and feldspar grains are surrounded by thin clay coatings (cl). XPL. (E) Bw horizon of Echaporã pedotype (Inceptisol) characterised by incipient prismatic structures (see yellow dotted lines) separated by calcite coatings (arrowed). Pencil: 145 mm.

Figure 10. (A) Echaporã pedotype (Inceptisol) showed in a sketch where this is alternated at the base and at the top with unconfined deposits. See the text for description. (B) Kaingang pedotype (Vertisol) is a typically characterised by slickenside and mukkara structure in Bss and Bssk horizons. (C) Larger vision of the Kaingang pedotype (Vertisol) in which is possible to notice at the top of this

palaeosol profile the undulated surfaces that likely correspond to the gilgai surface of Vertisols and underlying the mukkara structure.

Figure 11. Weathering molar ratios of a section of Echaporã pedotypes (Inceptisol) alternated to deposits in the south-eastern sector of the upper part of the Bauru Group close to Echaporã town along the railway SP333. Al_2O_3/SiO_2 = clayeyness; Ba/Sr and Rb/Sr = leaching and hydrolysis; $\Sigma Bases/Al_2O_3$ = hydrolysis; C.I.A. ($100xAl_2O_3/ Al_2O_3+Ca_2O+NaO+K_2O$) = weathering index. Note the anomalous values of Ba/Sr, Rb/Sr, $\Sigma Bases/Al_2O_3$ and C.I.A in correspondence of the horizons Bk, Bwk and Ck and that the weathering molar ratios of A/Bw or Bw horizons do not vary significantly along the palaeosol profiles and are very similar to values of the C horizons or original deposits. See the text for more explanations.

Figure 12. Sketch showing the cyclical alternation between depositional processes and pedogenesis in the south-eastern sector of the upper portion of the Bauru Group. (A) Typical section in the south-eastern sector. The cyclicity of palaeosols/deposits is controlled by unconfined flow, probably developed at the terminal area of a distributive fluvial system. (B) High-concentrated and high-transport capacity flows deposited up to 3 m of tabular sandstone beds. (C) Inceptisols (Echaporã pedotype) developed over these deposits for a time of the order of 10^4-10^5 years. Palaeoclimatic data indicate subhumid conditions.

Figure 13. Plot of mean and standard deviation of mean annual precipitation (MAP) from physical and geochemical features of the palaeosols of the three study areas. NW: north-western area (number of measurements: 11). Medial NE: medial portion of the fluvial system of the north-eastern area (number of measurements: 4). Proximal NE: proximal portion of the fluvial system of the north-eastern areas (number of measurements: 2). SE: south-eastern area (number of measurements: 14).

Figure 14. (A) Principal component analysis (PCA) of the major and minor geochemical elements of the palaeosols of the three study sectors. See discussion in the text. (B, C) Plot of mean and standard deviation of percent weight distribution of Fe_2O_3 (B) and TiO_2 (C) of the three study sectors. NW: north-

western sector (number of samples: 51). NE: north-eastern sector (number of samples: 20). SE: south-eastern sector (number of samples: 16). (D) Ti/Al molar weathering ratio in three palaeosol succession of the three study sectors. Note the difference in the palaeosols of the different sectors and the constant value for the same profile of palaeosol. (E) Plot of mean and standard deviation of Ti/Al molar weathering ratio from palaeosols of the three study sectors. NW: north-western sector (number of samples: 51). NE: north-eastern sector (number of samples: 20). SE: south-eastern sector (number of samples: 16).

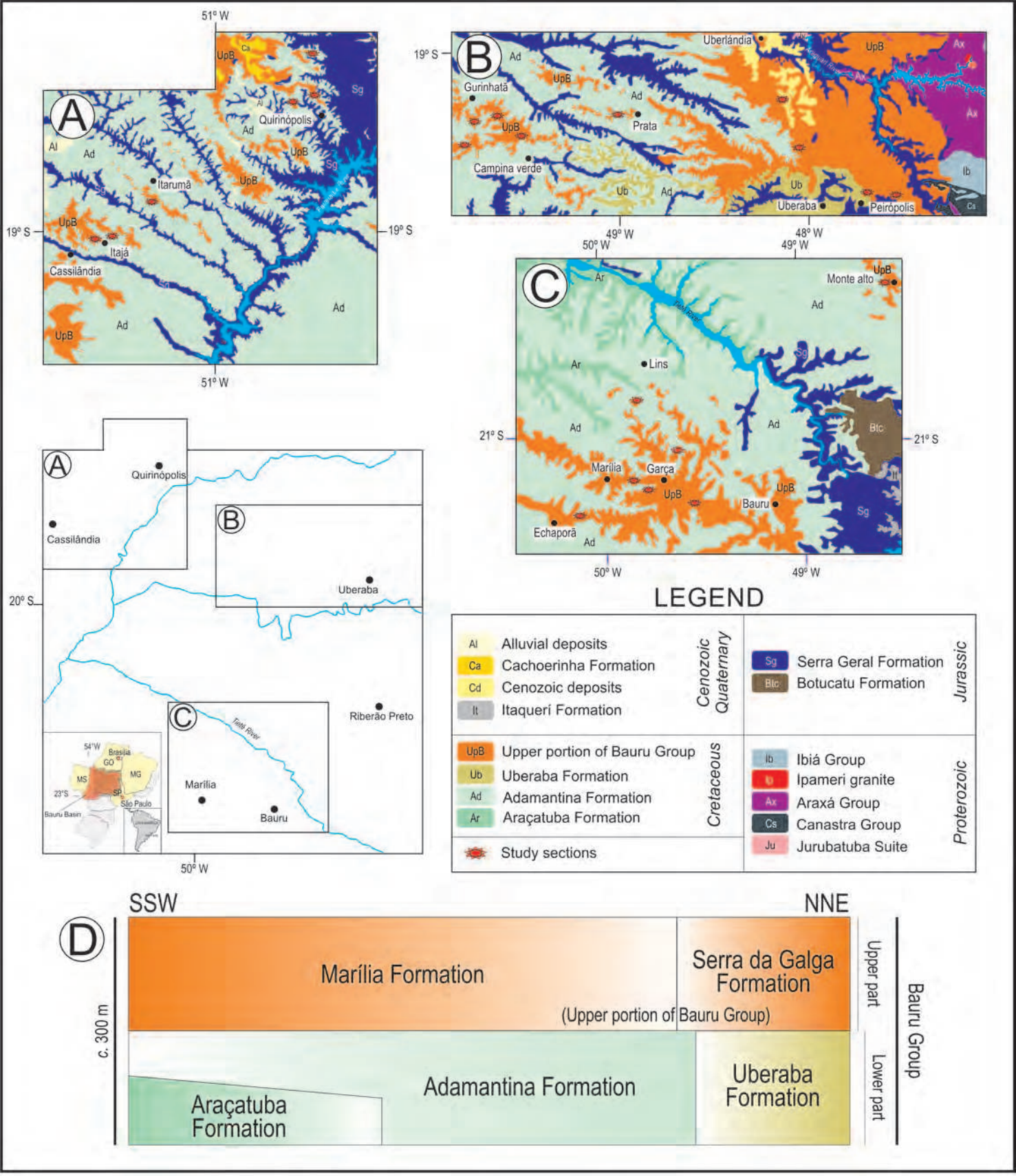
A
B
C
D
51° W
19° S
Quirinópolis
Itarumã
Itajá
Cassilândia
Uberlândia
Gurinhatã
Prata
Campina verde
Uberaba
Peirópolis
49° W
48° W
50° W
Monte alto
Lins
Marília
Garça
Bauru
Echaporã
21° S
20° S
Riberão Preto
Tietê River
Paraná River
Brasília
São Paulo
Bauru Basin
LEGEND
Alluvial deposits
Cachoerinha Formation
Cenozoic deposits
Itaqueri Formation
Cenozoic Quaternary
Serra Geral Formation
Botucatu Formation
Jurassic
Upper portion of Bauru Group
Uberaba Formation
Adamantina Formation
Araçatuba Formation
Cretaceous
Ibiá Group
Ipameri granite
Araxá Group
Canastra Group
Jurubatuba Suite
Proterozoic
Study sections
SSW
NNE
Marília Formation
Serra da Galga Formation
(Upper portion of Bauru Group)
Araçatuba Formation
Adamantina Formation
Uberaba Formation
c. 300 m
Upper part
Lower part
Bauru Group

FIGURE 1

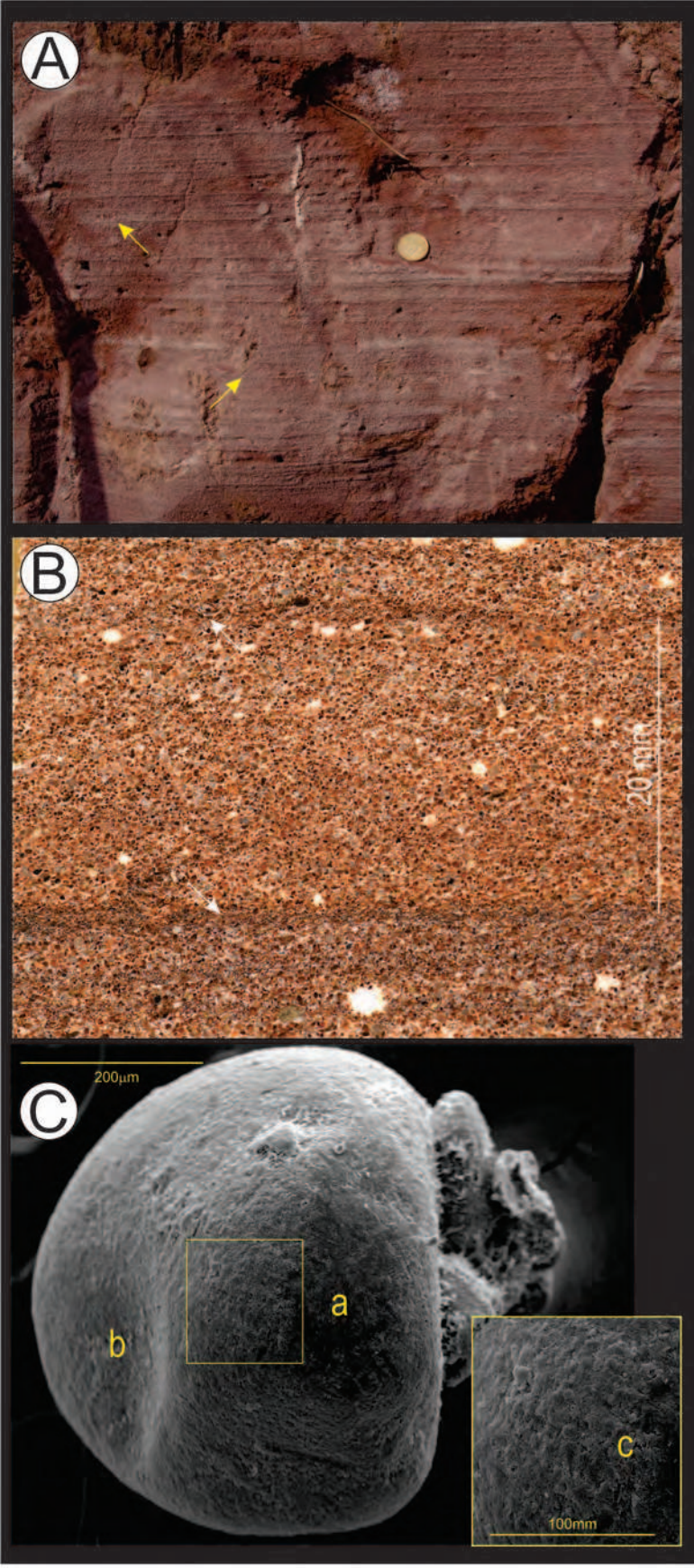

FIGURE 2

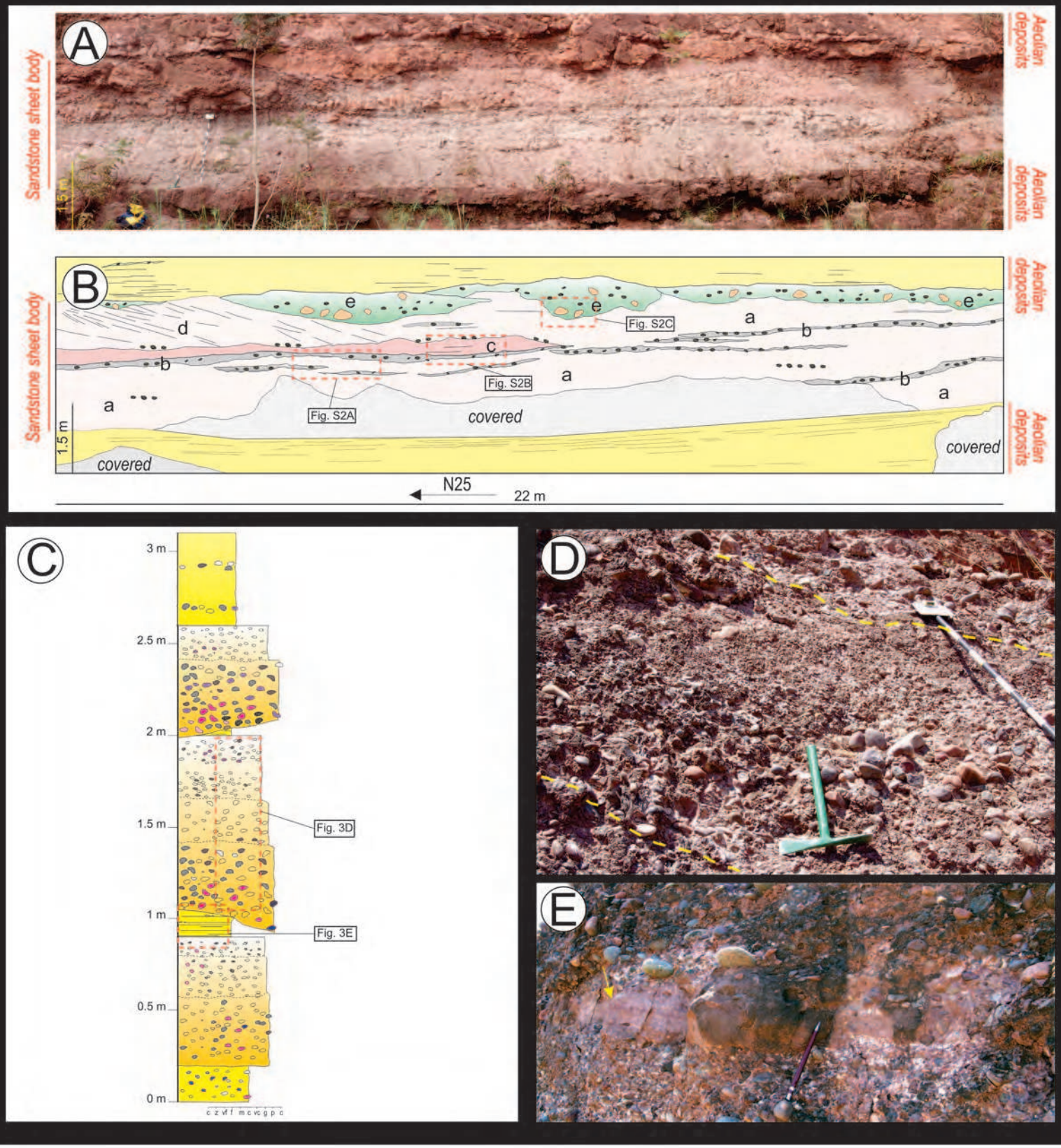
A
Sandstone sheet body
Aeolian deposits
Aeolian deposits
1.5 m
B
Sandstone sheet body
Aeolian deposits
Aeolian deposits
Aeolian deposits
a
b
c
d
e
Fig. S2A
Fig. S2B
Fig. S2C
covered
covered
covered
1.5 m
N25
22 m
C
3 m
2.5 m
2 m
1.5 m
1 m
0.5 m
0 m
Fig. 3D
Fig. 3E
D
E

FIGURE 3

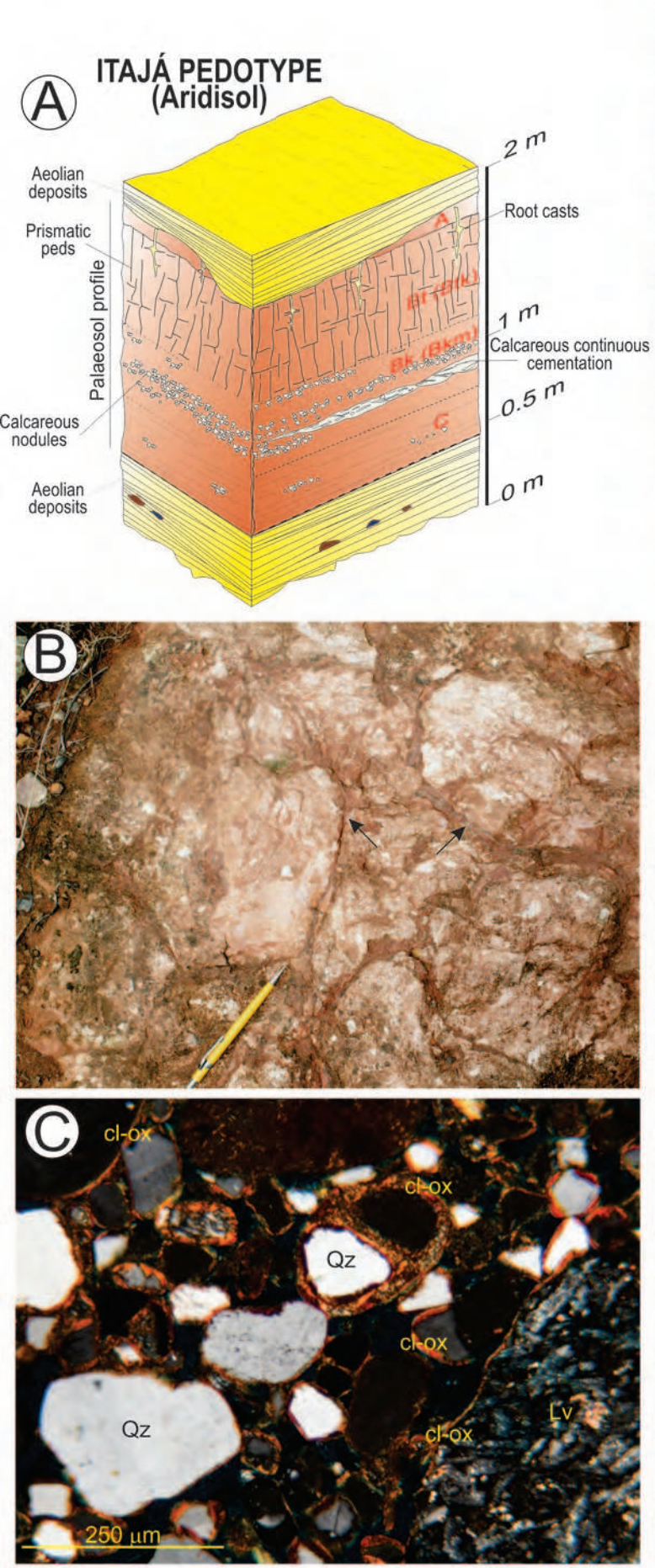
A
ITAJÁ PEDOTYPE
(Aridisol)
Aeolian deposits
Prismatic peds
Palaeosol profile
Calcareous nodules
Aeolian deposits
2 m
Root casts
1 m
Calcareous continuous cementation
0.5 m
0 m
A
Bt1 (Bk)
Bk (Bkm)
C
B
C
cl-ox
cl-ox
Qz
cl-ox
Qz
cl-ox
Lv
250 µm
D
E
Qz
Qz
Ls
c
c
500 µm
F
0.15 m
G

FIGURE 4

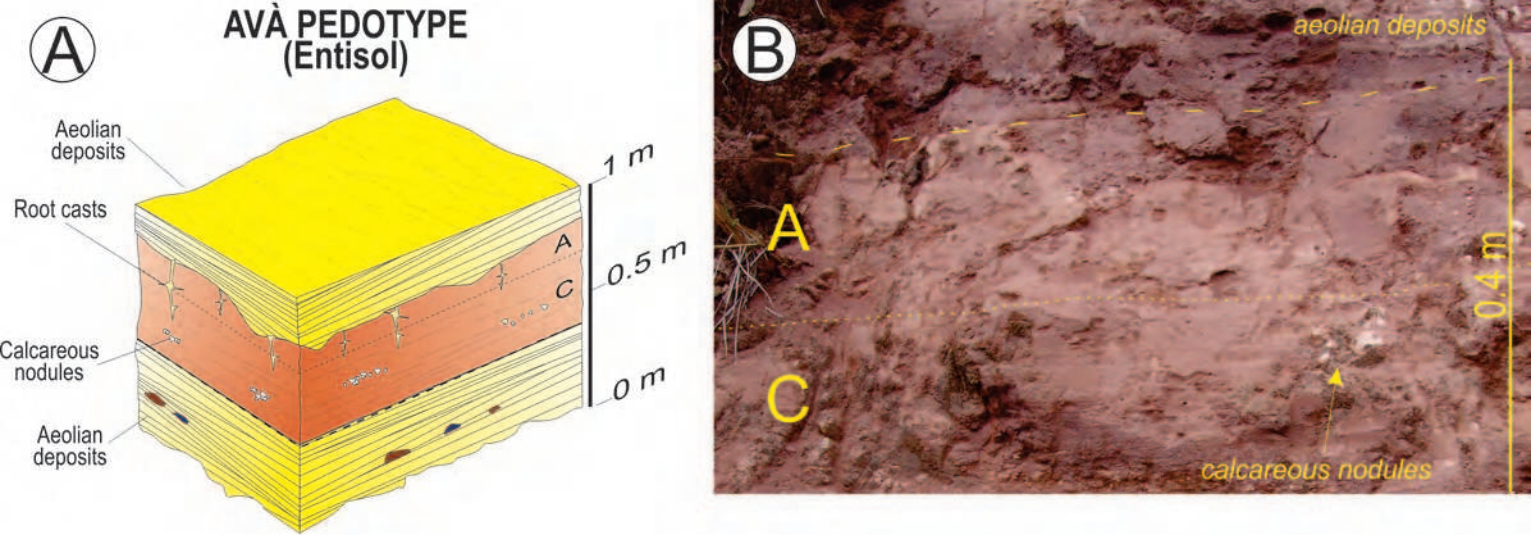
A
AVÀ PEDOTYPE
(Entisol)
Aeolian deposits
Root casts
Calcareous nodules
Aeolian deposits
A
C
1 m
0.5 m
0 m
B
aeolian deposits
A
C
0.4 m
calcareous nodules

FIGURE 5

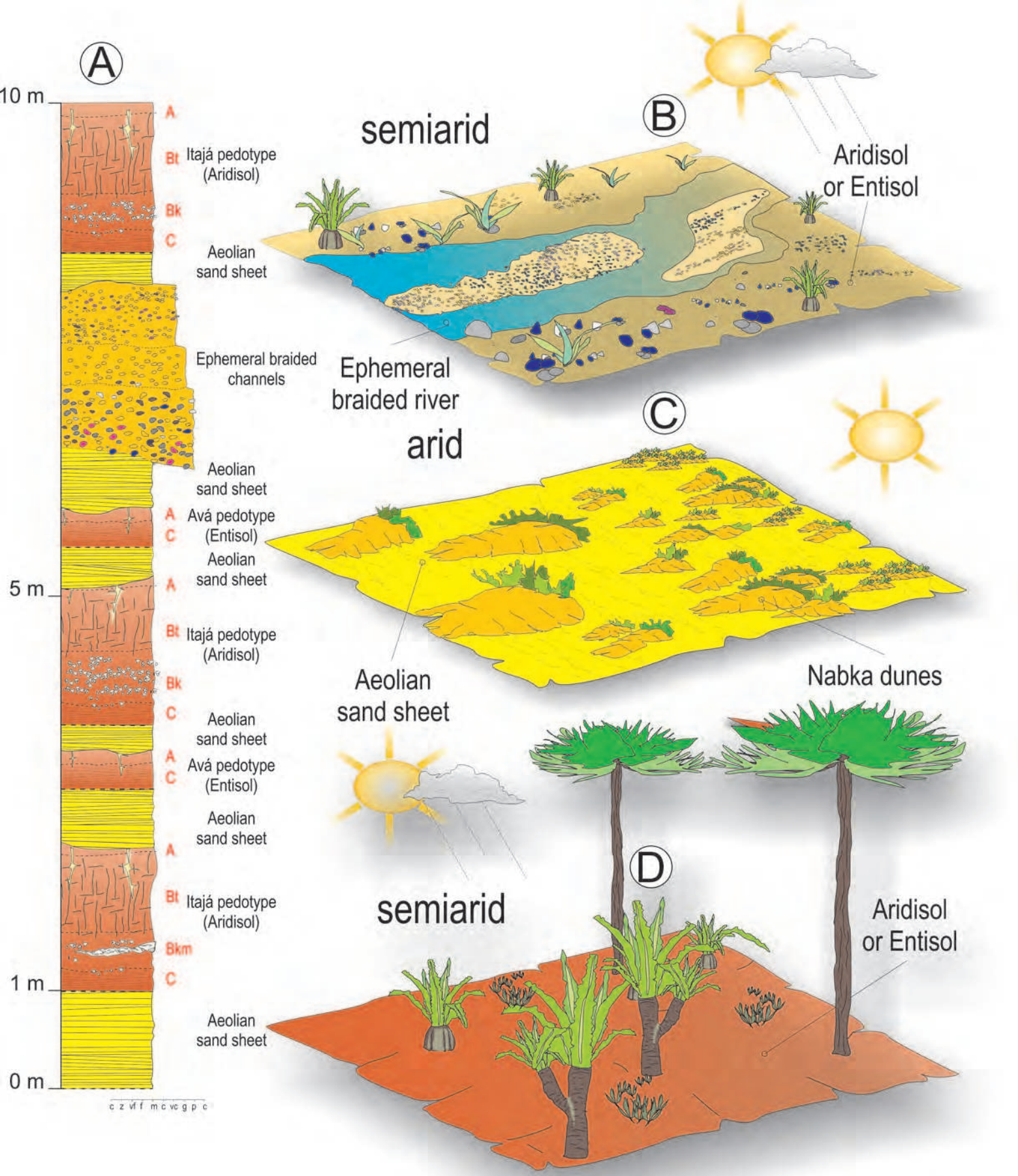
A
10 m
A
Bt
Itajá pedotype
(Aridisol)
Bk
C
Aeolian
sand sheet
Ephemeral braided
channels
Aeolian
sand sheet
A
C
Avá pedotype
(Entisol)
Aeolian
sand sheet
5 m
A
Bt
Itajá pedotype
(Aridisol)
Bk
C
Aeolian
sand sheet
A
C
Avá pedotype
(Entisol)
Aeolian
sand sheet
A
Bt
Itajá pedotype
(Aridisol)
Bkm
C
1 m
Aeolian
sand sheet
0 m
c z vf f m c vc g p c
B
semiarid
Aridisol
or Entisol
Ephemeral
braided river
C
arid
Aeolian
sand sheet
Nabka dunes
D
semiarid
Aridisol
or Entisol

FIGURE 6

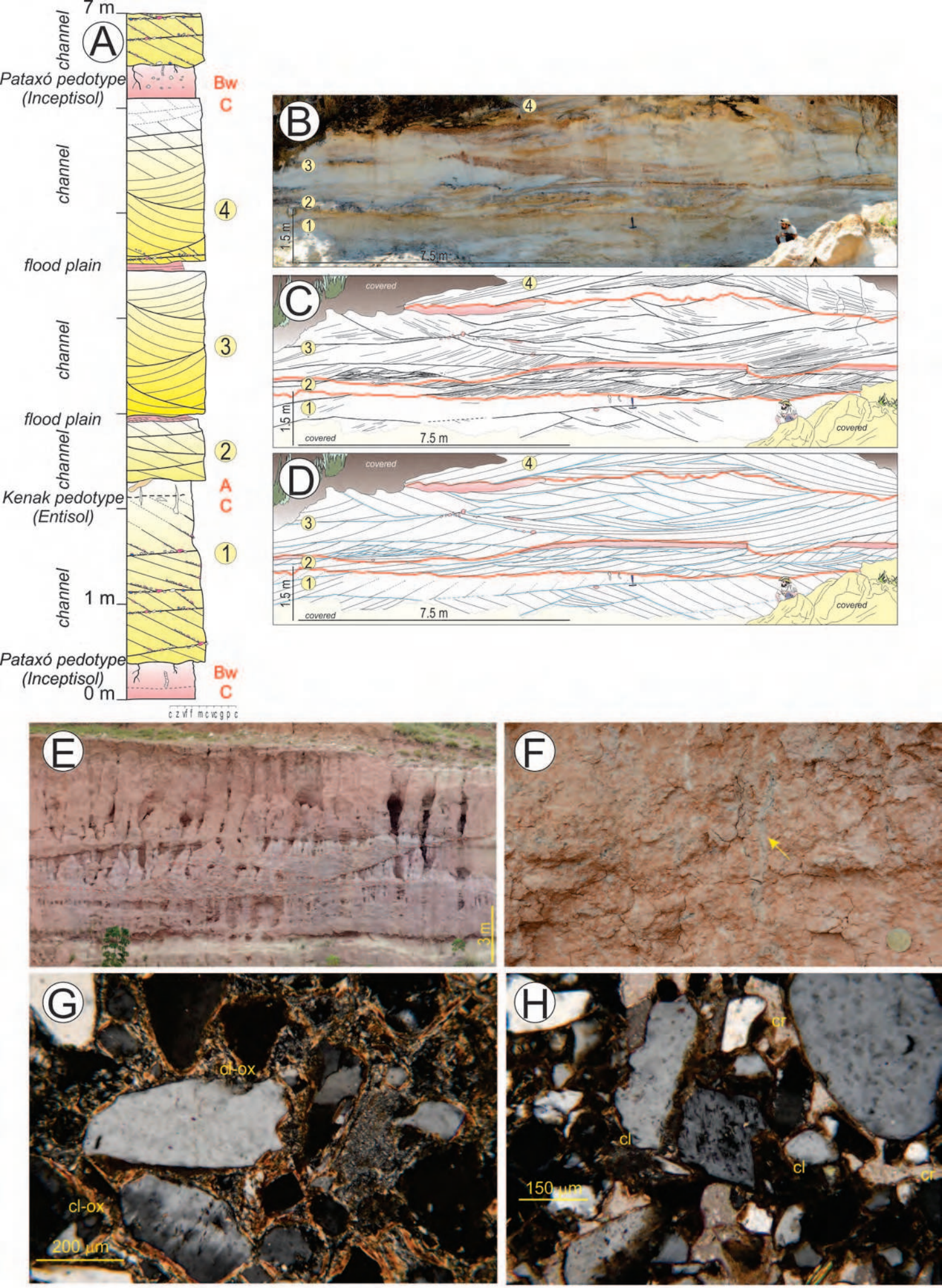
A
7 m
channel
Pataxó pedotype
(Inceptisol)
Bw
C
channel
4
flood plain
channel
3
flood plain
channel
2
A
C
Kenak pedotype
(Entisol)
1
channel
1 m
Pataxó pedotype
(Inceptisol)
Bw
C
0 m
c z vf f m c vc g p c
B
4
3
2
1
1.5 m
7.5 m
C
covered
4
3
2
1
1.5 m
covered
7.5 m
covered
D
covered
4
3
2
1
1.5 m
covered
7.5 m
covered
E
3 m
F
G
cl-ox
cl-ox
200 µm
H
cr
cl
cl
cr
150 µm

FIGURE 7

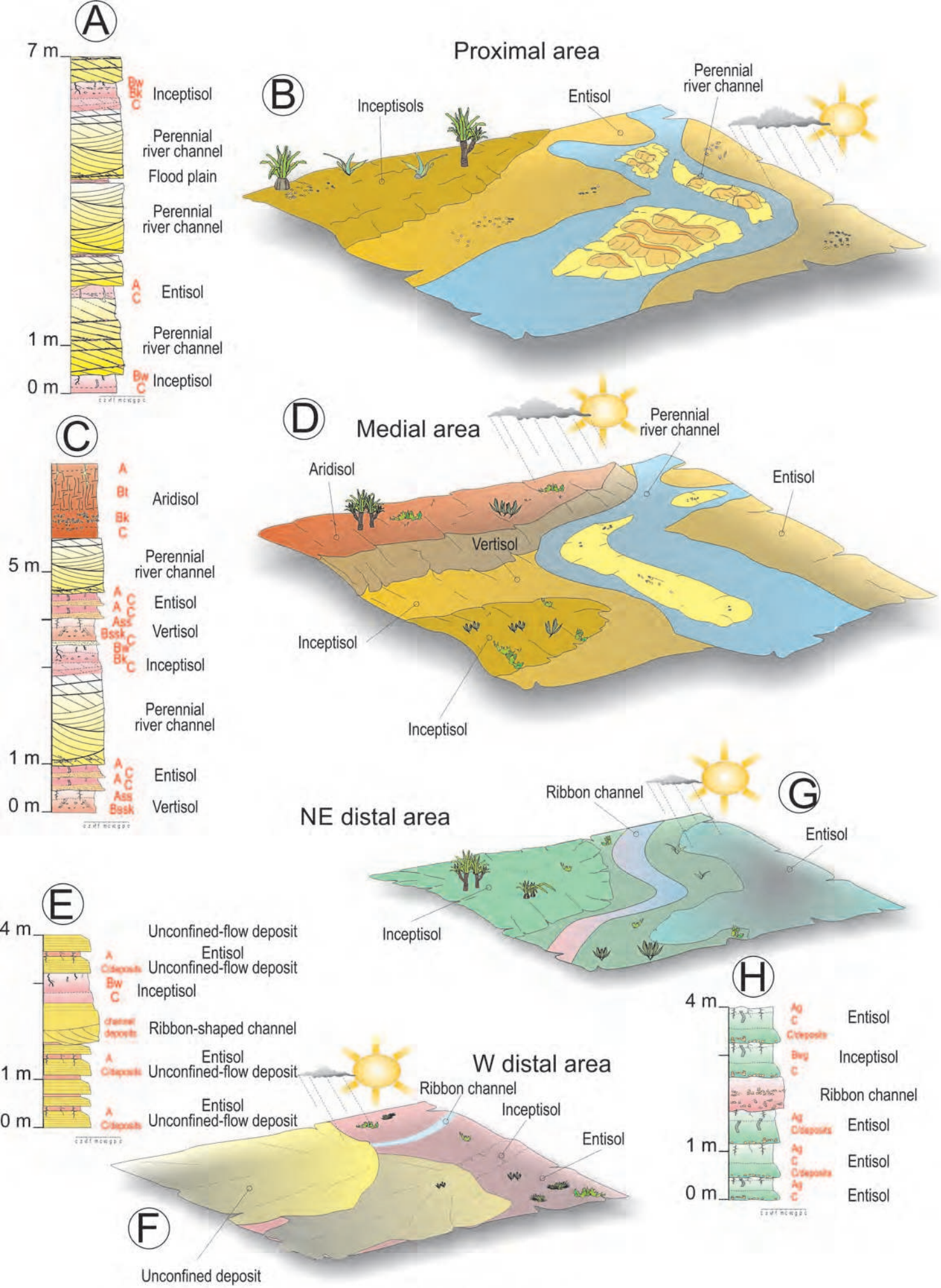
A
7 m
Inceptisol
Perennial river channel
Flood plain
Perennial river channel
Entisol
1 m
Perennial river channel
0 m
Inceptisol
B
Proximal area
Inceptisols
Entisol
Perennial river channel
C
Aridisol
5 m
Perennial river channel
Entisol
Vertisol
Inceptisol
Perennial river channel
1 m
Entisol
0 m
Vertisol
D
Medial area
Perennial river channel
Aridisol
Entisol
Vertisol
Inceptisol
Inceptisol
G
NE distal area
Ribbon channel
Entisol
Inceptisol
E
4 m
Unconfined-flow deposit
Entisol
Unconfined-flow deposit
Inceptisol
Ribbon-shaped channel
Entisol
1 m
Unconfined-flow deposit
Entisol
0 m
Unconfined-flow deposit
H
4 m
Entisol
Inceptisol
Ribbon channel
Entisol
1 m
Entisol
0 m
Entisol
W distal area
Ribbon channel
Inceptisol
Entisol
F
Unconfined deposit

FIGURE 8

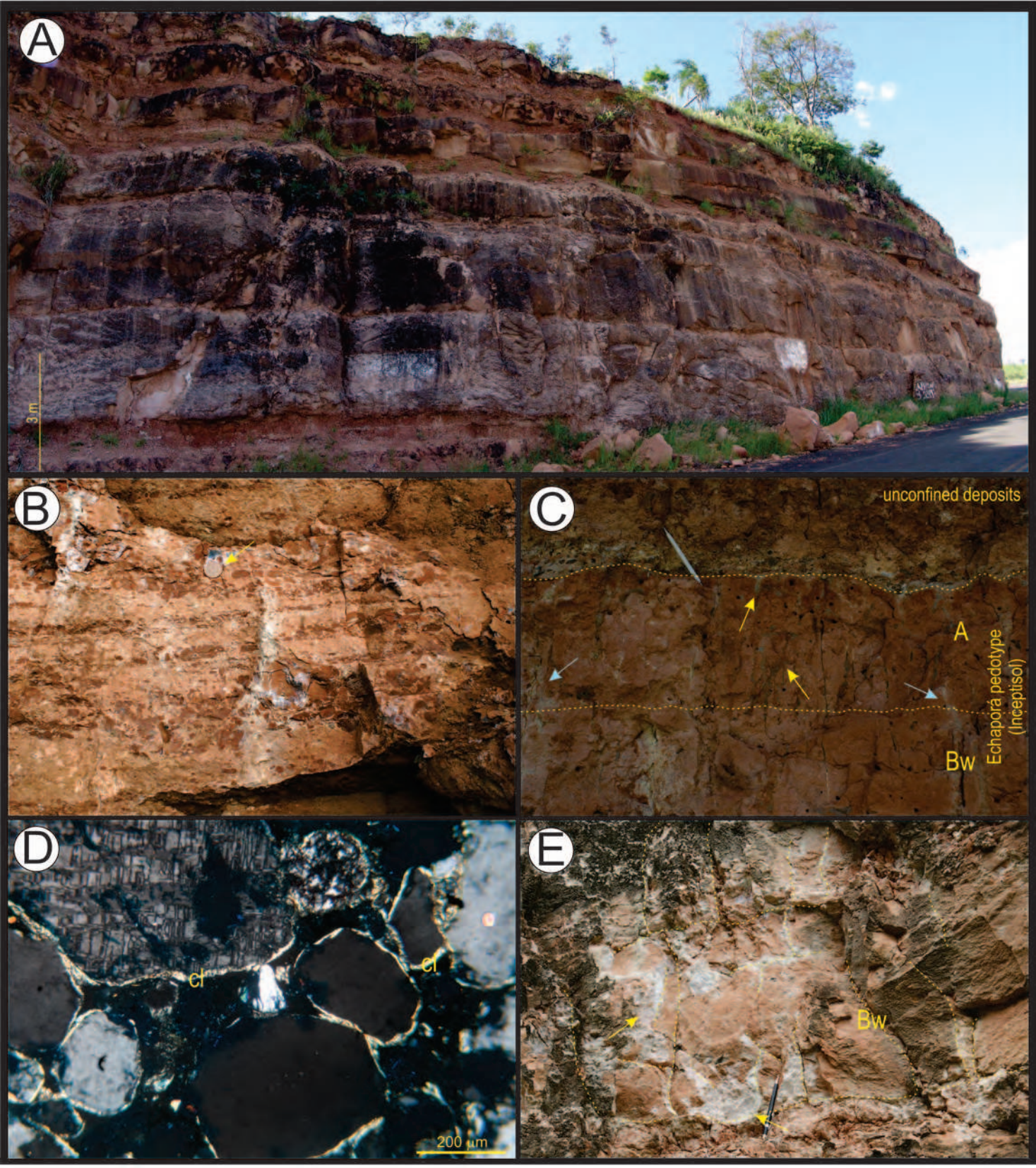
A
3 m
B
C
unconfined deposits
A
Bw
Echapora pedotype
(Inceptisol)
D
cl
cl
200 µm
E
Bw

FIGURE 9

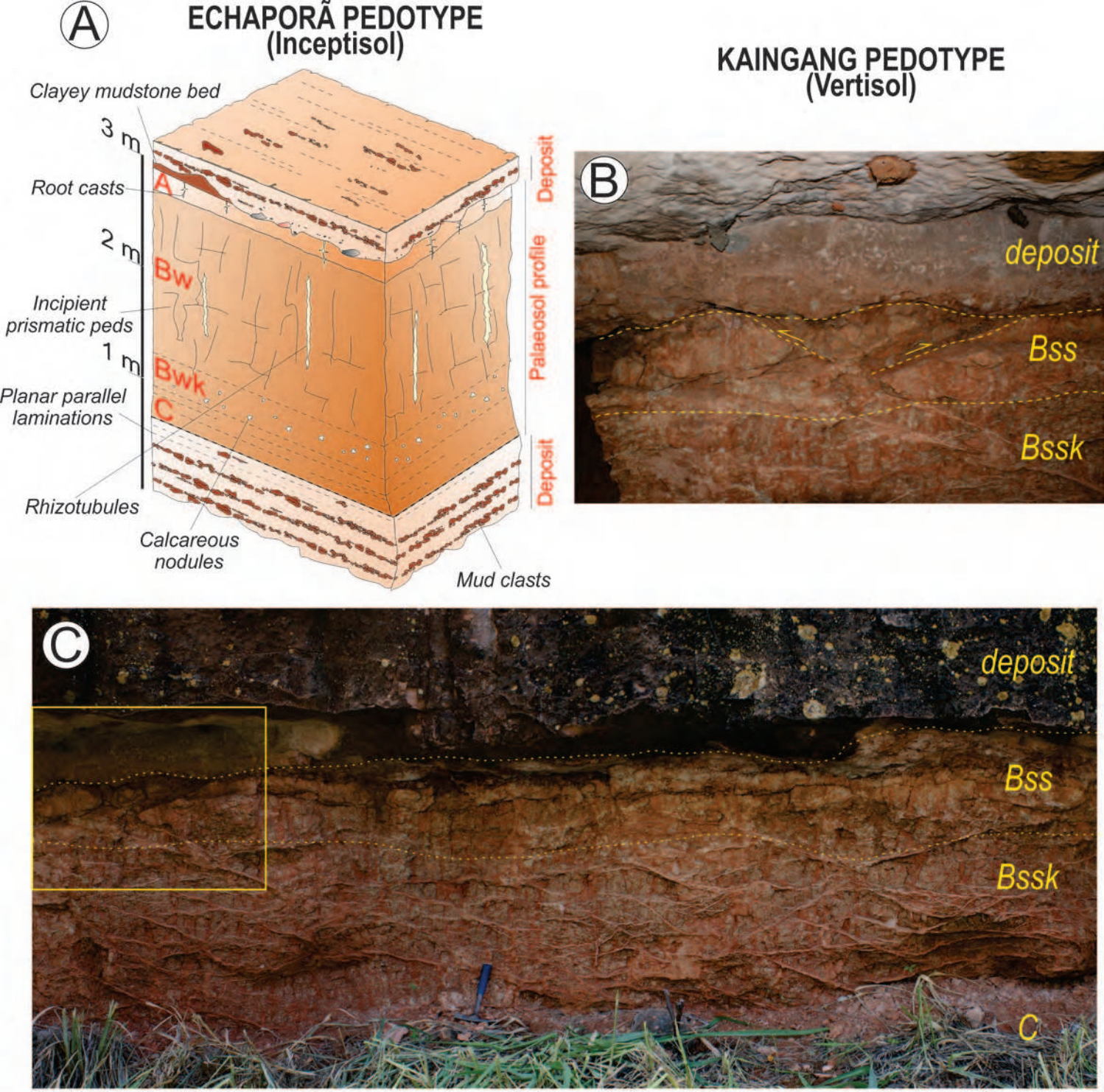
A
ECHAPORÃ PEDOTYPE
(Inceptisol)
Clayey mudstone bed
3 m
Root casts
A
2 m
Bw
Incipient
prismatic peds
1 m
Bwk
Planar parallel
laminations
C
Rhizotubules
Calcareous
nodules
Mud clasts
Deposit
Palaeosol profile
Deposit
KAINGANG PEDOTYPE
(Vertisol)
B
deposit
Bss
Bssk
C
deposit
Bss
Bssk
C

FIGURE 10

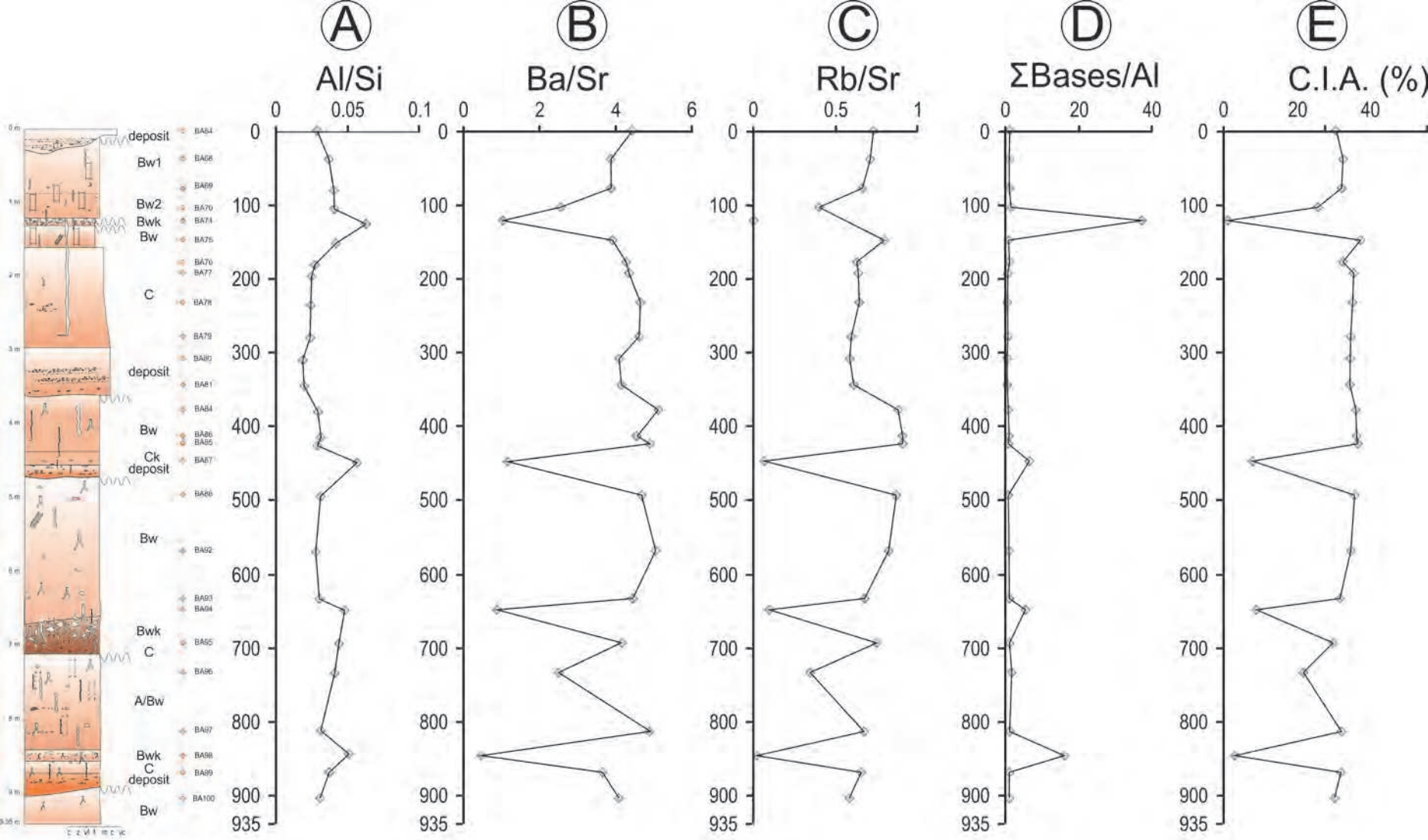
A
Al/Si
0
0.05
0.1
B
Ba/Sr
0
2
4
6
C
Rb/Sr
0
0.5
1
D
ΣBases/Al
0
20
40
E
C.I.A. (%)
0
20
40
0
100
200
300
400
500
600
700
800
900
935
deposit
Bw1
Bw2
Bwk
Bw
C
deposit
Bw
Ck
deposit
Bw
Bwk
C
A/Bw
Bwk
C
deposit
Bw

FIGURE 11

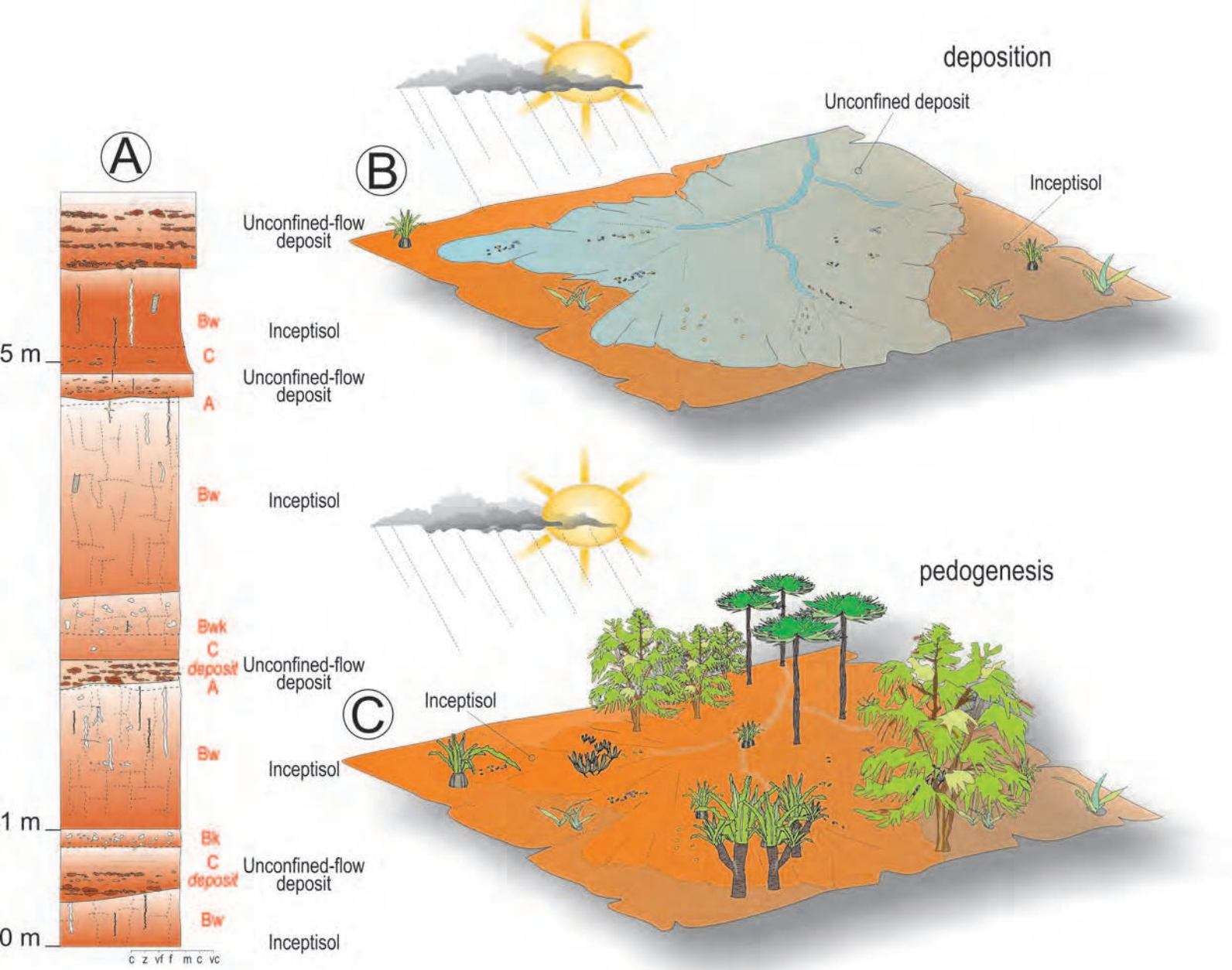
A
B
C
deposition
Unconfined deposit
Inceptisol
Unconfined-flow deposit
pedogenesis
Inceptisol
5 m
1 m
0 m
Bw
C
A
Bwk
C deposit
A
Bk
C deposit
c z vf f m c vc
Inceptisol
Unconfined-flow deposit
Inceptisol
Unconfined-flow deposit
Inceptisol
Unconfined-flow deposit
Inceptisol

FIGURE 12

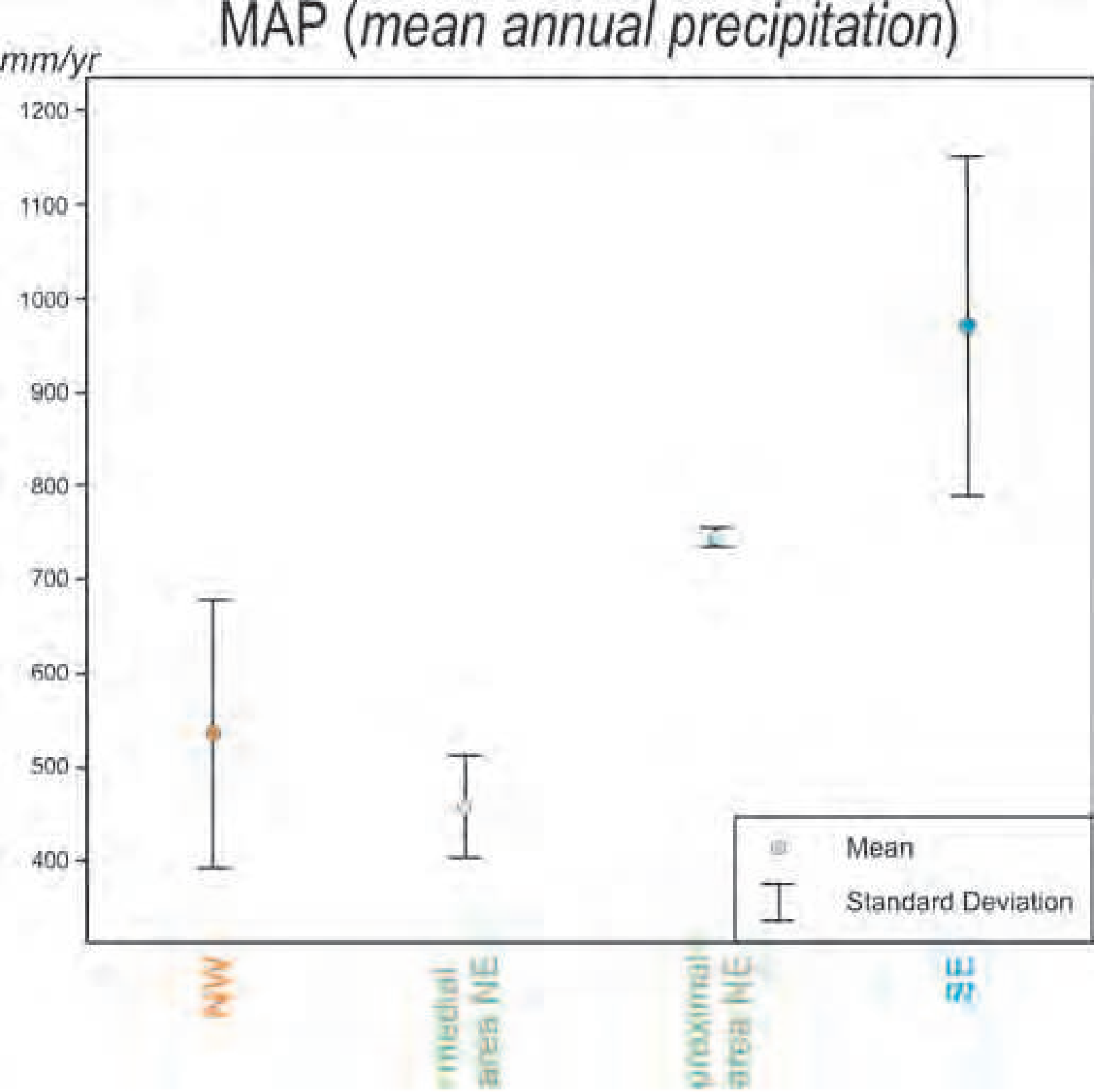
MAP (mean annual precipitation)
mm/yr
1200
1100
1000
900
800
700
600
500
400
Mean
Standard Deviation
NW
medial
area NE
proximal
area NE

FIGURE 13

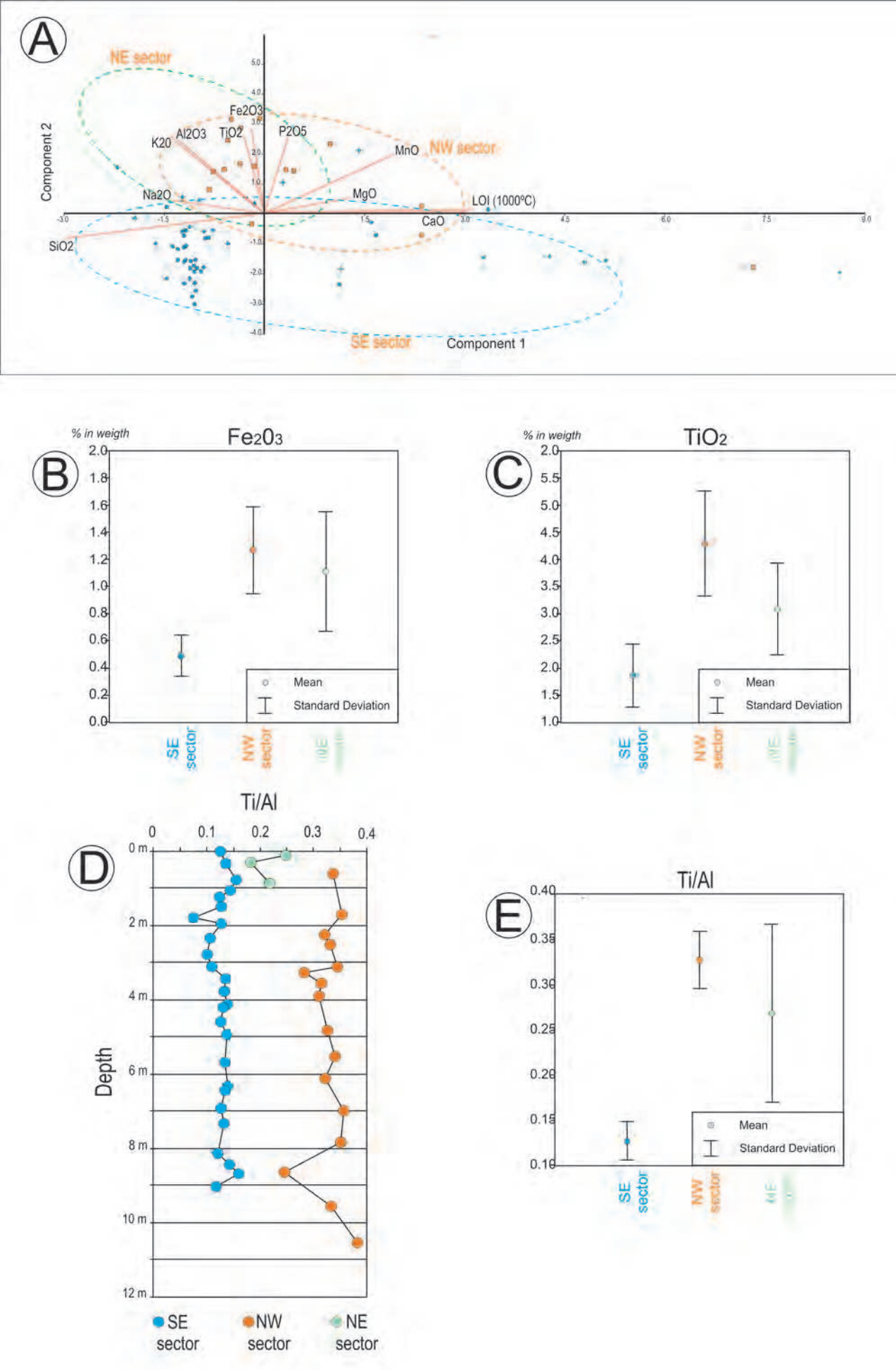
A
NE sector
Component 2
Fe2O3
K20
Al2O3
TiO2
P2O5
MnO
NW sector
Na2O
MgO
LOI (1000°C)
CaO
SiO2
SE sector
Component 1
B
% in weigth
Fe2O3
Mean
Standard Deviation
SE sector
NW sector
C
% in weigth
TiO2
Mean
Standard Deviation
SE sector
NW sector
D
Ti/Al
Depth
0 m
2 m
4 m
6 m
8 m
10 m
12 m
SE sector
NW sector
NE sector
E
Ti/Al
Mean
Standard Deviation
SE sector
NW sector

FIGURE 14

North-western sector								
DEPOSITS %	Planar-parallel, horizontal or low-angle, laminated sandstone beds (aeolian deposits) %	Sandstone sheet bodies (river deposits) %	Conglomerate sheet bodies (river deposits) %	PALAEOSOLS %	Itajá pedotype (Aridisol) %	Avá pedotype (Entisol) %	Vertisols %	Alfisols %
35	28	4	3	65	38	16	6	5

North-eastern sector								
	DEPOSITS %	Channelised %	Unchannelised %	PALAEOSOLS %	Krenak pedotype (Entisol) %	Pataxó pedotype (Inceptisol) %	Aranã pedotype (Vertisol) %	Mukuriñ pedotype (Aridisol) %
Proximal	63	Sheet sandstone bodies 57	Muddy sandstone beds 6	37	10	27	-	-
Medial	35	Sheet sandstone bodies 22	Muddy sandstone beds 13	65	34	14	10	7
Distal	75	Ribbon sandstone bodies 8	Tabular bed of sandstone grading to mudstone 62	25	17	8	-	-

South-eastern sector				
DEPOSITS %	Tabular sandstone beds %	PALAEOSOLS %	Echaporã pedotype (Inceptisol) %	Kaingang pedotype (Vertisol) %
8	8	92	90	2

TABLE S1

Major and minor oxides (weight percentage) of north-western sector													
Sample	Depth m	SiO_2	TiO_2	Al_2O_3	Fe_2O_3	MnO	MgO	CaO	Na_2O	K_2O	P_2O_5	LOI	Total
P2H1	60	83.08	1.02	3.87	3.51	0.042	2.64	0.92	0.09	1.27	0.058	3.8	100.3
P2H2	170	82.44	1.31	4.75	4.34	0.046	1.83	0.74	0.16	1.66	0.051	3.08	100.4
P2H3	225	61.18	1.03	4.11	3.56	0.058	4.5	10.31	0.09	1.23	0.054	13.6	99.7
P2H4	250	75.56	1.36	5.25	4.41	0.082	3.4	2.21	0.1	1.49	0.055	6.04	100
P2H5	310	74.47	1.36	5.05	4.48	0.069	3.15	3.36	0.14	1.62	0.072	6.38	100.2
CI 1	325	32.06	0.394	1.78	1.59	0.041	12.47	20.93	0.03	0.37	0.056	29.8	99.5
CI 2	355	82.29	1.26	5.12	4.52	0.069	1.68	0.53	0.17	1.78	0.08	2.81	100.3
CI 3	390	65.75	0.814	3.35	3.23	0.052	4.05	9.62	0.04	0.76	0.079	12	99.8
CI 4	485	78.14	1.35	5.28	4.55	0.038	2.81	1.53	0.15	1.93	0.084	4.59	100.4
CI 5	550	76.46	1.37	5.15	4.52	0.06	2.31	2.62	0.19	1.89	0.085	4.93	99.6
CI 6	610	72.7	1.35	5.36	4.46	0.04	3.02	3.71	0.17	2.01	0.074	6.72	99.6
CI 7	695	74.45	1.66	5.95	5.28	0.103	2.89	2.19	0.21	2.11	0.096	5.4	100.3
CI 8	780	73.3	1.59	5.81	5.21	0.049	2.75	3.33	0.2	2.09	0.173	5.81	100.3
CI 9	865	75.37	1.25	6.55	4.42	0.069	3.05	1.87	0.2	2.34	0.094	5.1	100.3
CI 10	955	73.19	1.62	6.21	5.51	0.068	2.23	3.18	0.21	2.24	0.122	5.27	99.8
CI 11	1050	63.48	1.49	5	5.19	0.065	1.86	10.01	0.21	1.81	0.131	10.4	99.6

Major and minor oxides (weight percentage) of north-eastern sector													
Sample	Depth m	SiO2	TiO2	Al2O3	Fe2O3	MnO	MgO	CaO	Na2O	K2O	P2O5	LOI	Total
P1 top	25	77.22	1.744	7.78	4.32	0.083	1.85	1.11	0.15	2.23	0.325	2.9	99.7
P1 inter	65	76.04	1.619	8.46	4.83	0.076	1.94	1.39	0.18	2	0.324	3.16	100
P1 base	100	81.6	0.615	7.62	2.39	0.026	1.6	0.87	0.12	2.1	0.159	2.72	99.8
P2 top	690	82.99	1.22	6.32	3.1	0.033	1.53	0.22	0.1	2.25	0.055	2.19	100
P2 inter	705	86.35	0.703	5.53	1.91	0.025	1.15	0.17	0.1	2.13	0.045	1.79	99.9
P2 base	770	83.45	1.053	6.18	2.92	0.072	1.32	0.34	0.15	2.19	0.142	2.02	99.8
PCT-1	30	77.81	0.689	8.55	3.32	0.065	1.68	1.19	0.25	2.41	0.133	3.7	99.797
PCT-2	60	71.95	0.608	7.72	2.93	0.059	1.51	5.58	0.22	2.15	0.079	7.02	99.826
PCT-3	90	55.15	0.488	5.92	2.39	0.102	1.11	17.1	0.18	1.63	0.102	15.8	99.972
PCT-4	120	83.02	0.322	7.45	1.53	0.03	1.19	0.74	0.22	2.33	0.055	2.94	99.827
PI5-1	870	79.1	1.616	5.83	3.22	0.055	1.5	2.83	0.09	2.2	0.216	3.15	99.807
PI5-2	910	56.74	1.274	3.92	2.14	0.039	1	17.57	0.08	1.49	0.129	15.6	99.982
PI5-3	935	80.23	1.676	6.07	3.24	0.036	1.34	1.58	0.12	2.21	0.089	3.24	99.831
PI5-4	945	75.41	1.738	7.86	4.25	0.048	1.9	1.56	0.16	3.02	0.135	3.71	99.791
PI4-1	1170	51.27	0.993	6.83	3.25	0.087	1.76	17.03	0.13	2.38	0.426	15.8	99.956
PI4-2	1220	54.54	1.022	7.92	3.9	0.181	2	13.9	0.16	2.75	0.487	13.4	100.26
PI4-3	1250	54.15	1.031	8.14	4.05	0.116	2.14	13.55	0.15	2.76	0.351	13.5	99.938
PI1-1	1740	75	1.387	4.08	2.49	0.05	1.04	7.18	0.07	1.29	0.078	7.18	99.845
PI1-2	1780	75.22	1.23	4.58	3.02	0.059	1.45	5.92	0.06	1.56	0.08	6.67	99.849
PI1-3	1820	71.88	1.162	4.34	2.71	0.062	1.25	8.38	0.07	1.39	0.07	8.53	99.844
TRI-TOPO	15	89,02	0,586	4,66	1,76	0,037	0,5	0,04	0,06	1,12	0,027	2,01	99,82
TRI-INTER	40	90,23	0,535	4,02	1,51	0,027	0,46	0,05	0,05	0,97	0,023	1,99	99,865
TRI-BASE	80	87,64	0,644	5,2	2,03	0,049	0,64	0,05	0,06	1,24	0,028	2,26	99,841

Major and minor oxides (weight percentage) of south-eastern sector													
Sample	Depth m	SiO_2	TiO_2	Al_2O_3	Fe_2O_3	MnO	MgO	CaO	Na_2O	K_2O	P_2O_5	LOI	Total
BA64	0	86.65	0.427	4.35	1.63	0.016	1.51	1.03	0.19	1.19	0.042	2.9	99.9
BA68	35	83.8	0.562	5.31	1.8	0.022	1.91	0.93	0.29	1.42	0.05	3.25	99.3
BA69	80	82.45	0.697	5.75	2.28	0.02	2.06	1.12	0.28	1.45	0.058	3.49	99.6
BA70	105	80.46	0.639	5.66	2.21	0.025	1.94	2.46	0.28	1.45	0.062	4.29	99.5
BA74	125	19.55	0.205	2.1	1.1	0.14	1.32	41.25	0	0.35	0.004	33.8	99.8

BA75	150	82.97	0.596	5.97	2.28	0.021	2.43	0.44	0.3	1.42	0.055	3.44	99.9
BA76	180	87.79	0.248	4.13	1.32	0.014	1.33	0.69	0.2	1.18	0.048	2.49	99.4
BA77	195	89.44	0.387	3.87	1.57	0.021	0.96	0.31	0.18	1.19	0.041	1.74	99.7
BA78	235	90.38	0.323	3.84	1.41	0.018	0.84	0.33	0.18	1.19	0.042	1.55	100.1
BA79	280	89.87	0.29	3.68	1.29	0.02	0.87	0.41	0.16	1.08	0.036	1.71	99.4
BA80	310	91.96	0.262	3.06	1.13	0.015	0.52	0.28	0.13	1	0.033	1.27	99.6
BA81	345	91.67	0.336	3.2	1.23	0.018	0.55	0.29	0.14	1.05	0.037	1.16	99.7
BA84	380	86.93	0.457	4.38	1.51	0.015	1.54	0.24	0.2	1.39	0.037	3.14	99.8
BA86	415	86.13	0.508	4.67	1.63	0.013	1.57	0.28	0.2	1.49	0.04	3.27	99.8
BA85	425	87.15	0.443	4.36	1.52	0.015	1.59	0.22	0.15	1.41	0.04	3.14	100
BA87	460	54.86	0.521	5.26	2.34	0.125	1.93	16.54	0.11	1.19	0.044	16.8	99.7
BA88	495	86.57	0.494	4.59	1.7	0.014	1.6	0.34	0.18	1.46	0.041	3.33	100.3
BA92	570	87.37	0.442	4.21	1.4	0.017	1.38	0.39	0.17	1.4	0.039	2.93	99.7
BA93	635	86.03	0.495	4.53	1.65	0.021	1.5	0.8	0.21	1.44	0.042	3.47	100.2
BA94	650	62.18	0.534	5.12	2.13	0.044	1.73	13.07	0.17	1.29	0.055	13.6	99.9
BA95	695	80.92	0.598	6.04	2.38	0.019	1.92	1.6	0.29	1.58	0.058	5	100.4
BA96	735	80.91	0.585	5.67	2.32	0.038	1.84	3.67	0.24	1.47	0.052	2.8	99.6
BA97	815	86.18	0.435	4.58	1.61	0.015	1.51	0.82	0.22	1.31	0.045	3.52	100.3
BA98	845	38.79	0.376	3.37	1.51	0.068	1.34	28.18	0.14	0.69	0.06	24.9	99.4
BA99	870	82.01	0.663	5.3	2.51	0.023	1.73	1.17	0.22	1.25	0.06	4.34	99.3
BA100	905	85.53	0.412	4.54	1.76	0.014	1.31	1.16	0.17	1.27	0.049	3.75	100

Trace elements (ppm) of of south-eastern sector

Sample	Depth m	Ba	Ce	Cr	Cu	Ga	La	Nb	Nd	Ni	Pb	Rb	Sc	Sr	Th	V	Y	Zn	Zr
BA64	0	319	24	42	3.4	3.7	14	10	10	8.1	8	33	5	46	2.6	51	6.6	14.4	172
BA68	35	340	27	61	4.5	5.9	15	15	16	12.7	10.9	39	6	56	5.1	56	7.5	19.7	188
BA69	80	370	36	87	5.4	5	<13	18.4	15	13.5	9.4	40	9	61	5	61	8.6	22.2	222
BA70	105	390	35	206	4.2	4.4	18	17.5	22	12.4	11.2	38	7	97	4.3	65	9.2	22.4	208
BA74	125	704	17	12.9	<1.5	4.4	31	6.6	<8	9.9	17.5	4.2	16	418	<2	33	19.9	10.8	54
BA75	150	307	36	46	4.9	6	18	13.3	21	12.9	9.1	39	10	50	5.8	71	8.7	20.5	205
BA76	180	349	16	19.7	4.1	4.9	13	8	<8	8.3	7.3	32	5	52	4.3	41	5.9	14.2	100
BA77	195	346	20	39	3.6	2.7	14	8.8	16	8.2	9.1	32	4	51	5.9	49	5.7	13.8	125
BA78	235	371	24	90	2.3	3	16	7.8	<8	7.8	8.9	32	4	51	3.6	53	5	15.9	104
BA79	280	368	20	155	2	2.6	19	7.9	10	8.5	9.4	30	5	51	2.9	64	5.6	14.4	99
BA80	310	309	11	62	3.1	<2	<13	7	<8	5	7.4	27.7	<3	48	<2	36	6.3	10	107
BA81	345	318	14	51	3	3.3	<13	8.1	8	6.3	8.8	29.4	<3	49	2.3	48	6.2	11.8	110
BA84	380	353	16	57	3.4	6.2	15	14.5	17	9.7	10.4	38	4.5	44	3.5	43	7.4	15.2	190
BA86	415	328	24	45	4.8	6.3	16	15.7	21	10.1	10	41	3.3	46	5.4	46	8.5	14.6	210
BA85	425	345	23	32	4.7	6.1	17	13.6	13	9.9	10.3	39	4.7	45	6	43	8.4	14	183
BA87	460	798	50	41	4.5	7	38	19.8	31	17	24.7	33	9	430	5.6	56	18.5	23.8	153
BA88	495	344	30	39	5.3	6.4	16	14.9	12	9.8	10.8	40	3.3	47	4.2	50	7.7	14.8	201
BA92	570	371	18	34	3.5	4.6	21	14	14	8.1	10.6	38	5.3	47	4.9	48	6.1	14.4	194
BA93	635	410	22	35	4.5	5.9	16	15.5	15	9.1	12.4	39	4.3	59	4.6	52	7.7	15.1	195
BA94	650	487	41	41	4.6	6.3	39	21.6	23	14.8	15.4	35	9.9	345	5.2	61	13.5	24.5	182
BA95	695	410	25	42	8.2	8.8	19	18.7	26	14.6	10.1	46	5.7	63	4.5	73	10.9	24	224
BA96	735	475	36	44	7.7	7.5	26	18.4	33	13.4	13	41	5.1	121	5.9	73	12	23.1	203
BA97	815	420	18	36	4.6	5.9	16	13.1	<11	9.3	10.1	36	3.3	55	4.4	55	7.2	16	171
BA98	845	472	38	21	<1	5.2	32	12.7	21	10.3	13.8	15.8	10.9	611	3.4	30	13.5	17	143
BA99	870	320	31	60	5.7	7	19	14.6	26	13.6	11.3	36	5.1	56	5	79	10.4	21	285
BA100	905	364	17	36	3.9	6.1	10	10.9	11	10.5	9.1	33	4.6	57	2.7	57	6.9	16.7	159

TABLE S2

Molecular weathering ratios of south-eastern sector							
Sample	***Horizons***	**Depth m**	**Clayeyness Al/Si**	**Leaching Ba/Sr**	**Leaching Rb/Sr**	**Hydrolysis ΣBases/Al**	**CIA**
BA64	deposit	0	0.03	4.42	0.74	1,68	55.6
BA68	Bw1	35	0.04	3.87	0.71	1,61	58.9
BA69	Bw1	80	0.04	3.87	0.67	1,61	58.6
BA70	Bw2	105	0.04	2.57	0.4	2,02	46.5
BA74	Bwk	125	0.06	1.07	0.01	37,5	2.71
BA75	Bw	150	0.04	3.92	0.8	1,5	67.8
BA76	C	180	0.03	4.28	0.63	1,51	59.1
BA77	C	195	0.03	4.33	0.64	1,18	64.3
BA78	C	235	0.03	4.64	0.64	1,12	63.7
BA79	C	280	0.02	4.6	0.6	1,19	62.8
BA80	deposit	310	0.02	4.11	0.59	1,02	62.9
BA81	deposit	345	0.02	4.14	0.61	1,03	62.8
BA84	Bw	380	0.03	5.12	0.89	1,41	65.9
BA86	Bw	415	0.03	4.55	0.91	1,37	65.6
BA85	Bw	425	0.03	4.89	0.89	1,42	66.7
BA87	deposit	460	0.06	1.18	0.08	6,92	14.3
BA88	Bw	495	0.03	4.67	0.87	1,42	64.8
BA92	Bw	570	0.03	5.04	0.83	1,42	62.7
BA93	Bwk	635	0.03	4.43	0.68	1,58	57.4
BA94	Bwk	650	0.05	0.9	0.1	5,82	16.8
BA95	C	695	0.04	4.15	0.75	1,65	54.2
BA96	A/Bw	735	0.04	2.5	0.35	2,35	39.6
BA97	A/Bw	815	0.03	4.87	0.67	1,55	58.3
BA98	Bwk	845	0.05	0.49	0.03	16,5	6.06
BA99	deposit	870	0.04	3.65	0.66	1,55	58
BA100	Bw	905	0.03	4.07	0.59	1,56	54.7

TABLE S3

SECTORS	(i)**Depth Bk horizon** MAP(mm/y) = 137.24 + 6.45D - 0.013D2 SE +147 mm/y	(ii)**Chemical alteration -** CIA-K MAP(mm/y) = 221.1e0.0197(CIA-K) SE +181 mm/y	(ii)**Chemical alteration -** (ΣBases/Al MAP(mm/y) = -259.31 (ΣBases/Al) + 759 SE +235 mm/y	(iii) **Chemical alteration - CALMAG** MAP(mm/y) = 22.69 (CALMAG)– 435.8 SE = ± 108 mm	**MEAN**
north-western	322 - 358 - 401 - 498 - 679	518 - 595 - 691 - 775	502 - 541	no data	535
proximal north-eastern	no data	no data	737 - 752	no data	744
medial north-eastern	406 - 532		431	460	457
south-eastern	814 - 899	633 - 803 - 873 - 895 - 899 - 905 - 1090 - 1142 - 1145 - 1174 - 1182 - 1229	no data	no data	977

TABLE S4

Formation time, Ft (yr)			
	Ft (yr) = 17.7 (Bt thickness, cm)^2 + 645.8 (Bt thickness, cm) Sheldon (2003)	**Ft (calcium carbonate nodules) = 3.92 x (nodule diameter, mm)$^{0.34}$** Retallack (2005)	**MEAN**
North-western sector	367,533 – 356,749 – 201,620 – 163,097 – 145,316 – 112,715 – 95,049 – 73,704 – 66,352 – 59,354 – 46,425 – 46,425	no data	144,528
South-eastern sector	38,595 – 14,856 - 8,917	6,7	15,594

TABLE S5

SECTORS	*Channel deposits*	*Interchannel deposits*	*Palaeosol types*	*Source of the clastic material*	*Fluvial drainage direction*	*Relationships between palaeosol and deposits*	*Palaeosols formation time*	*Inferred palaeoclimate*
Northwestern	- 7% of the total thickness - Intermittent or ephemeral braided rivers	- 28% the total thickness - aeolian deposits of nabkha dunes	- 65% of the total succession - Commonly Aridisols and Entisols	- Mafic volcanic and sedimentary rock source	- Stream flows southward directed	- Aridisols and Entisols alternate with deposits of aeolian sand sheet	- 10^4-10^5 yr, for Aridisols and less than 103 yr for Entisols	- Arid or semiarid climatic conditions - Aridisols indicate mean annual precipitation of c. 400-650 mm/yr
Northeastern	- From proximal to NW distal zone of fluvial system: from 70 to 20% of the total thickness and width/thickness ratio from >100 to <10 - No channel deposits in W distal zone.	- Over 70% of the succession, in W distal part constituted of tabular sandstones overlie by thin mudstone beds	- From proximal to medial portion of the fluvial system: from 20-55% to 45-80% of the thickness - In NW distal portion 80% of the total thickness, while in W distal portion palaeosols do not exceed 25%. - Commonly Inceptisols and less common Entisol and Vertisols	- Metamorphic rock source	- Stream flows northwest and west directed	- In proximal, medial and NE distal portion of the fluvial system, there are alternations of Entisols and deposits close to the active channel; while above abandoned fluvial belt deposits developed Inceptisols interlayered with channel deposits. - In W distal area Entisols are alternated with unconfined deposits	- Thousands of years for Inceptisol/channel deposits alternation - Hundreds of years for Entisols/deposits alternation	- Inceptisols indicate mean annual precipitation of c. 450-750 mm/yr
Southeastern	- No channel deposits	- Lower 0.1-0.6 m of sandstone beds showing sedimentary structures linked to high concentrated and unconfined subaqueous flows	- 90% of the total thickness - Well-developed Inceptisols, in some cases transitioning to Alfisols	- Felsic igneous and/or sedimentary rock source	- No palaeocurrent direction data	- Well-developed Inceptisols alternated with unconfined deposits	- Residence of well-developed Inceptisols of 103-104 yr.	- Climofunction applied to Inceptisols indicate mean annual precipitation >850 mm/yr.

TABLE S6

CYCLICAL ALTERNATION OF PALAEOSOLS/DEPOSITS

The palaeosol and aeolian deposits alternations were controlled by high frequency climate variations.
The recurrence time of the depositional events varies from <10^3 y (Entisols/deposits) to 10^4-10^5y Aridisols/deposits)
Low accommodation space generation

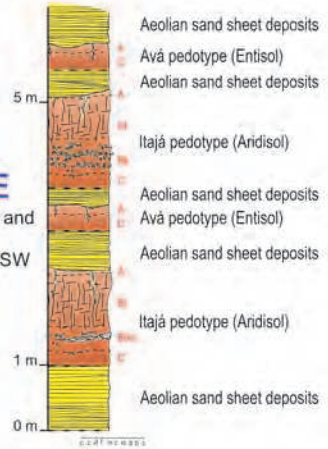

CLIMATE

Itajá pedotype (Aridisol)
is dominant

MAP = 535 mm/yr

Arid / semiarid alternations

CLASTIC SOURCE

Clastic source is from mafic volcanic and sedimentary rocks.
Palaeoflow directions are toward S-SSW

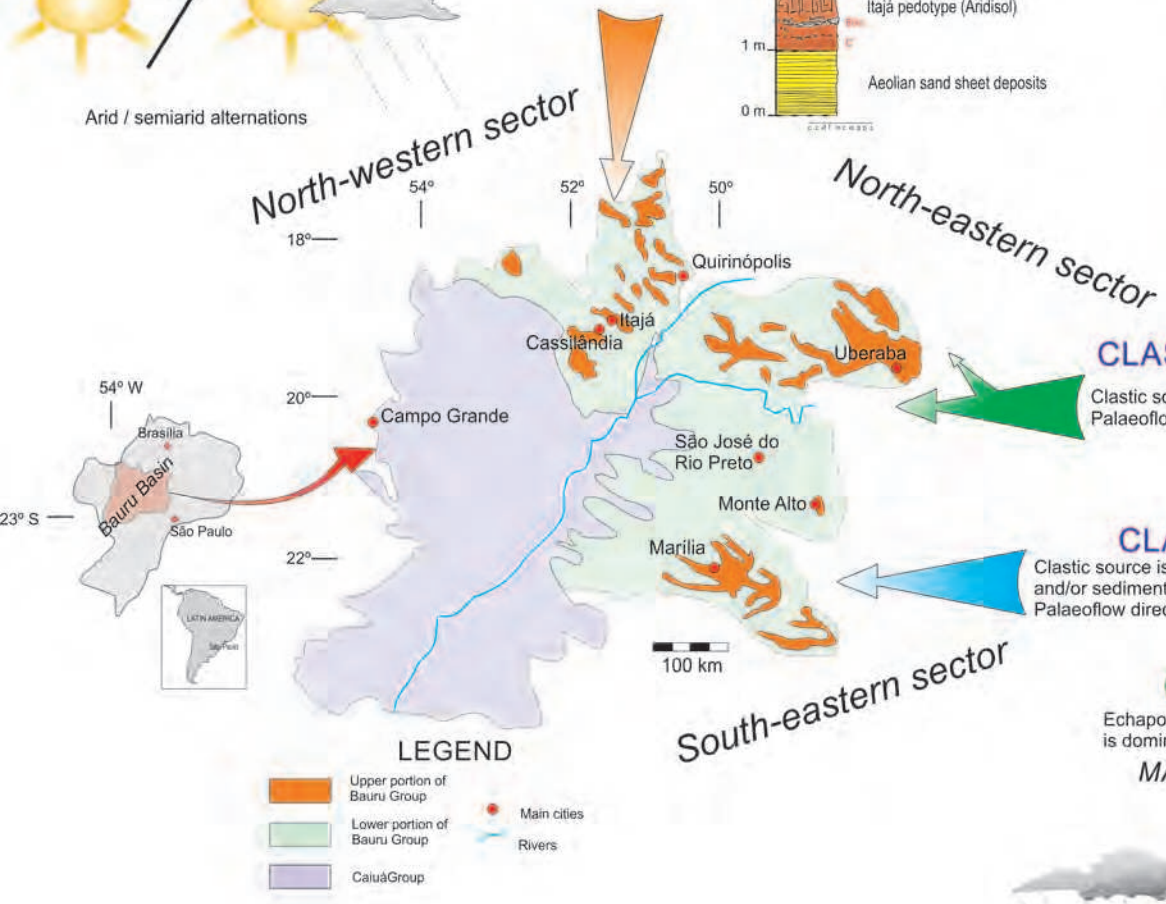

CLIMATE

Echaporã pedotype (Inceptisol)
is dominant

MAP 977 mm/yr

Subhumid climate

CLASTIC SOURCE

Clastic source is dominated by felsic intrusive magmatic and/or sedimentary rocks.
Palaeoflow directions are missing.

CLASTIC SOURCE

Clastic source is by prevalent metamorphic rocks.
Palaeoflow directions are toward W-NW

CLIMATE

Distal area

Krenk pedotype (Entisol)
is dominant

MAP = no data

Semiarid climate

Medial area

Krenk pedotype (Entisol)
is dominant

MAP = 457 mm/yr

Subhumid climate

Proximal area

Pataxó pedotype (Inceptisol)
is dominant

MAP = 744 mm/yr

Subhumid climate

CYCLICAL ALTERNATION OF PALAEOSOLS/DEPOSITS

The palaeosol and alluvial plain deposits alternances were controlled by channel and overbank river depositional processes.
The recurrence time of the depositional events varies from<10^3 y (Entisols/deposits) to >10^3y (Inceptisols/deposits).
High accommodation space generation

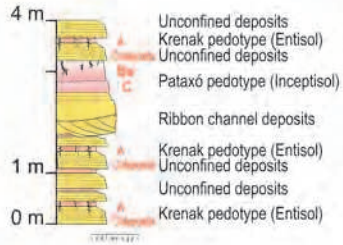

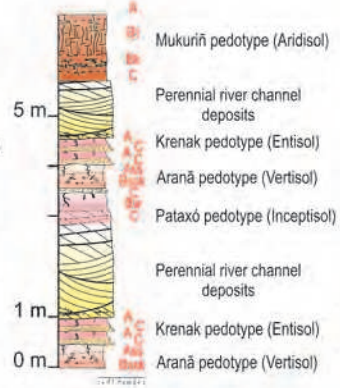

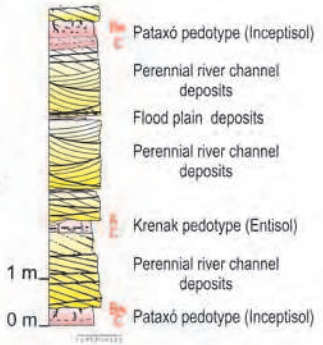

CYCLICAL ALTERNATION OF PALAEOSOLS/DEPOSITS

The palaeosol and tabular sheet deposits alternances were controlled by cyclical paroxysmal unconfined flows.
The recurrence time of the depositional events is c. 10^4 y (Inceptisols/deposits).
Intermediate accommodation space generation

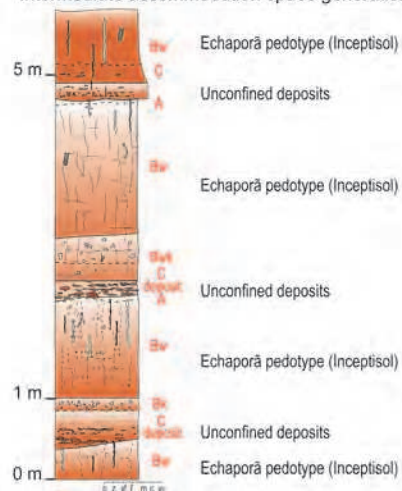

SUPPLEMENTARY MATERIAL

CAPTIONS

Figure S1. (A-D) North-western sector. (A) Petrography composition of the aeolian sandstones of "planar-parallel, horizontal or low-angle, laminated sandstone beds". (B) Clast composition of the river conglomerates of the "conglomerate sheet bodies". (C) Petrography composition of the river sandstones of "sandstone sheet bodies". (D) Petrography composition of the sandstone of the Iatajá pedotype (Aridisols). Note as the volcanic component of the sandstone decreases from fluvial through aeolian deposits to palaeosols suggesting the progressive loss of these clasts due to physical and chemical weathering (Basilici and Dal Bó, 2010). (E-G) North-eastern sector. (E) Petrography composition of the river sandstones of "Sheet sandstone bodies" of the proximal area. (F) Clast composition of the pebbles preserved in river sandstones of "Sheet sandstone bodies" of the proximal area. (G) Petrography composition of the sandstone of the Pataxó pedotype (Inceptisol). (H) South-eastern sector. Petrography composition of the sandstone of the Echaporã pedotype (Inceptisol). See text for discussion.

Figure S2. A. Sandstone tabular bodies. Close-up of poorly sorted and structureless sandstones (a) interlayered with sandy conglomerate lens (b). B. Sandstone tabular bodies. Close-up of sandstones shows planar parallel laminations (c), interlayered to structureless sandstones (a) and lenticular beds of sandy conglomerate (b). Coin: 25 mm. C. Sandstone tabular bodies. Close-up of the intraformational conglomerate. Dashed lines separate the muddy sandstone intraformational clasts. Pencil: 145 mm. D. Conglomerate and sandstone tabular bodies. Basalt and quartzarenite pebbles and cobbles clasts with ventifact shape. Coin: 25 mm.

Figure S3. Figure 20. Rose-diagram of palaeodirections of fluvial flows extracted from fabric and sedimentary structures of the north-western and north-eastern areas. (A, B) Statistical

distribution of dip of discoidal imbricated pebble- and cobble-sized clasts. The palaeoflow is opposed to the dip. (C, D). Statistical distribution of foreset dip of cross stratifications.

Figure S4. (A-C). Laminated sandstones deposited by climbing wind ripples (aeolian deposits in the picture) overlay an eroded surface of a palaeosol profile. Figure B emphasise the sedimentary structures of the photograph (Figure A) and figure C is an interpretation. D. Medial portion of the fluvial distributary system. Sedimentary structures and bounding surfaces as observed by field drawings (Modified from Soares et al., 2020a). E. Medial portion of the fluvial distributary system. Desk-based interpretation of a river channel with a larger width/thickness ratio and lesser grain size in comparison with the proximal areas channel deposits.

Figure S5. Factor loading of the components 1 (P1) and 2 (P2) extracted by the Principal component analysis (PCA) of the major and minor geochemical elements of the palaeosols of the three study sectors. See discussion in the text.

Table S1. Percentage distribution of the thickness of the architectural elements in the three study sectors. See text for details and discussions.

Table S2. Weight distribution of major, minor, and trace (only for the south-eastern sector) elements of samples of palaeosols of the three study sectors.

Table S3 of Supplementary Material. Some weathering molar ratio of major, minor, and trace elements of samples of palaeosol of the south-eastern sector.

Table S4. Mean annual precipitation (MAP) of the three study areas obtained from different climofunctions. (i) From Retallack (2005); (ii) from Sheldon et al. (2002); (iii) from Nordth and Driese (2010).

Table S5. Quantitative values of the time of development (formation time) of palaeosols in north-western and south-eastern sectors. See text for details and discussions.

Table S6. Main difference in palaeopedological and sedimentological aspects of the three sectors of study.

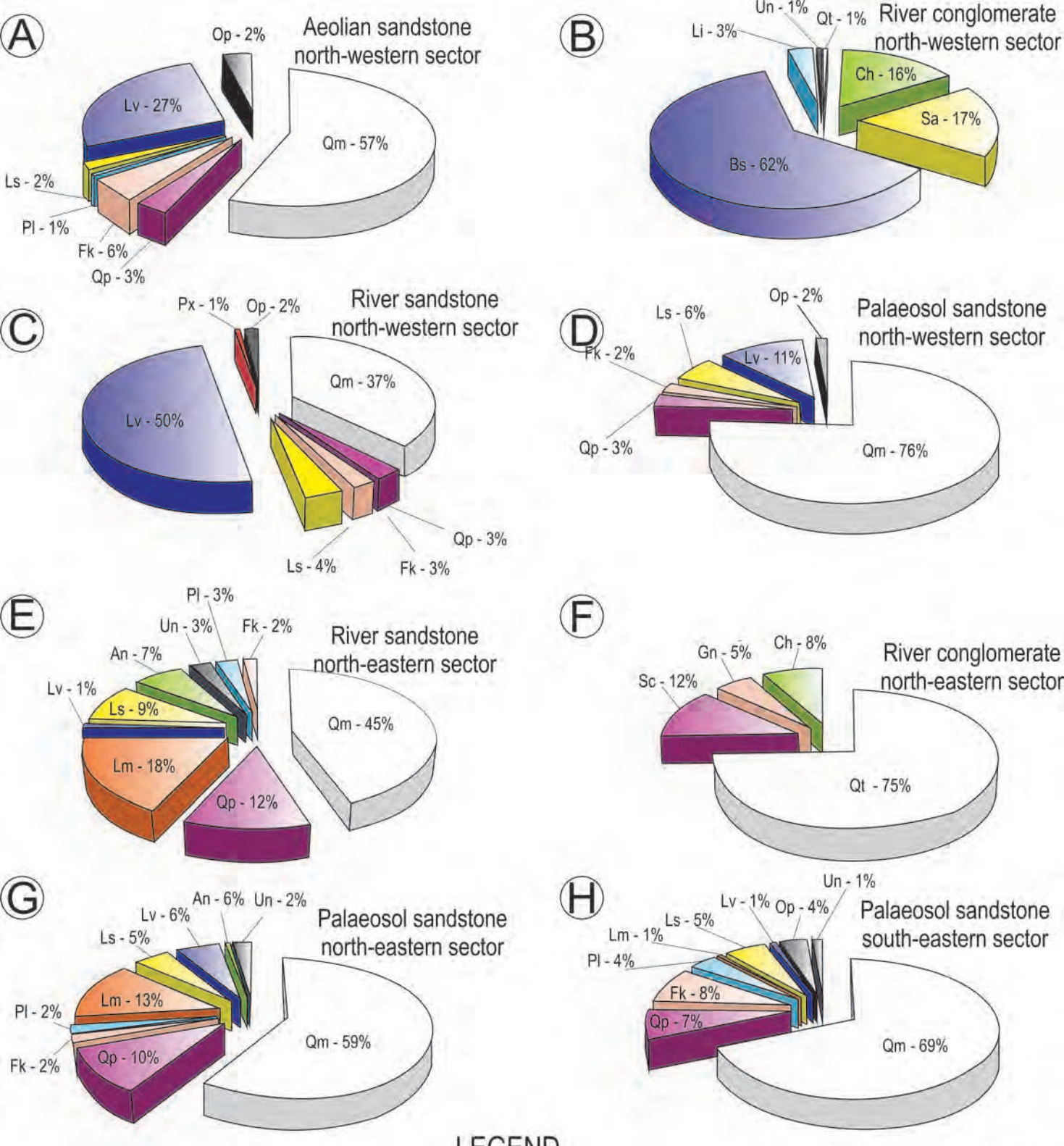
A
Aeolian sandstone
north-western sector
Op - 2%
Lv - 27%
Qm - 57%
Ls - 2%
Pl - 1%
Fk - 6%
Qp - 3%
B
River conglomerate
north-western sector
Un - 1%
Qt - 1%
Li - 3%
Ch - 16%
Sa - 17%
Bs - 62%
C
River sandstone
north-western sector
Px - 1%
Op - 2%
Qm - 37%
Lv - 50%
Qp - 3%
Ls - 4%
Fk - 3%
D
Palaeosol sandstone
north-western sector
Op - 2%
Ls - 6%
Fk - 2%
Lv - 11%
Qp - 3%
Qm - 76%
E
River sandstone
north-eastern sector
Pl - 3%
Un - 3%
Fk - 2%
An - 7%
Lv - 1%
Ls - 9%
Qm - 45%
Lm - 18%
Qp - 12%
F
River conglomerate
north-eastern sector
Gn - 5%
Ch - 8%
Sc - 12%
Qt - 75%
G
Palaeosol sandstone
north-eastern sector
An - 6%
Un - 2%
Lv - 6%
Ls - 5%
Lm - 13%
Pl - 2%
Qm - 59%
Fk - 2%
Qp - 10%
H
Palaeosol sandstone
south-eastern sector
Un - 1%
Lv - 1%
Op - 4%
Ls - 5%
Lm - 1%
Pl - 4%
Fk - 8%
Qp - 7%
Qm - 69%
LEGEND
Sandstone petrography
Volcanic lithic fragments (Lv)
Sedimentary lithic fragments (Ls)
Metamorphic lithic fragments (Lm)
Amphibole (An)
Plagioclase (Pl)
Monocrystalline quartz (Qm)
Polycrystalline quartz (Qp)
K-Feldspar (Fk)
Opaque minerals (Op)
Pyroxene (Px)
Undetermined (Un)
Pebble and cobble composition
Basalt (Bs)
Sandstone (Sa)
Chert (Ch)
Limestone (Li)
Quartzite (Qt)
Schist (Sc)
Gneiss (Gn)
Undetermined (Un)

FIGURE S1

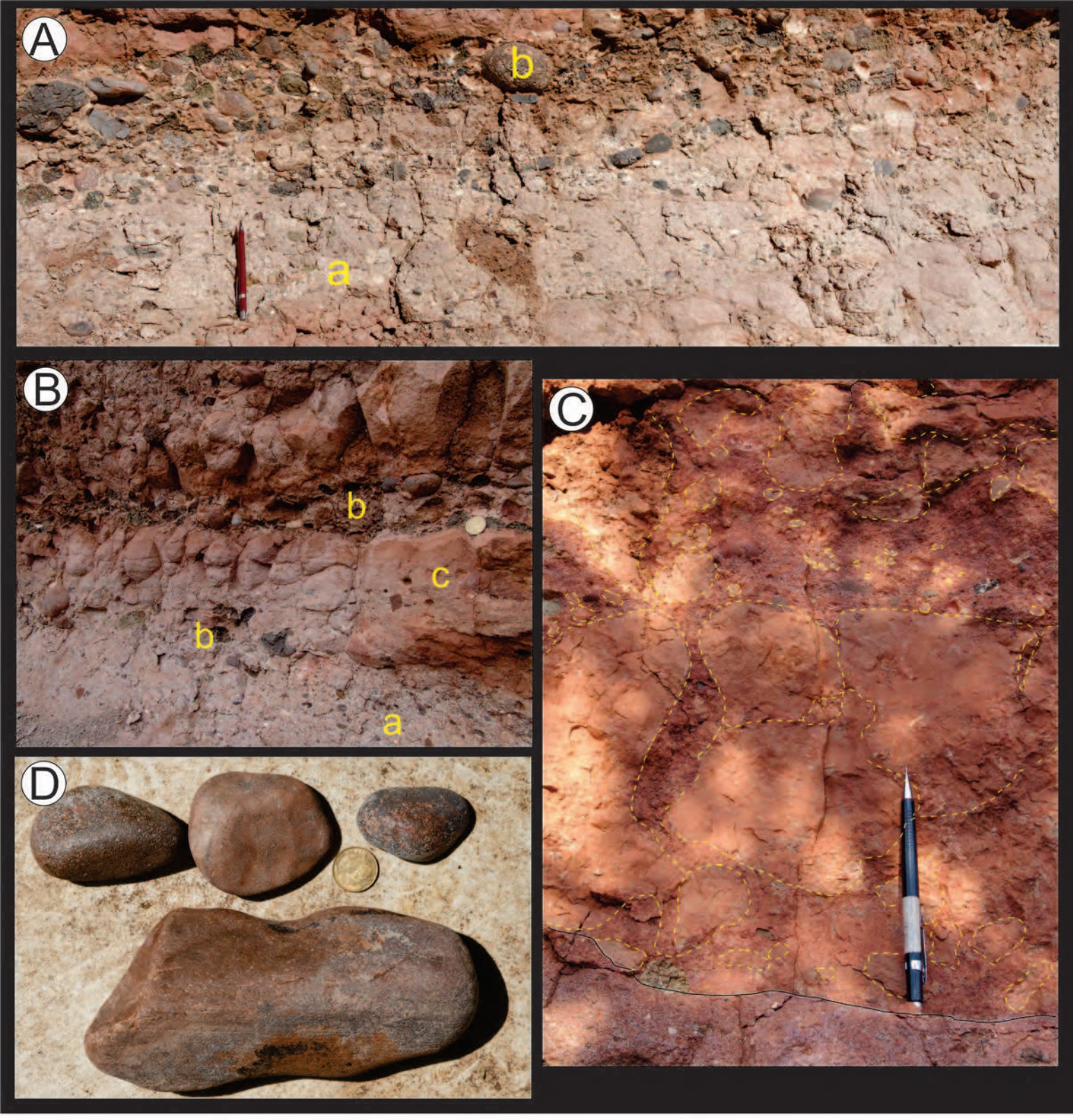

FIGURE S2

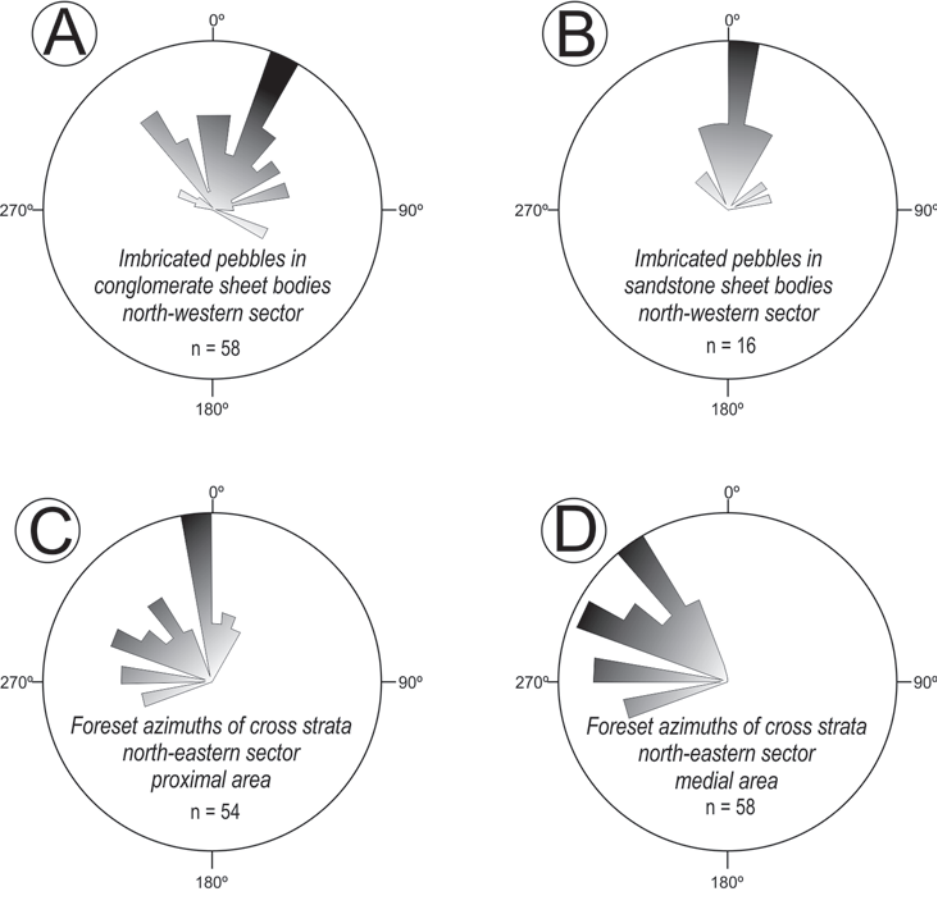
A
0°
270°
90°
180°
Imbricated pebbles in conglomerate sheet bodies north-western sector
n = 58
B
0°
270°
90°
180°
Imbricated pebbles in sandstone sheet bodies north-western sector
n = 16
C
0°
270°
90°
180°
Foreset azimuths of cross strata north-eastern sector proximal area
n = 54
D
0°
270°
90°
180°
Foreset azimuths of cross strata north-eastern sector medial area
n = 58

FIGURE S3

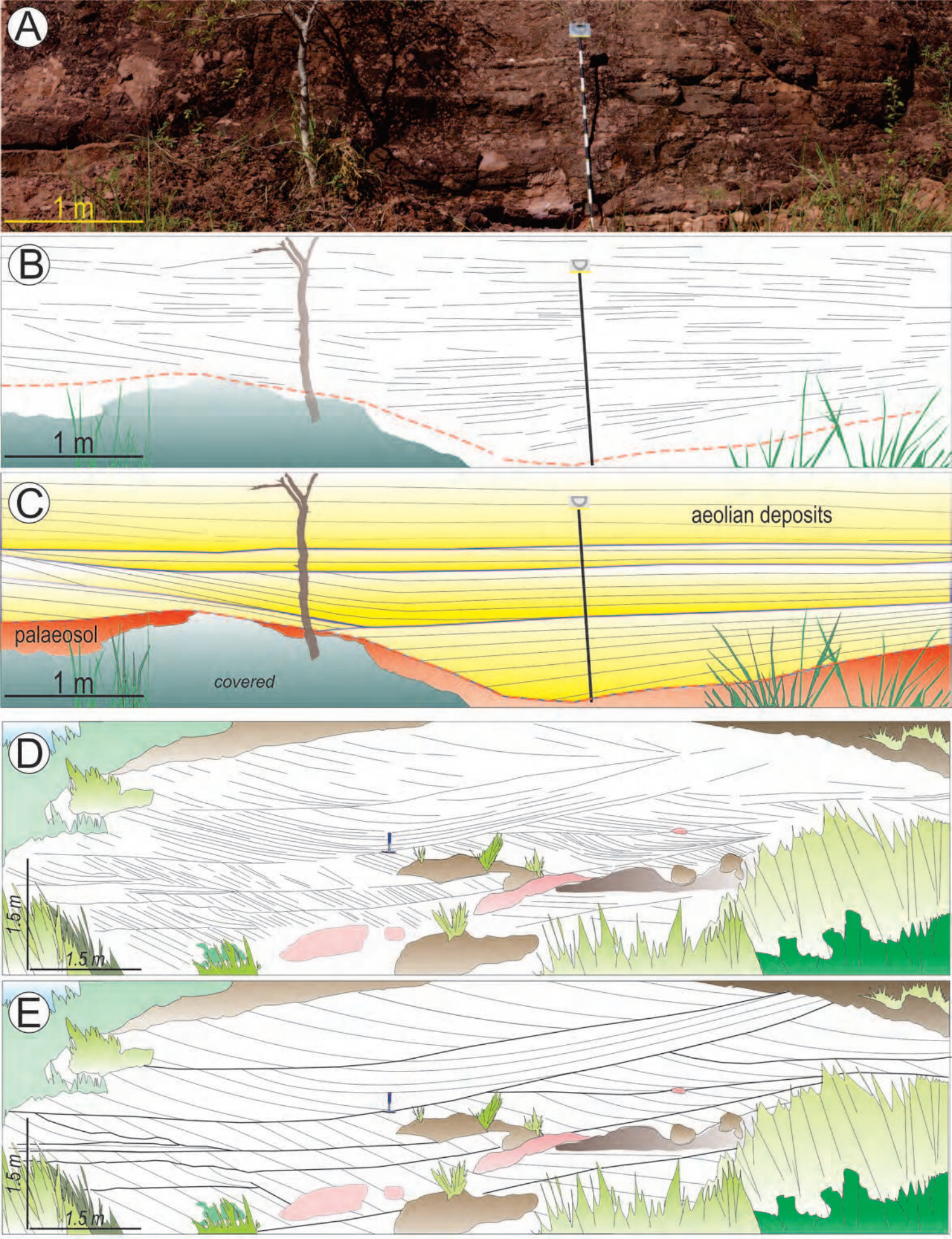
A
1 m
B
1 m
C
aeolian deposits
palaeosol
1 m
covered
D
1.5 m
1.5 m
E
1.5 m
1.5 m

FIGURE S4

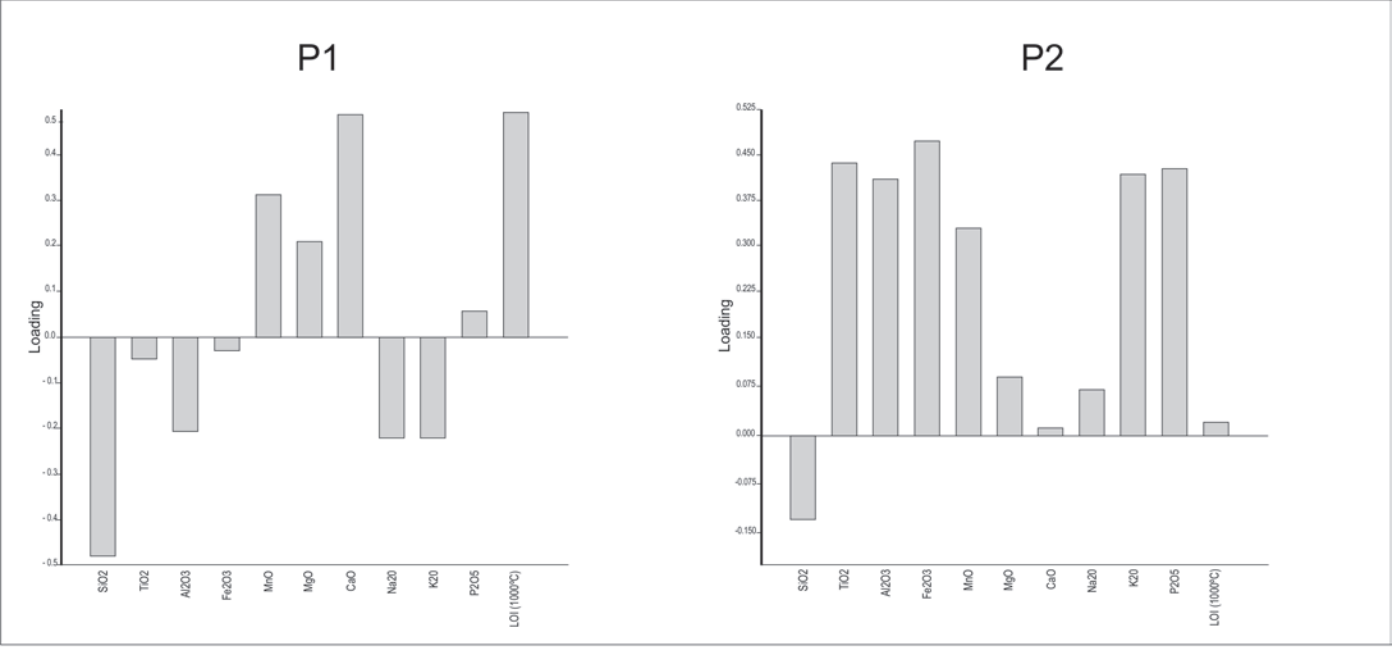
P1
Loading
0.5
0.4
0.3
0.2
0.1
0.0
-0.1
-0.2
-0.3
-0.4
-0.5
SiO2
TiO2
Al2O3
Fe2O3
MnO
MgO
CaO
Na2O
K2O
P2O5
LOI (1000°C)
P2
Loading
0.525
0.450
0.375
0.300
0.225
0.150
0.075
0.000
-0.075
-0.150
SiO2
TiO2
Al2O3
Fe2O3
MnO
MgO
CaO
Na2O
K2O
P2O5
LOI (1000°C)

FIGURE S5